ENGINEERING GEOLOGIC AND GEOTECHNICAL ANALYSIS OF PALEOSEISMIC SHAKING USING LIQUEFACTION EFFECTS: PART II. FIELD EXAMPLES

Russell A. Green[1], Stephen F. Obermeier[2], and Scott M. Olson[3]

University of Michigan, Department of Civil and Environmental Engineering
Report UMCEE 04-08

Key words: paleoliquefaction, paleoseismic, liquefaction, earthquake, Wabash Valley, New Madrid

August 22, 2004

[1] Assistant Professor, Department of Civil and Environmental Engineering, University of Michigan, 2372 G.G. Brown Building, Ann Arbor, Michigan, 48109-2125, rugreen@engin.umich.edu
[2] Emeritus, U.S. Geological Survey, Reston, Virginia and EqLiq Consulting, Rockport, Indiana, sobermei@yahoo.com
[3] Geotechnical Project Manager, URS Corporation, 1001 Highlands Plaza Drive West, Suite 300, St. Louis, Missouri, 63110, 314-429-0100, 314-429-0462 (fax), scott_olson@urscorp.com

ABSTRACT

I. INTRODUCTION
II. PROCEDURE FOR PERFORMING BACK-ANALYSIS
Using Liquefaction Evaluation Procedures at Individual Sites to Estimate Likely Combination of a_{max} and M (Step 5).
Determine representative in-situ soil index (e.g., $N_{1,60cs}$) of source stratum of liquefied soil
Determine combinations of a_{max}-M required to induce liquefaction
Use regional attenuation relationship(s) to estimate credible bedrock a_{max}-M combinations possible at the site
Back-analyses of non-liquefied sites.
Integrating Individual Site Back-Calculations in Regional Assessment of the Magnitude of the Paleoearthquake (Step 6).
III. CASE STUDY – ASSESSMENT OF THE CHANGE IN LIQUEFACTION SUSCEPTIBILITY AT PALEOLIQUEFACTION SITES
Background Information
Field Setting
Observed Liquefaction Effects and In-Situ Testing
Results and Interpretations
Discussion of Factors Affecting Interpretation
IV. CASE STUDY – REGIONAL ANALYSIS OF THE VINCENNES EARTHQUAKE
Background Information
Geological and engineering geological studies
Geotechnical studies
Selection of Representative Penetration Resistance
Site PB
Site MA
Back-Calculation Results
Discussion of Back-Calculations for Vincennes Earthquake
Influence of various attenuation models
Influence of bedrock motion amplification
Influence of back-calculation technique
Potential aging effects
V. SUMMARY AND CONCLUSIONS
VI. ACKNOWLEDGMENTS
VII. REFERENCES

APPENDIX I. SITE AMPLIFICATION FACTORS

APPENDIX II. VINCENNES EARTHQUAKE BACKGROUND INFORMATION

ENGINEERING GEOLOGIC AND GEOTECHNICAL ANALYSIS OF PALEO-SEISMIC SHAKING USING LIQUEFACTION EFFECTS: FIELD EXAMPLES

by: Russell A. Green, Stephen F. Obermeier, and Scott M. Olson

ABSTRACT

The greatest impediments to the widespread acceptance of back-calculated ground motion characteristics from paleoliquefaction studies typically stem from three uncertainties: (1) the significance of changes in the geotechnical properties of post-liquefied sediments (e.g., "aging" and density changes), (2) the selection of appropriate geotechnical soil indices from individual paleoliquefaction sites, and (3) the methodology for integration of back-calculated results of strength of shaking from individual paleoliquefaction sites into a regional assessment of paleoseismic strength of shaking. Presented herein are two case studies that illustrate the methods outlined in Olson et al. (2004) for addressing these uncertainties. The first case study is for a site near Memphis, Tennessee, wherein cone penetration test data from side-by-side locations, one of liquefaction and the other of no liquefaction are used to readily discern that the influence of post-liquefaction "aging" and density changes on the measured in-situ soil indices is minimal.

In the second case study, twelve sites that are at scattered locations in the Wabash Valley and that exhibit paleoliquefaction features are analyzed. The features are first provisionally attributed to the Vincennes Earthquake, which occurred around 6,100 years BP, and are used to illustrate our proposed approach for selecting representative soil indices of the liquefied sediments. These indices are used in back-calculating the strength of shaking at the individual sites, the results from which are then incorporated into a regional assessment of the moment magnitude, M, of the Vincennes Earthquake. The regional assessment validated the provisional assumption that the paleoliquefaction features at the scattered sites were induced by the

Vincennes Earthquake, in the main, which was determined to have M~7.5. The uncertainties and assumptions used in the assessment are discussed in detail.

I. INTRODUCTION

The study of paleoliquefaction effects to assess the characteristics of prehistoric earthquakes is gaining an increasingly prominent role in evaluating seismic hazard, especially in regions that experience infrequent earthquakes. However, questions remain regarding the use of geotechnical data for paleoearthquake investigations because of the uncertain influence of changes in the geotechnical properties after the sediments have liquefied (e.g., aging and density changes), and additionally, questions remain regarding uncertainties in how to implement existing analytical procedures for performing the back-calculations and how to interpret the results. In a companion paper (Olson et al., 2004), the authors propose new methods for analyzing and interpreting paleoliquefaction manifestations, which should reduce the uncertainties in the back-calculated earthquake parameters. The focus of the present paper is to detail two case studies that illustrate those proposed methods. The case studies are associated with paleoearthquakes in the New Madrid and Wabash Valley Seismic Zones (Figure 1).

The first case study in this paper illustrates the authors' recommended approach (Olson et al., 2004) for assessing the significance of effects related to aging, density changes, and other factors affecting liquefaction susceptibility at paleoliquefaction sites. Although penetration resistance is known to increase with time in some deposits that have liquefied (e.g., Olson et al., 2001), few paleoliquefaction studies have attempted to account for this phenomenon, undoubtedly as a result of the lack of guidance on the subject. The site analyzed in this case study is located near Memphis, Tennessee. At the site there is an extensive bank exposure, hundreds of meters long, where both marginal liquefaction effects and no liquefaction effects exist, side-by-side, in deposits having the same age and having the same initial depositional environment. Here, the geologic and liquefaction susceptibility conditions at the site are very good for demonstrating the authors' proposed method, because the effects of liquefaction on subsequent liquefaction susceptibility can be compared directly.

The second case study illustrates multiple facets of paleoliquefaction analyses, including: the appropriate selection of soil parameters for assessing liquefaction susceptibility by using field observations in sectional view at sites located in the both the meizoseismal zone and beyond; and the integration of data from multiple sites into a regional assessment of the strength of shaking of a paleoearthquake, even when uncertainty exists regarding whether all the features analyzed resulted from the same causative earthquake. This second case study makes use of extensive paleoliquefaction data that were collected a few years ago in the Wabash Valley Seismic Zone (Figure 1). In particular, twelve sites having paleoliquefaction features were used to assess the characteristics of the causative motions. Most or all the features previously had been attributed to the same large paleoearthquake, estimated to have occurred near Vincennes, Indiana, about 6,100 yr BP ±200 yrs – hereafter referred to as the "Vincennes Earthquake" (e.g., Munson and Munson, 1996; Pond and Martin, 1996; and Obermeier, 1998). Although previous studies have been performed on this paleoearthquake, questions have remained regarding whether the observed liquefaction features were actually induced by the Vincennes Earthquake, whether the geotechnical interpretation of field data was correct, and whether the previously assessed magnitude (M~7.5) of the Vincennes Earthquake is valid.

Our re-assessment of the Vincennes Earthquake employs a variant of the procedure devised by Pond and Martin (1996), using the same raw field data. These data were obtained prior to the development of the proposed recommendations for site selection outlined in Olson et al. (2004). Still, the interpretation and analysis of the data presented herein generally accords with the recommendations of Olson et al. (2004). Particularly, the authors critically consider the role of ground-failure mechanism, in addition to the severity of liquefaction at the site, in establishing representative in-situ soil indices used to back-calculate the strength of shaking. Also, four regionally applicable acceleration attenuation relations are used to characterize the paleoearthquake, which were not available at the time when Pond and Martin (1996) conducted their study. In order for the authors to cross-check the back-calculated earthquake magnitude, the attenuation

relations were used in conjunction with both the cyclic stress and the Green-Mitchell energy-based liquefaction evaluation procedures (Green, 2001).

II. PROCEDURE FOR PERFORMING BACK-ANALYSES

The overall thrust of the procedure proposed by Olson et al. (2004) is to address and reduce many of the uncertainties inherent in field data collection techniques and existing back-analysis techniques. The procedure consists of six steps:

(1) Plan field work with consideration of regional seismological and geotechnical issues that affect site selection, data interpretation, and details of back-analysis. Olson et al. (2004) discuss these issues in detail.

(2) Perform field work in light of engineering geologic recommendations of Obermeier et al. (2001, 2004) and data collection techniques suggested by Olson et al. (2004).

(3) Estimate the provisional location of the energy center of the paleoearthquake, as detailed in Obermeier et al. (2001, 2004).

(4) Use a regional magnitude bound relationship and the distance from the energy center to the most distal site of liquefaction (R_{ec_max}) to estimate magnitude. (Obermeier et al., 2001; Olson et al., 2004)

(5) Perform back-calculations using liquefaction evaluation procedures at individual sites to estimate likely combinations of peak ground surface acceleration (a_{max}) and earthquake magnitude (M).

(6) Integrate results from individual sites into a regional assessment to verify the estimated provisional location of the energy center of the paleoearthquake and to estimate the magnitude of the paleoearthquake.

The primary focus of this paper is to illustrate Steps (5) and (6). The analytical portions of these two steps are described below. Central to these steps is the proper interpretation of field data (e.g., SPT logs or CPT soundings) for use in the assessment of the paleoearthquake, which is given considerable attention in our case studies.

Using Liquefaction Evaluation Procedures at Individual Sites to Estimate Possible Combinations of a_{max} and M (Step 5).

For illustration purposes the steps presented below are in reference to the cyclic stress liquefaction evaluation procedure, although the overall approach applies equally to the Green-Mitchell energy-based procedure, as well as most other liquefaction evaluation procedures. In the discussion below the in-situ soil index is quantified in terms of $N_{1,60cs}$ (i.e., the standard penetration test (SPT) N-value, normalized and adjusted for overburden stress, hammer energy, rod length, fines content, etc. per Youd et al., 2001). However, the approach is applicable to any in-situ soil indices for which liquefaction evaluation procedures have been developed (e.g., q_{T1cs}, V_{s1}). The following steps apply to sites containing liquefaction features.

Determine representative in-situ soil index (e.g., $N_{1,60cs}$) of source stratum of liquefied soil. For a site containing a liquefaction feature, estimate the representative value of $N_{1,60cs}$ of the soil layer that is most susceptible to liquefaction. Olson et al. (2004) discuss techniques to estimate a representative value of $N_{1,60cs}$ from measured field values for sites studied in sectional or plan view, as well as factors that affect the interpretation of the "representative" value.

Determine combinations of a_{max}-M required to induce liquefaction. Once a representative $N_{1,60cs}$ is determined for the soil layer most susceptible to liquefaction, all a_{max}-M combinations required to induce liquefaction can be determined by setting the factor of safety against liquefaction (FS_{liq}) equal to one, e.g.:

$$FS_{liq} = \frac{CRR}{CSR_{M7.5}} = 1 \qquad [1]$$

Thus by substituting expressions for CRR and $CSR_{M7.5}$ into Eq. [1] (see Olson et al., 2004 for corresponding expressions), a_{max} can be expressed as a function of M:

$$a_{max} = CRR\left(N_{1,60cs}\right) \cdot MSF(M) \cdot K_{\sigma} \cdot \frac{g \cdot \sigma'_{vo}}{0.65 \cdot \sigma_{vo} \cdot r_d} \qquad [2]$$

Figure 2 shows a plot of Eq. [2].

<u>Use regional attenuation relationship(s) to estimate credible bedrock a_{max}-M combinations at the site.</u> As illustrated in Figure 2a, the boundary corresponding to Eq. [2] (and a factor of safety of unity) separates combinations of a_{max}-M that are sufficient to induce liquefaction from combinations that are insufficient. Of particular interest are the a_{max}-M combinations that are sufficient to induce liquefaction, and as may be observed from Figure 2a, these combinations are infinite in number and can vary widely. To narrow this range, regional attenuation relations are used to deterministically define credible a_{max}-M combinations for the site. For a given site condition, most attenuation relations are formulated with three variables: a_{max}, M, and site-to-source distance (R), with a_{max} usually being the dependent variable (i.e., a_{max} = f(M, R)). The dashed line in Figure 2b is a plot of an attenuation relation where R set equal to the distance from the paleoliquefaction site to the provisional location of the energy center of the earthquake (determined in Step 3), and M is varied from 5.5 to 8.5. [Note: The estimated location of the energy center is referred to as "provisional" because it is based on the assumption that the liquefaction features were primarily induced by a single, large earthquake. The validity of this assumption is later assessed in Step 6.] Therefore, the dashed line in Figure 2b represents the likely accelerations at the paleoliquefaction site corresponding to various potential causative earthquake magnitudes. As indicated in this figure, the portion of the attenuation relation that plots above and to the right of the FS_{liq} = 1 line defines a_{max}-M combinations that could possibly have caused liquefaction at the site. The intersection of the boundary line (i.e., FS_{liq} = 1 line) and the attenuation relation is the lower bound a_{max}-M combination operative at the site. All other possible a_{max}-M combinations sufficient to induce liquefaction at the site have $FS_{liq} < 1$, and therefore yield higher values for a_{max} and M.

In many geographic regions throughout the world, attenuation relations do not exist for all site conditions. For example, in the central and eastern US (CEUS), available attenuation relations are primarily for rock sites. A variety of approaches of varying

degrees of sophistication can be used to relate the a_{max} for a rock site to the corresponding value for soil conditions. The topic is discussed further in Appendix I.

Back-analyses of non-liquefied sites. The preceding discussion applies to the back-analysis of sites that liquefied. Consequently, the resulting a_{max}-M combination is a lower-bound estimate for each paleoliquefaction site. By following the same procedures for sites that did not liquefy during a paleoearthquake, an upper bound estimate of the a_{max}-M combination for each site can be determined.

Integrating Individual Site Back-Calculations in Regional Assessment of the Magnitude of the Paleoearthquake (Step 6).

To make a reasonable interpretation of the individual site data computed in Step 5, a regional assessment of the a_{max}-M combinations for all the study sites needs to be performed. The regional assessment incorporates the back-analyses from both sites of liquefaction (i.e., lower bound values) and of no liquefaction (i.e., upper bound values). Several approaches can be used for the regional assessment, but the authors recommend the one illustrated in Figure 3.

In Figure 3, the a_{max} value determined for each site is plotted as a function of the corresponding distance from the site to the provisional energy center, with various styles of filled symbols being used for liquefied sites and open symbols being used for the sites that did not liquefy. The "+" and "-" signs indicate opposite directions from the energy center. For example, for strike-slip faults where the location and orientation of the fault and the direction of paleofault movement is known, the "+" and "-" could correspond to directions of forward and reverse rupture directivity in the fault-parallel direction. In this case, a corresponding plot would be made for paleoliquefaction sites located in the fault-normal directions, with "+" and "-" representing opposite fault-normal directions. For case studies where the location and orientation of the fault and direction of paleofault movement are unknown, which is likely the case for most CEUS sites, the "+" and "-" could correspond to general opposing directions aligned with pertinent geologic features

(e.g., "+" and "-" could correspond to opposing directions parallel or perpendicular to known faults in the region).

As stated above, the various styles of filled symbols in Figure 3 represent sites that liquefied, while the open symbols represent sites of no liquefaction. Assuming all the liquefaction features were induced by the same causative paleoearthquake and the provisional location of the energy center is valid, a boundary giving a reasonable separation between the liquefaction and no liquefaction data should be apparent. The severity of liquefaction experienced at the sites and aging effects will influence where the data points plot with respect to this boundary. In general, sites that exhibit severe liquefaction effects that were manifested either as hydraulic fracturing or surface oscillations would tend to plot farther below the boundary than would sites that experienced marginal liquefaction. The reason for this is that a $FS_{liq} = 1$ was assumed in the back-analyses, while in fact the actual FS_{liq} was likely much less than one. On the contrary, sites that exhibit severe effects from lateral spreading will not necessarily tend to plot farther below the boundary than would sites that only experienced marginal lateral spreading. This is because even sites having a relatively high FS_{liq} (i.e. ~1) can experience severe lateral spreading in meizoseismal zones. By analogy, for sites that did not liquefy, sites having higher values of $N_{1,60cs}$ would generally tend to plot farther above the boundary than sites having lower values of $N_{1,60cs}$.

Three different symbols are used in Figure 3 to represent sites of severe, moderate, and marginal liquefaction effects. Marginal effects refer to those that are barely discernible (such as cracking of a fine-grained cap at the ground surface), or to effects that are weakly developed (such as the presence of very scattered small sand blows), consistent with the usage of Olson et al. (2004). Moderate refers to effects such as the development of lateral spreading with dikes on the order of 15 cm in width, or the development of scattered, large sand blows. Severe refers to sites having dikes on the order of 0.5 m in width or larger or having numerous large sand blows, or else it can refer to a locale where liquefaction effects have been so severe as to cause severe warping or distortion of the ground surface or of thick fine-grained strata at depth. Solid symbols are used for

marginal liquefaction sites. These sites are more likely to represent a threshold for liquefaction and should be weighted more heavily in the interpretation of magnitude.

Aging effects also will influence the position of data points in Figure 3. As outlined in Figure 10 of Olson et al. (2004), aging effects influence whether the back-calculated a_{max} values for liquefied sites are likely less than, greater than, or equal to the actual a_{max} experienced at the sites. In Figure 3, upward and downward pointing arrows are attached to the respective data points to indicate whether the back-calculated values for a_{max} are likely on the low and high sides, respectively, as determined from Figure 10 in Olson et al. (2004).

The trends noted above regarding the relative location of the data points in Figure 3 were stated without consideration of the quality of the data used in the back-calculations, which may vary significantly from site to site. To qualitatively rank the geologic data quality, we introduce the "field data quality" (FDQ) index which may be high, intermediate, or low. FDQ relates to the quality of and confidence in geologic interpretations at an individual study site, incorporating the following factors: (1) variability of geologic setting (e.g., braid-bar, point bar, etc.); (2) depth of potential source beds at the time of the earthquake; (3) depth of the groundwater table at the time of the earthquake; (4) mechanism of ground failure (e.g., hydraulic fracturing, lateral spreading, surface oscillation); and (5) severity of liquefaction, as it relates to making proper field interpretations. In turn, the quality of and confidence in the geologic interpretations are influenced by a number of factors, including the number, spacing, and locations of in-situ borings or tests; the vertical and lateral variability of sediments at the site; the method of observation (i.e., plan view versus sectional view); and the length and quality of the bank exposure at the site. These factors are qualitatively combined to assess the overall FDQ of an individual study site. In Figure 3, different symbols are used to represent three levels of the field data quality (FDQ): high, intermediate, and low. Sites having high FDQ would generally be expected to exhibit the trends noted above regarding the relative location of the data points in Figure 3, with the trends becoming less pronounced as the FDQ decreases.

The provisional location of the energy center was determined assuming that the paleoliquefaction features were primarily induced by the same paleoearthquake. The uniqueness of the boundary giving a reasonable separation between the data (particularly those having a high FDQ) for sites that did and did not liquefy when plotted as shown in Figure 3 allows this assumption to be checked, and also allows the magnitude of the paleoearthquake to be determined. As illustrated in Figure 4, three scenarios are shown. Scenario A represents the case where all the paleoliquefaction features resulted from a single, large earthquake located at the provisional location of the energy center. For such a scenario, it is likely that the back-calculated data points for the sites will be symmetrical about a vertical line drawn through the energy center (i.e., zero site-to-source distance). Using a regionally applicable a_{max} attenuation relation, and properly accounting for site amplification effects, the probable magnitude of the paleoearthquake corresponds to the contour of constant M that reasonably defines the upper limit of the data points for the sites that liquefied, as shown in the figure. Data points representing sites that did not liquefy generally would lie above the contour of constant M.

An alternative to Scenario A (i.e., the single, large earthquake scenario) is where the liquefaction features were generated by a large earthquake and other smaller earthquakes that occurred in the same general locale and time frame as the large earthquake. For this case the difference in the ages of the features generated by the large and smaller earthquakes would not be discernable using radiocarbon or other geologic or archeologic dating techniques. This case is illustrated as Scenario B in Figure 4, with the resulting plot of the data being very similar to that for Scenario A. The impact of Scenario B on the overall interpretation and the seismic hazard (compared to Scenario A) is likely to be small because a large earthquake likely would dominate the regional pattern of liquefaction features (and thus how the data plots in Figure 4).

The final scenario (Scenario C) illustrated in Figure 4 represents where the liquefaction features were induced by several small earthquakes occurring in the same general region at about the same time. As with Scenario B, the difference in the ages of the features

generated by the various earthquakes would not be discernable by means of dating techniques used by the geologic community. In contrast to Scenarios A and B, it is unlikely that a contour of constant M can be drawn using a regional attenuation relation that reasonably bounds the liquefaction data. Depending on the spatial distribution of the earthquakes, it is doubtful that the upper bound of the data points will be symmetrical about a vertical line drawn through the provisional location of the energy center. Also, the maximum a_{max} (i.e., the a_{max} at the hypothesized energy center) for Scenario C will be much lower than for Scenarios A and B (i.e., $H_1 > H_2$) in Figure 4.

The estimated magnitude from the regional assessment should be compared with the magnitude estimated using the magnitude bound method (Step 4). Although the relative reliability of the two estimates depends on the FDQ indices of the data used in the respective analyses, in general, it would be expected that the magnitude estimated following Steps 5 and 6 would yield a more credible result because site/profile specific information for multiple sites is explicitly taken into account in determining M.

III. CASE STUDY – ASSESSMENT OF THE CHANGE IN LIQUEFACTION SUSCEPTIBILITY AT PALEOLIQUEFACTION SITE

Geotechnical field investigations used to assess a paleoearthquake are inherently performed long after the earthquake, and pre-earthquake geotechnical field data are not available. As a result the influence of post-liquefaction changes (e.g., aging and density) in soil/state properties is uncertain, and this uncertainty can be significant. Olson et al. (2004) consequently recommended criteria for proper site selection and data interpretations as a means to reduce this uncertainty. In the following a case study involving a site near Memphis, Tennessee (Figure 5), is used to illustrate the approach proposed by Olson et al. (2004). The method involves performing in-situ tests at side-by-side locations of marginal liquefaction and no liquefaction, preferably where there is a large difference between the age of the liquefaction features and the age of the source bed, so that the effects of aging can be more readily discerned.

Background Information

Memphis, Tennessee, is an area of high seismic risk due to its close proximity to the New Madrid Seismic Zone (NMSZ; Figure 1), which was the source region of the very large earthquakes of 1811-12 (M~7.6 or 7.7±0.5; Wheeler and Perkins, 2000; Atkinson et al., 2000). Although several paleoseismic studies (other than paleoliquefaction) have been performed in the NMSZ during the last 10 years to estimate the strength of shaking of the 1811-12 earthquakes, the confidence in the results from these studies is not high. This lack of confidence has served as the impetus for using liquefaction-induced features to assess the strength of shaking (i.e., paleoliquefaction back-analyses).

Broughton et al. (2001) first discovered very young liquefaction features in the Memphis area, which were likely induced by the 1811-12 New Madrid earthquakes. The features were found only at scattered sites and were typically small, especially in the eastern Memphis area. None of these sites were accessible to a drill rig for CPT testing, prompting Obermeier to undertake a search for other sites farther east, along the Wolf River. The objective was to find a site having marginal liquefaction features that could be used to estimate the paleoseismic strength of shaking.

Field Setting

The general location of the 7-km long portion of the Wolf River searched by Obermeier is shown in Figure 5. This section lies just upstream of a portion of the river that was channelized (mainly straightened) about 20 years ago by the U.S. Army Corps of Engineers. Channelization in the search area has resulted in the river down-cutting about 3 m into the surficial deposits. The down-cutting extends downward through the fine-grained cap and well into a potentially liquefiable sand deposit. The river is also severely cutting laterally, resulting in a nearly continuous clean bank exposure many kilometers in length. Consequently, even marginal liquefaction effects can be observed readily.

The potentially liquefiable source bed consists of clean, medium- to fine-grained quartz sand that was deposited in a braided stream environment. Overlying the sand is a clayey silt deposit that typically ranges in thickness from 1.7 to 3 m (and rarely up to 5 m in

thickness). Due to the almost complete lack of weathering, the uppermost 0.5 to 0.6 m of clayey silt likely post-dates 1812. In general, the base of the fine-grained cap is sharply underlain by clean quartz sand. Occasionally there is a transition zone of sand intercalated with silt lenses.

Obermeier discovered very small dikes and sills in one relatively small stretch of the riverbank in 2001. Using the same method that Pond and Martin (1996) employed in the Wabash Valley, the depth of the water table at the time of the causative earthquake was estimated to be approximately 3 m (Obermeier et al., 2000). This estimate is based upon measuring liquefaction resistance with depth, in conjunction with widespread field observations of fluidization effects in potential source beds of sand, as discussed in Obermeier et al. (2004).

Observed Liquefaction Effects and In-Situ Testing

The dikes found by Obermeier were manifested as narrow (less than 1 to 2 cm in width), sand-filled tabular intrusions that cut up into the fine-grained cap. All the dikes pinched together in the overlying cap where it was impossible to use radiocarbon (or any other absolute) dating techniques to establish the age of the features. [Note: Exact dating of dikes typically requires conditions where the liquefied material vented to the ground surface having organics, or requires the dikes to cross-cut a relevant buried organic bearing stratum. At the Memphis sites, the pinching together of the dikes in an oxidized zone consequently precluded the use of dating techniques that utilize organics.] Sills manifested as narrow (less than 2 to 3 cm in thickness) sand intrusions running along the base of the fine-grained cap were also present at some locales of dikes. The liquefaction-induced features were scattered along an exposure several hundred meters in length. Because the features were virtually unweathered and very loose, they are clearly quite young. Also, based on the degree of pedological development and oxidization in the clayey silt deposits hosting the liquefaction-induced features, the features were obviously significantly younger than both the host and source deposits. It is estimated that the liquefaction features are hundreds of years in age, while the host deposits and source sands are likely of mid-Holocene age or older.

Cone penetration tests (CPT) were performed at seven locations along the top of the riverbank and extended to a depth of 20 m or more. The testing was performed under the direction of Dr. Paul Mayne and Mr. Billy Camp (Mayne and Camp, 2000). The soundings were set back a maximum of 6 to 9 m from the top of the riverbank, which was as close to the top of the near-vertical bank exposure as was safely possible to perform the testing. Soundings were performed at side-by-side locations of marginal and no liquefaction features.

Results and Interpretations

A plan view of the CPT sounding locations, relative to the bank exposure, is shown in Figure 6, with the sounding logs presented in Figure 7. These figures show that the sediments are quite uniform laterally, at least in terms of soil classification and strata thickness, making the site very suitable for assessing whether aging effects are significant. In Figure 7 the hatched zones designate the critical depth to liquefaction for each sounding, irrespective of whether liquefaction was induced. Small liquefaction features were observed at Wolf-5 and Wolf-6, at the respective critical depths. Additionally, fluidization effects were observed at Wolf-7 in the depth range 4 to 5 m, which is consistent with liquefaction having occurred in the depth range of 5 to 6 m.

The hatched zones shown in each sounding also indicate the authors' interpretation of the representative CPT tip resistances for the respective critical depths for liquefaction, where the representative CPT tip resistances were taken as the average minimum tip resistance over the critical depth range. The tip resistances were corrected for unequal end area effects, but were not corrected for thin layer effects (e.g., Lunne et al., 1997). Because the ground surface at the site is level and the loosest sandy soils were located over a narrow range of depths (see Figure 7), overburden-normalized CPT tip resistances (q_{T1}) show trends similar to the values of q_T. As may be observed from the soundings, only small differences in CPT tip resistance of the loosest sands typically occur from one sounding to another, but the differences are clearly distinguishable and relatable to the

occurrence or non-occurrence of liquefaction. The following observations and interpretations are made, following the logic outlined in Figure 10a of Olson et al. (2004).

- The minimum value of q_{T1} at the location of marginal liquefaction effects [i.e., q_{T1}(min, marg liq)] is only slightly less than the minimum q_{T1} values at adjacent locations of no liquefaction [i.e., q_{T1}(min, no liq)].

- The higher values of q_{T1}(min) at the locations of no liquefaction increase incrementally with lateral distance from the location of marginal liquefaction (i.e., Wolf-5 and -6), with the exception of Wolf-4. The authors hypothesize that although Wolf-4 exhibited a slightly lower q_{T1}(min) value than Wolf-6, the limited thickness of the loose layer in Wolf-4 would be unable to produce a sufficient volume of water to form even marginal liquefaction features. In contrast, at Wolf-6 there are numerous thin layers that have nearly the same low values of q_{T1}. These multiple layers produced a sufficient volume of water to develop small liquefaction features.

- There is a large difference between the ages of the liquefaction features (likely about 200 years old) and the source deposit that liquefied (likely at least several thousands of years, as noted above).

Based on the above observations, any decrease in post-earthquake penetration resistance likely recovered quickly to a value close to its pre-earthquake value, and aging over the few hundreds of years since the formation of the features (~200 years, if caused by the 1811-12 New Madrid earthquakes) likely has been relatively minor. Consequently, the authors conclude that the current value of q_{T1} is representative of the corresponding value had it been measured shortly after the earthquake (on the order of months). Accordingly, the current value of q_{T1} is appropriate for assessing the a_{max} experienced at the site. Furthermore, the adjacent CPT soundings at locations of no liquefaction can be used to bracket the range of potential a_{max} experienced at the site.

Using the above observations as a guide, the authors' back-calculations indicate that the value of a_{max} estimated from individual CPT soundings varies by only 16%, and the value of M varies by only 0.2 units. These values consider all of the soundings performed at the site; the back-calculated values from the closest "marginal liquefaction" and "no liquefaction" soundings are nearly identical. [Note: The purpose of the above example was to illustrate the assessment of the significance of aging at a site of marginal liquefaction. The authors made no attempt to assess rigorously the strength of shaking of the causative earthquake, which would require an extensive field investigation and an integrated regional assessment of the results of back-calculations from multiple paleoliquefaction features.]

Discussion of Factors Affecting Interpretation

The Wolf River site is nearly ideal to illustrate whether aging effects or any other effects related to the occurrence of liquefaction are significance at a site of marginal liquefaction. Because it was determined that these effects were minimal at this site, representative q_{T1} values were readily determined for use in the back-analysis. Additionally, this site clearly illustrates the influence of minor changes in liquefaction resistance, as reflected in q_T values, and the influence of cumulative thickness of the liquefiable sediments on the manifestation of liquefaction features.

The correspondence of the formation of liquefaction features and CPT tip resistances at critical depths, such as that at the Wolf River site, may not be readily found during the course of all paleoliquefaction investigations, making proper interpretation of field data more difficult. Additionally, a study such as was done at the Wolf River site must carefully evaluate geotechnical factors that can influence interpretations. For example, the presence of a dense sand layer immediately overlying a liquefied layer could dilate in undrained shear during earthquake shaking and "absorb" excess water expelled by an underlying liquefied source bed. This could preclude the formation of more extensive and/or severe liquefaction features or prevent the formation of any liquefaction features, even though liquefaction did occur locally. As may be observed from the Wolf River soundings, there is a denser sand layer immediately above the critical depth to

liquefaction. However, based on the excellent association between liquefaction effects and the q_T values at multiple test locations, the authors do not believe that this dense layer had much influence on the manifestation of the liquefaction features.

Another factor that can add uncertainty to field interpretations is capillarity. The estimation of the depth of the water table at the time of the paleoearthquake can be complicated by capillarity, particularly in very fine-grained sand deposits. However, the significance of capillarity can be determined by comparing penetration data taken at various times when the depth of the water table differs. Another approach is illustrated for the Wolf River case study. There, capillarity must have had no more than a minor role in interpretations on the basis of both the regional observations of the location of source beds for liquefied sands (Obermeier et al., 2000), and on the basis of the excellent correspondence at the Wolf River site between liquefaction effects and q_T values.

In summary, in order to eliminate many issues that are commonly encountered in various field settings, multiple CPT soundings (or other in-situ tests) should be performed at adjacent locales where liquefaction and no liquefaction features are observed. Also, wherever possible, the tests should be done in conjunction with detailed sectional view observations of liquefaction effects at various depths in various strata, as was done for the Wolf River site.

IV. CASE STUDY – REGIONAL ANALYSIS OF THE VINCENNES PALEOEARTHQUAKE

The largest earthquake in the 200-year historic record of the Wabash Valley of Indiana-Illinois (Figure 1) is M 5.8. However, it is clear from the sizes and abundance of paleoliquefaction features discovered in the region about 10 years ago that much larger Holocene earthquakes had occurred (Obermeier et al., 1993). What is not known about the paleoliquefaction features is what they represent in terms of the number of earthquakes, their ages, source regions, and magnitudes. The case study presented below illustrates how these questions can be answered, with particular emphasis on the largest

paleoearthquake that occurred in the Wabash Valley, the "Vincennes Earthquake." The analysis is twofold. First, the regional size distribution of the liquefaction features is determined to estimate the tectonic source region (i.e., the energy center) of the earthquake. Next, the regional pattern of shaking intensity that caused the features is determined using geotechnical/seismological procedures to evaluate the magnitude of the earthquake.

Background Information

The energy center for the Vincennes Earthquake is estimated to have been located near the town of Vincennes, Indiana, with the event occurring around 6,100 yr BP +/- 200 yrs (i.e., approximately 5000 calendar years ago) (Munson and Munson, 1996). As shown in Figure 8, Vincennes, Indiana, is on the border of southern Indiana and Illinois, in the heart of the lower Wabash Valley. Also shown in Figure 8 are the locations of liquefaction features that are attributed to the Vincennes event (Munson and Munson, 1996; Hajic and Wiant, 1997; and Obermeier, 1998). The following sections provide information from previous studies of the Vincennes Earthquake, upon which the analyses and interpretations presented herein are built.

Geological and engineering geological studies. The locations of prehistoric liquefaction features previously attributed to the Vincennes Earthquake (and provisionally attributed to the Vincennes Earthquake for the initial phase of our study) are shown in Figure 8. These sites were found by searching banks of streams and sand pits (i.e., sectional view observations). The searched bank heights typically ranged from 3 to 6 m, with the strata that liquefied being visible at many locales when the rivers were low. Despite the venting of sand and gravel onto the ground surface at many sites, the depositional/oxidizing environments of the hosting sediments prevented use of radiocarbon dating for precise determination of age at more than a few of the paleoliquefaction features (Munson and Munson, 1996; Hajic and Wiant, 1997). Consequently, the regional size distribution of the liquefaction features played a significant role in the determination of whether the features likely resulted from a single large earthquake, or alternatively, from several regionally distributed, smaller events.

Using the regional size distribution of the liquefaction features, in conjunction with radiocarbon, archeological, stratigraphic, and pedological data, the energy center for the Vincennes event was estimated to have been near Vincennes, Indiana. Many of the data for the Indiana sites were collected and analyzed by Munson and Munson (1996), with the data from Illinois sites coming from Hajic and Wiant (1997). The criteria for interpreting the seismic origin of the liquefaction features, which were almost exclusively sand-filled dikes, and for using the regional size distribution of the liquefaction features for locating the energy center of the event are given in Obermeier et al. (1993, 2001) and Obermeier (1996). An overview of the considerations made in the interpretation process follows.

Field studies show that at about 6,100 yr BP widespread liquefaction occurred at many places over a region hundreds of square kilometers in areal extent (Figure 8), with the largest (i.e., widest) concentrated in a relatively small zone near Vincennes, Indiana (Munson and Munson, 1996; Hajic and Wiant, 1997). This relatively small zone was centrally located to a wide region of dikes having approximately the same age. In the vicinity of Vincennes, the dike widths at several scattered sites exceed 0.6 m and are as wide as 2.7 m (e.g., Munson and Munson, 1996; Hajic and Wiant, 1997), whereas outside this zone the dikes are much narrower.

Traveling south of Vincennes in both Indiana and Illinois, the maximum dike widths decrease as a function of distance. The most credible interpretation of this observation is that the liquefaction features were induced by a single, large earthquake centered near Vincennes. This scenario is given further credence by the fact that very extensive field searches south of Vincennes have failed to provide evidence of other paleoearthquakes whose ages are even remotely near 6,100 yr BP. An alternative hypothesis, albeit believed by the authors to be less credible that the single large earthquake scenario, is that more than one earthquake occurred within several hundred years of 6,100 yr BP (e.g., Munson and Munson, 1996; Hajic and Wiant, 1997), creating some of the liquefaction-induced dikes near Vincennes and southward.

North-northeast of Vincennes there is an unusual abundance of dikes in the banks of the Eel River (see Figure 8), many of which are 0.15-0.5 m wide (Munson and Munson, 1996). The source sediments along Eel River typically are very thick, clean sands. This differs from the gravelly sands found in most other large stream valleys in the lower Wabash Valley region (P.J. Munson, oral comm. 2003), which are less conducive to the formation of liquefaction features than the sediments along the Eel River. Additionally, extensive man-made channelization of the lower part of the Eel River has resulted in relatively clean bank exposures, facilitating the observation of any dikes that are present.

A plausible interpretation of the abundant dikes observed along the Eel River is that these features were induced by a large paleoearthquake, other than the Vincennes event, which was centered near the Eel River about 100 km to the north-northeast of town of Vincennes. Given the respective estimated ages of the liquefaction features found south of Vincennes and the features along the Eel River, this second earthquake would have to have occurred within a few hundred years of the Vincennes event. However, the second large paleoearthquake hypothesis is not supported by field evidence. If there had been two large paleoearthquakes, some sites along the Wabash River north of Vincennes likely would have liquefied during both, resulting in the vertical stacking of vented sand and gravel deposits. No evidence of such stacking has been found, despite observations of venting onto many now-buried pedological horizons that are well exposed in the riverbanks. Therefore, a single, large earthquake with an energy center at Vincennes appears to be the most credible hypothesis.

For additional overviews of the interpretations of the paleoliquefaction features in the Wabash Valley region, the reader is directed to Munson et al. (1997), Hajic and Wiant (1997), and Obermeier (1998).

Geotechnical studies. Utilizing the preferred interpretations of Munson and Munson (1996) for matching various liquefaction features with their causative paleoearthquakes, Pond and Martin (1996) evaluated the strength of shaking of the Vincennes Earthquake

for the scenario of a single, large paleoearthquake centered near Vincennes. Pond and Martin (1996) performed standard penetration tests (SPT) at numerous liquefaction sites, mainly along the Wabash River. At all sites the borings were located on the tops of the riverbanks near the liquefaction features, but set back 15 m or more from the steep banks. Three to five borings (and sometimes more) typically were drilled at each site. Where possible the borings were located along the strike of the dikes, which typically could be seen only in sectional view along the riverbanks. At some sites additional borings were performed 30 to 60 m perpendicular to strike of the dikes. Many of the sites tested were far from the meizoseismal zone, in which there were only one or two small dikes scattered in a long exposure. However, a few of the sites tested experienced severe liquefaction, particularly those located in the meizoseismal zone, as evidenced by wide lateral spreads and warped ground.

Pond and Martin (1996) analyzed the field data to determine the strength of shaking of the paleoearthquake, generally selecting the representative penetration resistance for the liquefied stratum as the largest of the minimum SPT $N_{1,60cs}$ values measured in boring(s) near dikes at a site. Stated alternatively, Pond and Martin determined the minimum SPT $N_{1,60cs}$ value in the liquefied stratum for each boring located near a dike at a site. From these minimum values, they selected the largest as the representative penetration resistance for the liquefied layer. This $N_{1,60cs}$ value was then used in conjunction with the cyclic stress liquefaction evaluation procedure (e.g., Seed and Idriss, 1971; Youd et al., 2001) to back-calculate the earthquake magnitude. The interpretation of the SPT boring logs and the procedure for back-calculating the magnitude of the paleoearthquake presented herein differ somewhat from those used by Pond and Martin. For example, in selecting the representative penetration resistance (i.e., SPT $N_{1,60cs}$ value) of a liquefied stratum at a site, the authors explicitly consider the mechanism of ground failure and the severity of liquefaction (see Olson et al., 2004). Also, the authors used both the cyclic stress liquefaction evaluation procedure and the Green-Mitchell energy-based procedure to back-calculate the strength of the earthquake shaking. In the back-analyses, we used four recently proposed, regionally applicable, peak ground acceleration attenuation

relations. These attenuation relations were not available at the time Pond and Martin performed their study.

In the following sections additional information is given regarding: (1) the authors' approach to selecting representative penetration resistances; (2) the results of the back-analyses; and (3) the interpretations of the results and a discussion of factors affecting the interpretations.

Selection of Representative Penetration Resistance

Olson et al. (2004) recommend that SPT borings be drilled primarily at sites that experienced marginal liquefaction, preferably with borings drilled at side-by-side locations where small liquefaction-induced features are present and where no liquefaction-induced features are present. The recommended procedure serves the dual function of allowing the upper and lower limits of ground shaking to be assessed, as well as enabling the qualitative assessment of the effect of aging and density change on the penetration resistance. For convenience, the guidelines recommended by Olson et al. (2004) for various ground-failure mechanisms are repeated in Table 1 of this paper. Unfortunately, no data sets have ever been collected for the Vincennes Earthquake following the guidelines recommended by Olson et al. (2004). Therefore, the authors interpreted and analyzed the available SPT data presented in Pond and Martin (1996) using the guidelines in Table 1 to the extent possible. Pond and Martin (1996) drilled borings at many sites where liquefaction appears to have ranged from marginal to relatively severe. Fortunately, many of these sites are hundreds of kilometers in length and have many dikes, with the source beds for some dikes of marginal liquefaction effects being identifiable.

As may be observed from Table 1, the ground failure mechanism plays an important role in the selection of the representative $N_{1,60cs}$ values for the liquefiable stratum. Interpretations of ground-failure mechanisms of the liquefaction features associated with the Vincennes Earthquake were made largely by Obermeier, using first-hand field observations in conjunction with information from published reports. For the sites

analyzed in this study, ground failure typically was caused by either lateral spreading or hydraulic fracturing. At some sites only one mechanism was operative, whereas at others at least two mechanisms were operative.

The geologic setting often significantly influences the mode in which liquefaction is manifested. For example, hydraulic fracturing may occur as a result of liquefaction of a localized body of susceptible sand. However, major lateral spreading involving movement of a horizontal slab hundreds of feet wide commonly requires laterally extensive liquefaction, which is enhanced by continuous, laterally extensive sandy strata. Additionally, a highly variable depositional setting can introduce uncertainty in assessing which sand strata actually liquefied. Braid-bar deposits, which were commonplace at the sites analyzed, are especially prone to this problem. Fortuitously for this study, the field data from the braid-bar deposit sites generally were easily interpreted as a result of the sectional view observations made at the sites. Contrary to the discontinuous braid-bar deposits, some of the sites investigated along the Wabash River were extensive point-bar deposits that were relatively uniform for large distances (often hundreds of meters laterally).

The following discussion uses two sites to illustrate the role of ground-failure mechanism on the authors' selection of the representative penetration resistances. Brief descriptions of the liquefaction features and a summary of the borings and interpretations for the twelve sites analyzed as part of this study (Figure 8) are provided in Appendix II.

Site PB. Site PB is a more than 4 km long bank exposure that is at least 5 m high everywhere. Figure 9 shows a vertical section of the site profile, the Unified Soil classification of the soil strata, the boring locations and measured SPT N-values, and the elevation of the ground surface and groundwater table at the time of the earthquake (~6,100 yr BP). The bank at the site is cleanly scoured by annual flooding, which has presented numerous occasions through the years for examination of liquefaction effects. Two dikes that resulted from lateral spreading were observed at the site, one 0.15 m wide and the other 0.7 m wide. Based on the ages of deposits at the site and field geologic

interpretations, the 0.7 m wide dike is believed to have formed by movement of sediment to the south. Aerial photos show that all granular deposits at the site were laid down as point-bar deposits, while the river was operating in a meandering mode (Obermeier et al., 1993). The plan-view pattern of scroll bars makes it clear that ages of these deposits increase northward, and that a lateral spread could have developed only by movement of a block of sediment, extending from the 0.7 m wide dike and going southward at least 75 m. Additional background information about this site is given in Appendix II.

Figure 10 shows a plan view of the boring locations. As may be observed from this figure, boring B2 is located near the 0.7 m wide dike and boring B1 near the 0.15 m wide dike. A considerable quantity of gravel was vented to the ground surface at the location of the 0.7 m wide dike. Field observations by Obermeier and other investigators, which were made in various years after flooding had scoured clean the banks at the site, revealed that none of the strata in the bank exposures had liquefied. Therefore, the only plausible source stratum is buried and is in the zone on Figure 9 below about 5.2 m from the current ground surface. For a site of severe liquefaction resulting from lateral spreading, the representative penetration resistance is the highest minimum value that is common among borings located along the length of the lateral spread (see Table 1). From the measured SPT data shown in Figure 9, normalized and adjusted per the procedures given Youd et al. (2001), the authors selected a representative SPT blow count of $N_{1,60cs}$ = 21.5 blows per foot (bpf) (N = 20 bpf), at a depth of 6.1 m from the ground surface at the time of the earthquake (which corresponds to a depth of 8.5 m from the current ground surface).

Site MA. At site MA, numerous small dikes are scattered along an approximately 500-m long bank exposure. Figure 11 provides a vertical section of the profile and also shows the locations of numerous small dikes that vented onto the ground surface. Figure 12 shows a plan view of the site and the location of all the dikes that vented to the surface. All the dikes were relatively narrow in width, with the widest being 0.1 m. When the river level is low, the riverbanks at the site are cleanly exposed to a depth of about 7 m, exposing the stratum that likely liquefied. Consequently, it was observed that all

fluidization effects were restricted to the immediate vicinity of the base of the individual dikes, which precludes lateral spreading as the ground-failure mechanism. The only realistic candidates are hydraulic fracturing and surface oscillations, but the limited lateral extent of fluidization effects strongly suggests that the predominant mechanism was hydraulic fracturing. Additional background information about this site is given in Appendix II.

For a site of liquefaction effects from hydraulic fracturing or surface oscillations such as site MA, the representative penetration resistance is the highest minimum value that is common among multiple boring performed in the proximity of individual liquefaction features (see Table 1). As shown in Figure 11, the highest minimum SPT $N_{1,60cs}$ values in the liquefied stratum at three of the borings (B2, B3, and B5) range from 12.6 to 19.1 bpf (N ranging from 9 to 14 bpf), with lower values at borings B1 and B4. The authors selected a representative SPT blow count of $N_{1,60cs}$ = 13.2 bpf (N = 9.5 bpf), at a depth of 2.3 m below the ground surface at the time of the earthquake (which corresponds to a depth of 3.2 m below the current ground surface).

Back-Calculation Results

The authors analyzed twelve sites exhibiting liquefaction features that were provisionally attributed to the Vincennes Earthquake, to include sites PB and MA discussed above. Table 2 lists the operative failure mechanism at each site, as well as the severity of liquefaction. These assessments were made based on first-hand field interpretations of the sites by Obermeier and by published site descriptions (e.g., Pond and Martin, 1996; Munson and Munson, 1996). Using this information in conjunction with boring logs for the sites and the guidelines presented in Table 1, the critical depth to liquefaction and corresponding representative penetration resistance values were determined for each site. These values are included in Table 2. Note that for two of the sites (YO and PL), two possible critical depths were identified, reflecting unknowns for the sites.

Following Step 5 of the proposed procedure, the lower bound estimates of a_{max}-M combinations requisite to induce liquefaction at each site were back-calculated using both

the stress- and energy-based liquefaction evaluation procedures (Youd et al., 2001 and Green, 2001, respectively). For the stress-based procedure, we used both the Andrus and Stokoe (1997) and Seed et al. (1983) magnitude scaling factors in separate back-calculations for each site. Also, for both the stress- and energy-based procedures, we performed separate back-calculations for each site using four regionally applicable attenuation relations: Somerville et al. (2001), Atkinson and Boore (1995), Toro et al. (1997), and Campbell (2001, 2003). These relations were used to compute the peak ground accelerations for rock site conditions, and the NEHRP (1998) site response coefficients were used to relate the rock accelerations to corresponding a_{max} values at the surface of the soil profiles (Appendix I). All the profiles analyzed were considered NEHRP Site Class D, with the exception of site PL. Due to shallow bedrock at site PL, no site adjustments were made to the bedrock acceleration values. The back-calculated a_{max}-M combinations are listed in Table 3.

Following Step 6 of the proposed procedure, we integrated the back-calculated results for the individual sites into a regional assessment of the Vincennes Earthquake, as shown in Figures 13a-d. In this set of figures, "+" and "-" distance from the energy center correspond roughly to north and south directions, as most of the sites fell along this alignment. The one exception was a thirteenth site (site HA), which is located to the east of the energy center, along the East Fork of the White River (Figure 8). Due to the large uncertainty regarding whether the features at site HA were actually induced by the Vincennes Earthquake, it was excluded from our regional assessment. The values plotted in Figure 13 were back-calculated using the stress-based procedure in conjunction with the Andrus and Stokoe (1997) magnitude scaling factors. The magnitude contours in this set of plots were computed using the attenuation relations mentioned above, with the NEHRP site amplification factors applied for Site Class D (i.e., at all distances, the accelerations from the attenuation relations were multiplied by the site response coefficients for NEHRP Site Class D conditions (Appendix I)). For consistency between the individual site data and attenuation relationship contours in Figure 13, the a_{max} values for site PL listed in Table 3 were multiplied by 1.6 (i.e., the corresponding NEHRP site response coefficients for Site Class D and level of rock acceleration). [Recall: No site

amplification factors were used in the back-calculations for site PL due to shallow bedrock.]

The last column in Table 2 gives the field data quality (FDQ) index for each of the sites, ranging from high to low (Appendix II provides details on how the FDQ values were determined for each of the sites). Even though assigning FDQ indices requires judgment, more weight should be given to the data having higher FDQ indices in the regional assessment of M. Also, comparing Figure 13 to Figure 3, it may be noticed that Figure 13 does not have any "no liquefaction" data and no arrows are used to indicate the influence of aging effects at the sites. This is because Pond and Martin (1996) did not perform in-situ testing at sites that did not exhibit liquefaction features and because the impact of aging could not be discerned from the field data reported by Pond and Martin (1996).

Based on the set of plots shown in Figure 13, and similar plots not presented in this paper for the stress-based procedure using Seed et al. (1983) magnitude scaling factors and the energy-based procedure, the authors estimate that the magnitude of the Vincennes Earthquake was approximately M 7.5. (For comparison, Pond and Martin (1996) estimated a magnitude of 7.7 for this event.) A more detailed discussion of the back-calculations and the assessed magnitude of the Vincennes Earthquake is given in the next section.

Discussion of Back-Calculations for Vincennes Earthquake

Our estimate of M~7.5 using Figure 13 is based largely on the orderly progression of a_{max}-M values on the M 7.5 contour for the sites south of the energy center located at Vincennes (i.e., sites VW, PB, and MA). All three of these sites have high FDQ indices. Additionally, four sites north of Vincennes also have high FDQ indices: SM, RF, PA, and WO, yielding back-calculated M values of 6.2, 7.2, 7.2, and 7.6, respectively, for the cyclic stress procedure (used in conjunction with the Andrus and Stokoe (1997) MSF and the Somerville et al. (2001) attenuation relation – as shown in Figure 13a). The relatively low magnitude back-calculated for site SM (i.e., M 6.2) is attributed to the fact that the site experienced severe hydraulic fracturing, and as such, would tend to yield a relatively

low back-calculated M. In contrast, site RF experienced severe lateral spreading, and as such, may or may not yield a relatively low back-calculated M. Accordingly, the sites north of the energy center having high FDQ indices add credence to the M 7.5 estimate, and all of the sites with high FDQ indices indicate that the location of the energy center of the paleoearthquake is consistent with the provisional energy center used in the back-calculations.

The remaining sites north of the energy center (i.e., YO, TH, BG, NP, and PL) have intermediate and low FDQ indices and yield a range of back-calculated M values. It is unclear from Figure 13 whether the scatter in the data for these sites is attributable to low FDQ indices or whether the features were induced by an earthquake other than the Vincennes event having an energy center 75-100 km northeast of Vincennes, as suggested by Munson and Munson (1996). However, the uncertainty in the causative earthquake for these five sites does not diminish the interpretation of data from sites having high FDQ indices.

Influence of various attenuation models. We used four regionally applicable attenuation relations in the back-calculations, namely Somerville et al. (2001), Atkinson and Boore (1995), Toro et al. (1997), and Campbell (2001, 2003). All of these relations are based on theoretical models in some fashion or another and have not been directly validated using strong motion observational data because of the lack of such data in the CEUS. All of these relations express a_{max} as a function of earthquake magnitude (M; specifically moment magnitude, M_w) and site-to-source distance (R). However, the relations use differing definitions for site-to-source distance and were developed for use over differing M and R ranges. Also, the a_{max} values computed using the attenuation relations correspond to different combinations of the peak accelerations of the two horizontal components of motion and for different site conditions. Table 4 lists the attenuation relations and pertinent model details. Additionally, Figure 14 shows plots of the attenuation relations (a_{max} as a function of site-to-source distance) for a M 7.5 earthquake. As illustrated in Table 3 and Figure 13, the magnitudes back-calculated using the different attenuation relations are in good agreement. If such were not the case, a

logic tree could be used to combine the results, such as is done in combining the results from probabilistic seismic hazard analyses performed using different attenuation relations, etc. (e.g., Kulkarni et al., 1984).

Table 4 indicates that none of the attenuation relations define site-to-source distance in terms of the horizontal distance to energy center (r_{ec}), which is the only measure that can be determined from most paleoliquefaction field investigations (Obermeier et al., 2004). For small magnitude events (M<5.5), the difference between the various site-to-source distances is likely negligible (e.g., Ambraseys 1988; Youd, 1991). However for large magnitude events, the following relationships would be expected between the r_{ec} and the other site-to-source distances: $r_{ec} \geq r_{jb}$; $r_{ec} \geq r_{rup}$; and $r_{hypo} \leq r_{ec\_hypo} \leq r_{hypo}$, where r_{ec_hypo} is the hypocentral depth computed assuming that the horizontal distance to the energy center is equal to the epicentral distance. In computing r_{ec_hypo}, Pond and Martin (1996) assumed a focal depth of 10 km for the Vincennes Earthquake, which corresponds to the approximate maximum depth for CEUS earthquakes in non-rifted domains (Somerville et al., 2001).

Based on expected relationships between the r_{ec} and the other site-to-source distances noted above, the magnitude of the Vincennes Earthquake is overestimated using Somerville et al. (2001), Campbell (2001, 2003), and Toro et al. (1997), with the assumption $r_{ec} = r_{jb} = r_{rup}$ (i.e., the site-to-source distances used in the attenuation relation in the back-calculations are larger than or equal to actual site-to-source distances). Correspondingly, the magnitude may be under- or over-estimated using Atkinson and Boore (1995), with the assumption $r_{ec\_hypo} = r_{hypo}$ (i.e., the site-to-source distances used in the attenuation relation in the back-calculations are either less than, greater than, or equal to actual site-to-source distances). However, the relatively close agreement of the magnitudes back-calculated using the different attenuation relations (Table 3 and Figure 13) leads the authors to believe that the amount of over- and under-estimations due to the inconsistencies in the measure of site-to-source distance is relatively small for this case study.

Influence of bedrock motion amplification. The four attenuation relations above were used to compute the peak acceleration for rock conditions (i.e., NEHRP Site Class A or B/C-boundary). However for the back-analyses, the a_{max} at the surface of the soil profiles is needed. As discussed in Appendix I, the peak acceleration for rock conditions can be multiplied by a site amplification factor to determine the corresponding a_{max} for the site condition of interest. It is preferred that site-specific site amplification factors be developed for each site from a series of numerical site response analyses of the site using representative ground motion time histories. Alternately, region-specific amplification factors can be used where available, e.g., the region-specific factors developed by Romero and Rix (2001) for the upper Mississippi embayment. [Note: The selection/synthesis of representative ground motions for large magnitude CEUS earthquakes is not a trivial undertaking, particularly as the magnitude of the event is yet unknown. Additionally, the soil profile and soil properties need to be characterized down to bedrock, with the required soil properties depending on the computer code used to perform the site response analyses. A detailed discussion of the issues involved with selection of ground motions and the performance of site response analyses is beyond the scope of this paper.]

For the paleoliquefaction sites analyzed in this case study, the NEHRP site amplification factors for Site Class D (Appendix I) were used in conjunction with the peak acceleration attenuation relations for rock to estimate the a_{max} at the soil surface, with the exception of site PL where shallow bedrock was present. The four attenuation relations used in the analyses and adjusted using the NEHRP site amplification factors for Site Class D are shown in Figure 14b for M 7.5 event. The attenuation relations with the NEHRP site amplification factors applied were used to back-calculate the values listed in Table 3.

The use of the generic NEHRP site amplification factors in this case study is a large source of uncertainty in the back-calculated values. As discussed in Green and Cameron (2003) and Cameron and Green (2004), the amplification of motions through the soil column is dependent on both the frequency content of the motion and the dynamic response characteristics of the profile. The NEHRP site amplification factors only take

into account the dynamic response characteristics of the profile, and do not account for the frequency content of the earthquake motion. However, until site-specific amplification factors are developed for the sites in question, the NEHRP factors probably provide reasonable results for the level of shaking of interest, and certainly suffice to illustrate the concepts proposed in Olson et al. (2004) and this paper.

Influence of back-calculation technique. The back-calculations were performed using the cyclic stress and energy-based liquefaction evaluation procedures, which are summarized in Olson et al. (2004). For the cyclic stress procedure, separate analyses were performed using the magnitude scaling factors (MSF) proposed by Andrus and Stokoe (1997) and by Seed et al. (1983), with the latter being almost identical to those of the Seed and Idriss (1982) shown in Figure 1 of Olson et al. (2004). It is worth noting that in the paleoliquefaction investigation of the 1755 Cape Ann Earthquake in Massachusetts, Ellis and de Alba (1999) state: "In this study, we applied MSF values proposed by Seed et al. (1983), which we consider appropriate to East Coast events." However, no further justification is given by Ellis and de Alba as to why they consider the Seed et al. (1983) MSF more appropriate for the eastern US than the various MSF proposed by others. Research is ongoing at the University of Michigan by R. Green to develop MSF, as well as the dimensionless stress reduction factor r_d, specifically for liquefaction evaluation in the CEUS.

As may be observed from Table 3, the magnitudes that were back-calculated using the energy-based procedure are slightly higher than those computed using the cyclic stress procedure. And, for the cyclic stress procedure, the magnitudes computed using the MSF proposed by Andrus and Stokoe (1997) are slightly higher than those computed using the MSF proposed by Seed et al. (1983). Although the energy-based procedure provides an independent assessment of the earthquake magnitude, the procedure has not undergone the years of scrutiny by the profession and subsequent modifications that the cyclic stress procedure has. Consequently, the authors believe that the values back-calculated using the cyclic stress procedure are more defensible than those computed using energy-based procedure. However, for detailed analyses wherein numerical site response analyses are

performed, as was discussed above for developing site-specific site amplification factors, the energy-based procedure is able to more accurately quantify the seismic demand (i.e., the amplitude and duration of motion) imposed on the soil than the cyclic stress procedure.

The authors' assessed value of M 7.5 for the Vincennes Earthquake is based primarily on the results from the cyclic stress procedure using the Andrus and Stokoe (1997) MSF. The authors prefer the Andrus and Stokoe (1997) MSF over the MSF proposed by Seed et al. (1983) because the former relation is in closer agreement to the Youd and Idriss (1997) recommended bounds (Figure 1: Olson et al., 2004). However, as with the results from the various attenuation relations, a logic tree could be used to combine the back-calculated values using the cyclic stress procedure with the two MSF and the values computed using the energy-based procedure.

Potential aging effects. Approximately 5000 calendar years have passed since the occurrence of the Vincennes Earthquake. Thus for the back-analysis, one must assess whether the contribution to penetration resistance from aging during this time period is significant. In many field settings, chemical bonding and/or mechanical grain readjustment account for much of the effects of aging (Olson et al., 2004). In the Wabash Valley, the granular deposits typically have a very significant portion (>5%) of limestone and dolomite grains. The authors suspect that these grains are prone to being dissolved by rainwater, which is slightly acidic. As a result the carbonate granular materials at shallow depths will be dissolved to some extent by downward seeping rainwater. Likely, this would significantly reduce any chemical or even mechanical aging effects at shallow depths.

If the carbonates were precipitating in underlying granular deposits to any extent, one would expect to see a thin zone (inches to a few feet) of granular material along the base of the cap that is cemented with carbonates. Such a zone has not been observed in the Wabash Valley, although it is commonly present in glacial slackwater deposits of southern Indiana and Illinois, as well as in northern Kentucky. One explanation for the

lack of a cemented zone in the Wabash Valley is that the granular deposits along the Wabash River are very permeable sands (often gravelly sands). At many places along the Wabash River, there is considerable groundwater flow through the shallow sands in response to seasonal lowering of the river, causing the groundwater to flow toward the river. This flow flushes the carbonates out of the coarse granular deposits at relatively shallow depths, precluding development of a cemented zone. In the glacial slackwater deposits mentioned above, the granular deposits are very fine and the nearest streams are relatively shallow, thereby limiting the groundwater flow and limiting the removal of carbonates from the deposits.

From experience in doing geotechnical work in the region, some geologically young point bar sands in the Wabash Valley exhibit SPT blow counts ranging from 0 to 2 bpf at shallow depths. Several of the sites analyzed in this investigation (BG, PA, PL, SM, and others) contain very loose clean sand deposits with blow counts ranging from 2 to 4 bpf at similar depths. Consequently, the effect of aging in the very loose granular deposits analyzed is unlikely to have been more than about 2 bpf during the past 5,000 years. For medium dense and dense sands in the region, the change in blow count as a result of aging (i.e., mechanical adjustment of grains) may be less.

V. SUMMARY AND CONCLUSIONS

The greatest impediments to the widespread acceptance of back-calculated ground motion characteristics from paleoliquefaction evaluations typically originate from the uncertainty in the influence of changes in the geotechnical properties of liquefied deposits on the back-calculated results (e.g., aging and density changes), from the uncertainty in how to use field data in the back-calculations, and from the uncertainty in how to integrate the back-calculated results from individual sites into a regional assessment of paleoseismic shaking. Using two case studies, the methods outlined in Olson et al. (2004) for minimizing these uncertainties were illustrated in this paper.

The first case study illustrated how performing in-situ engineering penetration tests at side-by-side locations, one of liquefaction and the other of none, can be used to readily

discern the significance of post-liquefaction changes in the deposit due to aging, density changes, etc. A site along Wolf River, near Memphis, Tennessee, is used to illustrate our proposed method. Based on the following observations and data collected at this site, we conclude that any decrease in post-earthquake penetration resistance likely recovered quickly to a value close to its pre-earthquake value, and density changes and aging over the few hundred years since the formation of the features (~200 years) has been minor:

- The minimum values of cone penetration resistance, q_{T1}, at the locations of marginal liquefaction effects were only slightly less than the minimum q_{T1} values at adjacent locations of no liquefaction. The potential source sands at both the sites of liquefaction and no liquefaction were from the same depositional situations, and were of essentially identical ages.
- The values of q_{T1} at the locations of no liquefaction increased incrementally with lateral distance from the locations of marginal liquefaction.
- There is a large difference between the ages of the liquefaction features and the source deposit that liquefied.

In the second case study, twelve sites that are at scattered locations in the Wabash Valley and that exhibit paleoliquefaction features were analyzed. The features were first provisionally attributed to the Vincennes Earthquake, which occurred around 6,100 years BP and centered near Vincennes, Indiana. The features were used to illustrate the approach outlined in Olson et al. (2004) for selecting representative soil indices of the liquefied sediments. These indices were used in back-calculating the strength of shaking at the individual sites, the results from which were then incorporated into a regional assessment of the moment magnitude, M, of the Vincennes Earthquake. The regional assessment showed that the paleoliquefaction features at least seven of the twelve sites investigated were induced by the Vincennes Earthquake. Due to the low-to-intermediate quality of some of the field data, it is uncertain whether the paleoliquefaction features at the remaining five sites were induced by the Vincennes Earthquake, or by another earthquake centered 75-100 km northeast of Vincennes. The greatest uncertainty in the assessed M~7.5 of the Vincennes Earthquake relates to the generic site amplification

factors used in the back-analyses (i.e., the NEHRP site amplification factors). However, until site-specific amplification factors are developed for the sites, the NEHRP factors likely provide reasonable results for the level of shaking of interest, and certainly suffice to illustrate the concepts proposed in Olson et al. (2004) and this paper.

VI. ACKNOWLEDGEMENTS

The authors gratefully acknowledge the helpful discussions with Drs. Eric Pond, Cheryl Munson, and Patrick Munson during the course of this study. Additionally, the patience exhibited by Dr. Ellis Krinitzsky in waiting for the completion of this manuscript is gratefully acknowledged.

VII. REFERENCES

Abrahamson, N.A. and Shedlock, K.M. (1997). Overview, Seismological Research Letters, 68(1): 9-23.

Ambraseys, N.N. (1988). Engineering Seismology, Earthquake Engineering and Structural Dynamics, 17: 1-105.

Andrus, R.D. and Stokoe, K.H., II, (1997). Liquefaction Resistance Based on Shear Wave
Velocity. Proc. NCEER Workshop on Evaluation of Liquefaction Resistance of Soils (T.L. Youd and I.M. Idriss, eds), Technical Report NCEER-97-0022: 89-128.

Atkinson, G.M. and Boore, D.M. (1995). New Ground Motions Relations for Eastern North America, Bulletin of the Seismological Society of America, 85: 17-30.

Atkinson, G., Bakun, B., Bodin, P., Boore, D., Cramer, C., Frankel, A., Gasperini, P., Gomberg, J., Hanks, T., Herrmann, B., Hough, S., Johnston, A., Kenner, S., Langston, C., Linker, M., Mayne, P., Petersen, M., Powell, C., Prescott, W., Schweig, E., Segall, P., Stein, S., Stuart, B., Tuttle, M., and Van Arsdale, R., (2000). Reassessing New Madrid, Proc., 2000 New Madrid Source Workshop,
[http://www.ceri.memphis.edu/usgs/reassessing_nm.pdf]

Bear, G.W., Rupp, J.A., Rudman, A.J. (1997). Seismic Interpretation of the Deep Structure of the Wabash Valley Fault System, Seismological Research Letters, 68(4): 624-640.

Broughton, A.T., Van Arsdale, R.B., and Broughton, J.H. (2001). Liquefaction Susceptibility Mapping in the City of Memphis and Shelby County, Tennessee, Engineering Geology, 62(1-3): 207-222.

Cameron, W.I. and Green, R.A. (2004). Soil Nonlinearity Versus Frequency Effects, Opinion Paper, International Workshop on the Uncertainties in Nonlinear Soil Properties and their Impact on Modeling Dynamic Response, March 18-19, 2004, Richmond Field Station, Berkeley, CA, 7pp.
[http://peer.berkeley.edu/lifelines/Workshop304/pdf/o_Green.pdf]

Campbell, K.W. (2003). Prediction of Strong Ground Motion Using the Hybrid Empirical Method and Its Use in the Development of Ground-Motion (Attenuation) Relations in Eastern North America, Bulletin of the Seismological Society of America, 93(3): 1012-1033.

Campbell, K.W. (2001). Development of Semi-Empirical Attenuation Relationships for the CEUS, USGS Annual Technical Summary.
[http://erp-web.er.usgs.gov/reports/annsum/vol43/ni/G0011.pdf]

Dobry, R., Borcherdt, R.D., Crouse, C.B., Idriss, I.M., Joyner, W.B., Martin, G.R., Power, M.S., Rinne, E.E., and Seed, R.B. (2000). New Site Coefficients and Site Classification Systems Used in Recent Building Code Provisions, Earthquake Spectra, EERI, 16(1): 41-67.

Ellis, C. and de Alba, P. (1999). Acceleration distribution and epicentral location of the 1755 "Cape Ann" earthquake from case histories of ground failure, Seismological Research Letters, 70(6): 758-773.

Green, R.A. (2001). Energy-Based Evaluation and Remediation of Liquefiable Soils, Ph.D. Dissertation, Virginia Polytechnic Institute and State University, 397 p.
[http://scholar.lib.vt.edu/theses/available/etd-08132001-170900/]

Green, R.A. and Cameron, W.I. (2003). The Influence of Ground Motion Characteristics on Site Response Coefficients, Proc., 7th Pacific Conf. on Earthquake Engineering, University of Canterbury, Christchurch, New Zealand, Feb. 13-15, Paper Number 90, 8pp.

Hajic, E.R. and Wiant, M.D. (1997). Dating of prehistoric earthquake liquefaction in southeastern and central Illinois: Final Report, submitted to the US Geological Survey, November, 1997, 57 p.

Idriss, I.M. (1991). Earthquake Ground Motions at Soft Soil Sites, Proc. Second International Conference on Recent Advances in Geotechnical Earthquake Engineering and Soil Dynamics, March 11-15, 1991, St. Louis Missouri, III: 2265-2272.

Idriss, I.M. (1990). Response of Soft Soil Sites During Earthquakes, Proc. H. Bolton Seed Memorial Symposium, (J.M. Duncan, ed.), University of California, Berkeley, May 1990, 2: 273-289.

Idriss, I.M. and Sun, J.I. (1992). SHAKE91: a computer program for conducting equivalent linear seismic response analyses of horizontally layered soil deposits, University of California, Davis.

Kulkarni, R.B., Youngs, R.R., and Coppersmith, K.J. (1984). Assessment of Confidence for Results of Seismic Hazard Analysis, Proc. 8th World Conference on Earthquake Engineering, Prentice-Hall, Inc., Englewood Cliffs, NJ, 1: 263-270.

Lunne, T., Robertson, P.K., and Powell, J.J.M. (1997). Cone Penetration Testing in Geotechnical Practice, Blackie Academic & Professional, 312 p.

Mayne, P. and Camp, W. (2000).
http://www.ce.gatech.edu/~geosys/Faculty/Mayne/Research/summer2000/wolf/wolf.htm

Munson, P.J., and Munson, C.A. (1996). Paleoliquefaction evidence for recurrent strong earthquakes since 20,000 yr BP in the Wabash Valley of Indiana: Final report, submitted to the US Geological Survey, March, 1996, 137 p.

Munson, P.J., Obermeier, S.F., Munson, C.A., and Hajic, M.R. (1997). Liquefaction evidence for Holocene and latest Pleistocene seismicity in the southern halves of Indiana and Illinois - a preliminary overview, Seismological Research Letters, 68(4): 521-536.

NEHRP (1998). NEHRP Recommended Provisions for Seismic Regulations for New Buildings and Other Structures, Part 1- Provisions: FEMA 302, Part 2-Commentary FEMA 303, Federal Emergency Management Agency, Washington DC.

Obermeier, S.F. (1996). Use of liquefaction-induced features for paleoseismic analysis – An overview of how seismic liquefaction features can be distinguished from other features and how their regional distribution and properties can be used to infer the location and strength of Holocene paleo-earthquakes, Engineering Geology, Elsevier Science, 44: 1-76.

Obermeier, S.F. (1998). Liquefaction evidence for strong earthquakes of Holocene and latest Pleistocene ages in the states of Indiana and Illinois, USA, Engineering Geology, Elsevier Science, 50: 227-254.

Obermeier, S.F. (1999). Seismic Liquefaction Features: Examples from Paleoseismic Investigations in the Continental United States, US Geological Survey Open-File Report 98-488.

Obermeier, S.F., Brack, J., van Arsdale, R., and Olson, S.M. (2000). Depth of Water Table for Paleoseismic Back-calculations, GSA Abstract with Programs, Annual Meeting, Denver, 23(7): 367.

Obermeier, S.F., Martin, J.R., Frankel, A.D., Youd, T.L., Munson, P.J., Munson, C.A., and Pond, E.C. (1993). Liquefaction evidence for one or more strong Holocene earthquakes in the Wabash Valley of southern Indiana and Illinois, U.S. Geological Survey Professional Paper 1536, 27 p.

Obermeier, S.F., Pond, E.C., and Olson, S.M. with contributions by Green, R.A., Mitchell, J.K., and Stark, T.D. (2001). Paleoliquefaction studies in continental settings: geologic and geotechnical factors in interpretations and back-analysis, US Geological Survey Open-File Report 01-029. [http://pubs.usgs.gov/openfile/of01-029]

Obermeier, S.F., Olson, S.M., and Green R.A. (2004). Field Occurrences of Liquefaction-Induced Features: A Primer for Engineering Geologic Analysis of Paleoseismic Shaking, Engineering Geology, Elsevier Science, (this volume).

Olson, S.M., Green, R.A., Obermeier, S.F. (2004). Engineering Geologic and Geotechnical Analysis of Paleoseismic Shaking Using Liquefaction Effects: A Major Updating, Engineering Geology, Elsevier Science, (this volume)

Olson, S.M., Obermeier, S.F., and Stark, T.D. (2001). Interpretation of penetration resistance for back-analysis at sites of previous liquefaction, Seismological Research Letters, 72(1): 46-59.

Pond, E.C. (1996). Seismic parameters for the central United States based on paleoliquefaction evidence in the Wabash Valley: PhD thesis, Virginia Polytechnic Institute, Dept. of Civil Engineering, Blacksburg, Virginia, 583 p.

Pond, E.C. and Martin, J.R., II, (1996). Seismic parameters for the central United States based on paleoliquefaction evidence in the Wabash Valley, Final Report Submitted to the USGS, August, 583 p. (also Pond, 1996).

Romero, S.M. and Rix, G.J. (2001). Ground Motion Amplification of Soils in the Upper Mississippi Embayment, Report No. GIT-CEE/GEO-01-1, School of Civil and Environmental Engineering, Georgia Institute of Technology.

Seed, H.B. and Idriss, I.M. (1971). Simplified procedure for evaluating liquefaction potential, Journal of the Soil Mechanics and Foundations Division, ASCE, 97(SM9): 1249-1273.

Seed, H.B. and Idriss, I.M. (1982). Ground Motions and Soil Liquefaction During Earthquakes, Monograph Series, Earthquake Engineering Research Institute, Oakland, CA, 134p.

Seed, H.B., Idriss, I.M., and Arango, I. (1983). Evaluation of Liquefaction Potential Using Field Performance, Journal of Geotechnical Engineering, ASCE, 109(3): 458-482.

Somerville, P., Collins, N., Abrahamson, N., Graves, R., and Saikia, C. (2001). Ground Motion Attenuation Relations for the Central and Eastern United States, Final Report submitted to the US Geological Survey.
http://erp-web.er.usgs.gov/reports/abstract/1999/cu/99HQGR0098.pdf

Toro, G.R., Abrahamson, N.A., Schneider, J.F. (1997). Model of Strong Ground Motions from Earthquakes in Central and Eastern North America: Best Estimates and Uncertainties, Seismologic Research Letters, 68(1): 41-57.

Wheeler, R.L. and Perkins, D.M. (2000). Research, methodology, and applications of probabilistic seismic-hazard mapping of the central and eastern United States – Minutes of a workshop on June 13-14, 2000, at Saint Louis University, U.S. Geological Survey Open File Report 00-0390.

Youd, T.L. (1991). Mapping of Earthquake-Induced Liquefaction for Seismic Zonation, Proc. Fourth International Conference on Seismic Zonation, Earthquake Engineering Research Institute, 1: 111-147.

Youd, T.L., and Idriss, I.M., eds., (1997). Proceedings of the NCEER Workshop on Evaluation of Liquefaction Resistance of Soils: Technical Report NCEER-97-0022, State University of New York, 276p.

Youd, T.L., Idriss, I.M., Andrus, R.D., Arango, I., Castro, G., Christian, J.T., Dobry, R., Finn, W.D.L., Harder, L.F., Hynes, M.E., Ishihara, K., Koester, J.P., Liao, S.S.C., Marcuson, W.F., Martin, G.R., Mitchell, J.K., Moriwaki, Y., Power, M.S., Robertson, P.K., Seed, R.B. and Stokoe, K.H. (2001). Liquefaction Resistance of Soils: Summary Report from the 1996 NCEER and 1998 NCEER/NSF Workshops on Evaluation of Liquefaction Resistance of Soils, Journal of Geotechnical and Geoenvironmental Engineering, ASCE, 127(4): 297-313.

APPENDIX I. SITE AMPLIFICATION FACTORS

In order of preference, the following approaches are currently recommended for determining a_{max} at the soil surface for use in liquefaction evaluations (Youd and Idriss, 1997, Youd et al. 2001):

1) Directly apply region-specific correlations relating peak horizontal acceleration at soil surface (a_{max}), earthquake magnitude, and site-to-source distance (i.e., ground surface acceleration attenuation relationships).
2) Perform site-specific ground response analysis.
3) Multiply the peak ground acceleration on a rock outcrop by an amplification factor appropriate for the site of interest.

Although the authors agree with the assigned preferences of the recommended approaches, the authors note that even regional ground surface attenuation relations may poorly predict ground surface accelerations if the subsurface stratigraphy of the study area varies significantly (e.g., site PL in this limited study). In addition, we note that option (2) requires acceleration time histories to perform the ground response analyses. Because of the lack of recorded strong ground motions in regions where paleoliquefaction studies are likely to be heavily relied upon (such as the CEUS), this option involves inherent uncertainty. Considerable judgment and expertise is required if this option is used, and expert seismologists should be involved in the development and selection of acceleration time histories. The issue of selecting/generating representative ground motion time histories for paleoliquefaction analyses is particularly difficult as the magnitude of the paleoearthquake is yet unknown. However, the initial estimate of M determined by the magnitude-bound method (Step 4) may be used as a guide to selecting a suite of appropriate input ground motion time histories. Additionally, an iterative approach may be employed wherein the regional assessment determined M is used as a guide to selecting a refined suite of appropriate input ground motion time histories to perform site response analyses.

As a result of lack of regional ground surface acceleration attenuation relations and the uncertainties related to the use of synthetic acceleration time histories in site response analyses, option (3) may be the most appropriate method to use for regions like the CEUS. Amplification factors are typically developed from earthquake case histories and relate the peak ground accelerations recorded on rock sites to those recorded on nearby soil sites. To avoid confusion, we will refer to the peak acceleration on rock outcrops as *pga* and the peak acceleration at the soil surface as a_{max}. Frequently referenced curves quantifying amplification factors for various soil conditions are shown in Figure I-1. Although these curves provide great insight into the qualitative behavior of various soil profiles subjected to different levels of earthquake motion, the contributions of the individual factors influencing the relationship between rock outcrop and the soil surface motion are indistinguishable. As a result, the amplification curves do not allow the explicit incorporation of site-specific information in determining a_{max}, other than *pga* and a general description of the soil profile.

Variations of the curves shown in Figure I-1 are also used in practice. In place of the general descriptions of the site conditions (e.g., rock, stiff soil, deep cohesionless soils, soft to medium stiff clay and sand, and soft soil), the site classifications presented in the NEHRP provisions often are used. The NEHRP provisions classify sites into one of five categories *A-E*, based on the average shear wave velocity ($v_{s\,ave}$) of the upper 30 m (100 ft) of the subsurface profile; an additional site class *F* is used for soils requiring special consideration (NEHRP 1998; Dobry et al. 2000). The site categories are defined as:

Site Class: *A* $v_{s\,ave} > 1524$ m/sec (5000 ft/sec)

B 762 m/sec (2500 ft/sec) $< v_{s\,ave} \leq 1524$ m/sec (5000 ft/sec)

C 366 m/sec (1200 ft/sec) $< v_{s\,ave} \leq 762$ m/sec (2500 ft/sec)

D 183 m/sec (600 ft/sec) $< v_{s\,ave} \leq 366$ m/sec (1200 ft/sec)

E $v_{s\,ave} < 183$ m/sec (600 ft/sec)

F Soils requiring site-specific evaluation

where:

$$v_{s\,ave} = \frac{30}{\sum_{i=1}^{n} \frac{d_i}{v_{s,i}}}$$

$v_{s\,ave}$ = The weighted average shear wave velocity for top 30 m (100 ft) of profile in m/sec.

d_i = The thickness of any layer between 0 and 30 m (100 ft) in m.

$v_{s,i}$ = The shear wave velocity in m/sec.

In addition to shear wave velocity, the NEHRP provisions allow Site Class to be defined in terms of undrained shear strength and SPT *N*-values. Once the site is classified, the amplification factor (F_a) can be determined from Table I-1. However, the amplification factors are specified in terms of the mapped short-period spectral acceleration (S_s), which is the spectral acceleration corresponding to a period of 0.2 sec.

Finally, the soil surface a_{max} is estimated as:

$$a_{max} = F_a \cdot pga$$
$$\approx F_a \cdot \frac{S_s}{2.5}$$

where S_s / 2.5 is approximately the rock outcrop *pga* (Dobry et al. 2000). A plot of a_{max} versus S_s / 2.5 is shown in Figure I-2. As may be seen in this figure, the amplification curves are similar to those shown in Figure I-1.

APPENDIX II. VINCENNES EARTHQUAKE BACKGROUND INFORMATION

This appendix contains basic information for the paleoliquefaction sites listed in Table 2, regarding length of back exposure, abundance and severity of liquefaction effects, ground failure mechanism, number of engineering borings, depth of water table, and other information pertinent for back-analysis of strength of paleoseismic shaking. Not included in our assessment of the influence of aging on the penetration resistance, which we discuss in the body of the paper.

Also in this appendix is our evaluation of the uncertainty for the value of the depth of the water table at the time of the earthquake (ATE), which we have taken from Pond and Martin (1996) and used to back-calculate the paleoseismic strength of shaking (Table 2). Our assessment of the uncertainty is based on schematic drawings and geotechnical data in Pond and Martin (1996), information in Munson and Munson (1996), personal field observations by Obermeier, and oral communication between S.F. Obermeier and E.C. Pond (2004).

The assigned FDQ indices are based in large part on the length of exposure in vertical section that was searched for liquefaction effects, in which potentially liquefiable sediments were observed throughout the exposure. Huge amounts of potentially liquefiable sandy sediments at various elevations in the exposures were observed at many scattered locales south of Vincennes (Figure 8), and to about 25 km north of Vincennes (to site RF). North of there, however, only exceptionally were potentially liquefiable sediments exposed in sectional view. The method used by Pond and Martin (1996) to determine the water table depth ATE for some of the northern sites was to extrapolate the water table depth ATE, regionally, from sites where the depth was narrowly bracketed (E.C. Pond, 2004, oral comm. with S.F. Obermeier). Whereas this method is suspected to be correct for estimating the water table depth ATE at most sites, the application of this method to any one site introduces considerable uncertainty at that site.

Finally, the $N_{1,60cs}$ listed for the sites were computed from the measured SPT N-values using the normalization and adjustment procedures in Youd et al. (2001).

Vincennes West (VW). The majority of this site experienced severe liquefaction, resulting in extensive lateral spreading, with one dike showing more than 0.75 m (2.4 ft) of horizontal movement. The bank exposure exceeds 350 m (1148 ft), and many dikes are scattered throughout. Lateral spreading was most severe at the southwest of the exposure. However, it appears that marginal hydraulic fracturing only occurred at the northeast end of the exposure. According to Pond and Martin (1996), "The liquefiable soils range from predominantly fine to medium sands at the SW end of the exposure to gravelly sands at the NE end. The largest dikes are associated with the fine to medium sands, and the smallest with the gravelly sediments."

Six SPT borings were drilled at scattered locations along the site. Both of the two borings (B-5 and B-6) near the dikes with gravelly sands yielded minimum $N_{1,60cs}$ values of about 30 bpf (N = 27 bpf) at a depth of 6.1 m (20 ft) below the ground surface ATE, where the ground failure mode was hydraulic fracturing. Thus, an $N_{1,60cs}$ of 30.3 bpf at depth of 6.1 m (20 ft) below the current ground surface was used in the back-calculations. We note that although Table 1 recommends the use of each individual boring at sites of marginal liquefaction with observations in sectional view, we used only a single, representative value here for two reasons. These are: (1) the minimum values of penetration resistance for the two borings are very similar; and (2) there were no borings drilled at a distance from the liquefaction features, i.e., at an adjacent "no liquefaction" site.

The water table depth ATE from Pond and Martin (1996) is approximately 1.5 m (5 ft), with respect to the estimated ground surface ATE. This value might be slightly shallow, but at most by only a meter or so. Thus the ATE depth of the water table from Pond and Martin (1996) is believed to be very good.

The FDQ for this site is high because of the clear-cut association of liquefaction effects in gravelly deposits with marginal hydraulic fracturing, and because of the very credible depth of the water table ATE from Pond and Martin (1996).

Seven Mile Island (SM). Scattered small dikes are located along a 200-m (656 ft) long bank exposure at this site. The source beds of gravelly sand could be seen at many places. Despite small dike widths, the source sediments for the dikes were severely disturbed at most places. The ground-failure mechanism for the dikes could not be definitively deduced from the field observations, but was almost certainly hydraulic fracturing.

Four SPT borings were drilled at the site, with three in proximity to one another where the ground disturbance was most severe. We assigned a representative minimum $N_{1,60cs}$ of 8.9 bpf (N = 7 bpf) at a depth of 2.4 m (7.75 ft) below the ground surface ATE because that value was the lowest in two borings nearest the dikes. Regardless of the correct value, any representative minimum value that could be chosen would be relatively low (< 10 bpf) at this site.

The water table depth ATE from Pond and Martin (1996) approximately is 0.23 m (0.75 ft), with respect to the estimated ground surface ATE. This value might be slightly too shallow, but at most by a meter or so. Thus the ATE depth from Pond and Martin (1996) is believed to be very good.

The FDQ for this site is high mainly because of the very credible depth of the water table ATE from Pond and Martin (1996).

Russellville Ferry (RF). A bank exposure about 400-m (1312 ft) long shows extensive dike development, with one being 1.5 m (4.9 ft) in width and others as much as 0.4 m (1.3 ft) wide. The region of wide dikes is clearly the result of lateral spreading, which occurred throughout the southernmost 250 m (820 ft) of the bank exposure. Six borings were drilled at scattered locations along the length of the exposure.

Field observations of dike fillings by Pond and Martin (1996, p. 127-8) permitted association of liquefaction effects with coarser (i.e., gravelly) sediments whose minimum $N_{1,60cs}$ values are 24.4 bpf (N = 19 bpf) at a depth of 3.2 m (10.5 ft) below the ground surface ATE in two of the borings (B3 and B6) that were taken in the region of lateral spreading.

The water table depth ATE from Pond and Martin (1996) is approximately 1.2 m (4 ft), with respect to the estimated ground surface ATE. This value might be slightly shallow, but at most by 0.3 m (1 ft) or so; the value could also be as much as 1 m (3 ft) too deep. Thus the ATE depth from Pond and Martin is believed to be very good for back-analysis.

The FDQ for this site is high, mainly on the basis of nearly duplicate, similar borings (and penetration resistances) in the gravelly deposit, and because of the very credible water table depth ATE from Pond and Martin (1996).

Palestine (PA). Two dikes located near one another were exposed in a 750-m (2460 ft) long bank exposure. The width of one was 15 cm (5.9 in), and the other was much smaller. The dike width of 15 cm (5.9 in) almost certainly indicates lateral spreading occurred at the site and developed the dike.

Four borings were drilled along the bank exposure, with two very near the dikes. According to Pond and Martin (1996, p. 130), the source bed was a gravelly sand stratum, which for the lateral spreading mechanism of ground failure has a minimum $N_{1,60cs}$ of 13.6 bpf (N = 12 bpf) in three of the four borings, at the boring depth of about 2.4 m (8 ft) below the ground surface ATE.

The water table depth ATE by Pond and Martin (1996) is approximately 2.3 m (7.5 ft), with respect to the estimated ground surface ATE, and appears to be a very good assessment.

The FDQ for this site is high on the basis of similar, scattered borings and the very credible water table depth ATE from Pond and Martin (1996).

Peankishaw Bend (PB). Lateral spreading at boring B-2 and everywhere south in the sketch for the site (Figure 9 and 10) has caused the ground to move horizontally more than 0.7 m (2 ft). In addition, extensive venting of sand and gravel took place through the dike nearest B-2.

Site PB is located in a more than 4-km (2.5 mi) long bank exposure that is at least 5 m (16.4 ft) high along its entire length. The bank is often severely and cleanly scoured by annual flooding, which has presented numerous occasions through the years for Obermeier to examine the deposits for liquefaction effects in the zone shown in Figure 9 as "Interbedded Lean Clay and Fine Sand (CL and SP)." This zone contains moderately thick (>1 m), clean sand deposits at nearly all places along the bank, and these sands have an engineering classification of "very loose" at places and are thereby highly susceptible to liquefaction (Pond and Martin, 1996). Despite this, no liquefaction effects have ever been found that originated from that zone. In addition, the fine-grained cap in the zone of lateral spreading shows no evidence of major disturbance. Thus, it has been concluded that the water table ATE was below this zone of CL & SP, and that liquefaction and lateral spreading originated in the underlying deposit, which is designated on Figure 9 as SP, SW, and SP-SM.

Figure 9 shows that at a depth of 8.5 m (28 ft) below the current ground surface, borings B-2, B-1, and B-3 show that the zone SP, SW, and SP-SM has $N_{1,60cs}$ values ranging from 21.5 to 24.7 bpf (N ranging from 20 to 23 bpf). Therefore, we selected a representative $N_{1,60cs}$ of 21.5 bpf (N =20 bpf) at a depth of 6.1 m (20 ft) below the ground surface ATE for the back-analysis.

The water table depth ATE from Pond and Martin (1996) is approximately 2.3 m (7.5 ft), with respect to the estimated ground surface ATE, but might be as much as a meter or more too shallow.

The FDQ for this site is high on the basis that scattered borings show good agreement for the representative penetration resistance, at essentially the same depth in all borings, which were located so as to intercept strata that liquefied and spread. And, whereas the water table could have been deeper than the ATE depth from Pond and Martin (1996), slightly increasing the depth ATE does not have a major influence on back-calculated value of strength of paleoseismic shaking.

York (YO). Numerous dikes (with paleosurface venting at many) were found in a 250-m (820 ft) long exposure of bank. The dikes are parallel to one another with several having widths of 8-10 cm (3.1-3.9 in), and their sum totals more that 0.5 m (1.6 ft). Lateral spreading clearly took place to the south of the dikes, toward a stream that was a tributary of the Wabash River.

Three borings were drilled at scattered locations along the lower half of the length of the lateral spread. The likely source stratum for the lateral spread is a 2-m (6.6 ft) thick zone of fine to medium sand with a trace of silt and gravel, which is located at a depth of about 8.5 m (28 ft) below the current ground surface. The minimum $N_{1,60cs}$ in the stratum is 5.1 and 7.1 bpf (N = 5 and 7 bpf) in two of the borings, and 12.1 bpf (N = 12 bpf) in the other. However, the minimum values occur at significantly differing depths, and so a much higher representative penetration value is probable. Thus the minimum $N_{1,60cs}$ is 5.1 bpf (N = 5 bpf) at a depth of 4.7 m (15.5 ft) below the ground surface ATE, with $N_{1,60cs}$ = 12.1 bpf (N = 12 bpf) at a depth of 4.9 m (16 ft) below the ground surface ATE being very plausible.

The water table depth ATE from Pond and Martin (1996) is approximately 3.1 m (10.3 ft), with respect to the estimated ground surface ATE. This depth could be no more than 0.3 m (1 ft) too shallow, but as much as 3 m (10 ft) too deep; thus there is considerable uncertainty in the depth of the water table ATE assessed by Pond and Martin (1996).

The FDQ for this site is low because of the uncertainty in the representative penetration resistance (which is at least 5.1 bpf, but possibly 12.1 bpf or higher), and because of the uncertainty in the water table depth ATE from Pond and Martin (1996).

Haysville (HA). Two small dikes about 25 m (82 ft) apart were found in a 300-m (984 ft) long bank exposure. The site is likely one of hydraulic fracturing. Two borings were conducted, one near each dike. The boring logs were very similar throughout their depths.

Although the features at this site have been attributed to the Vincennes Earthquake, there is still uncertainty as to whether this actually the case. Consequently, this site was not considered in the regional assessment of the magnitude of the Vincennes Earthquake.

Maunie (MA). Numerous small dikes are at scattered locations along an approximately 500-m (1640 ft) long bank exposure. Several scattered dikes vented to the ground surface. The dikes are mainly parallel to one another. The ground failure mechanism is not lateral spreading, in the main, but probably chiefly hydraulic fracturing and possibly with a small component of surface oscillation.

Banks are typically cleanly exposed when the river level is low, to a level equal to the water table depth ATD shown in Figure 11. Both fluidization effects in bank exposures and $N_{1,60cs}$ values in five boring logs show that all candidate source sands that liquefied and fluidized lie within the zone in Figure 11 designated as "Interbedded Clay and Sand (CL and SP)." Field observations made on several occasions show that the effects of fluidization are typically restricted to the immediate vicinity of the base of the dikes, and there have not been extensive lateral movements along the base of the cap. Thus hydraulic fracturing is probably the chief mechanism for forming the dikes.

The minimum $N_{1,60cs}$ values from three of the borings (B-2, B-3, and B-5) range from 12.6 to 19.1 bpf (N ranged from 9 to 14 bpf) at a depth of 2.3 m (7.5 ft) below the ground surface ATE, with lower $N_{1,60cs}$ values at the two other borings. Thus, we selected a representative $N_{1,60cs}$ of 13.2 bpf (N = 9.5 bpf) for the site as a whole.

The water table depth ATE by Pond and Martin (1996) is approximately 1.2 m (4 ft), with respect to the estimated ground surface ATE. This depth could be as much as 1 m (3 ft) too deep, but very probably was not because the site is an ancient terrace that is topographically elevated. Additionally, the actual value of water table depth ATE could have been no more than a few feet deeper than the ATE depth from Pond and Martin (1996). Thus ATE depth from Pond and Martin (1996) is very good for back-analysis.

The FDQ for this site is high for this site because of the numerous scattered borings having essentially the same value of minimum penetration resistance and because of the very credible water table depth ATE from Pond and Martin (1996).

Worthington (WO). Four dikes were at scattered locations along a 50-m (164 ft) long portion of a 150-m (492 ft) long bank exposure. The largest dike was 15 cm (5.9 in) wide, and the other three were much smaller and pinched together within the cap. Three borings were drilled at the site, at scattered locations in the vicinity of the dikes. All there boring logs were very similar to one another, making the ground-failure mechanism irrelevant for selection of a representative penetration resistance. We selected a representative $N_{1,60cs}$ of 14.1 bpf (N = 7 bpf) at a depth of about 2.7 m (9 ft) below the ground surface ATE.

The water table ATE value from Pond and Martin (1996) is approximately 1.5 m (5 ft), with respect to the estimated ground surface ATE. This value could be no more than about 0.6 m (2 ft) too shallow, but probably is not too deep. Thus the ATE depth from Pond and Martin (1996) is thought to be very good for back-analysis.

The FDQ for this site is high for the site because of the similarity of the boring logs at scattered, and because of the very credible water table depth ATE from Pond and Martin (1996).

Terre Haute (TH). Four small dikes within a 50-m (164 ft) long section are present in the middle of a 200-m (656 ft) long exposure of bank. Three borings were drilled, two near the dikes and one some 60 m (197 ft) away, in the section having no dikes. The dikes were likely caused by hydraulic fracturing or surface oscillations because of their small widths and the absence of evidence of an appropriate field setting for lateral spreading to have taken place.

The minimum values $N_{1,60cs}$ in all SPT borings were essentially the same, at the same depth. Therefore, the ground-failure mechanism plays no role in selection the representative $N_{1,60cs}$ of 16.8 bpf (N = 14.5 bpf), at a depth of 5.2 m (17 ft) below the ground surface ATE.

The water table depth ATE from Pond and Martin (1996) is approximately 0.76 m (2.5 ft), with respect to the estimated ground surface ATE. This depth might be as much as 3 m (10 ft) too shallow, which is significant.

The FDQ for this site is low mainly because of uncertainty in the water table depth ATE from Pond and Martin (1996).

Bowling Green (BG). Two small dikes close to one another and probably caused by lateral spreading were found in a 100-m (328 ft) long bank exposure. Four borings were drilled at scattered locations along the exposure, and all showed a zone of very loose silty sand (SP-SM) at a depth of about 5.3 m (17.5 ft) below the ground surface ATE. The representative $N_{1,60cs}$ for this site is probably at least 3.5 bpf (N = 3.5 bpf), and possibly significantly higher.

The water table ATE value by Pond and Martin (1996) is approximately 2.3 m (7.5 ft), with respect to the estimated ground surface ATE. This depth could be as much as 1.5 m (5 ft) too shallow or deep.

The FDQ for this site is low because the water table depth ATE from Pond and Martin (1996) has much uncertainty.

Newport (NP). A few dikes were found at scattered locations in a 75-m (246 ft) long bank exposure, with the largest one having a width of 0.24 m (0.8 ft). The dikes clearly formed by lateral spreading movement toward the Wabash River at the time of the earthquake.

Two widely spaced borings along the lateral spread show the presence of a stratum of loose sandy gravel. Both borings yielded a minimum $N_{1,60cs}$ of 7.1 bpf (N = 6 bpf) at a depth of 3.2 m (10.5 ft) below the ground surface ATE. We selected this value as a representative penetration resistance for the site.

The water table depth ATE from Pond and Martin (1996) is approximately 2.0 m (6.5 ft), with respect to the estimated ground surface ATE. There is a thin stratum of loose silty gravelly sand located slightly above the water table depth ATE from Pond and Martin (1996, p. 153); no liquefaction effects were observed to have originated in this stratum. On the basis of the density of this thin stratum, and the mechanics of seismic shaking, it is possible that liquefaction would have developed there if the water table had been above this stratum. Altogether, the range of possible values for the water table depth is thought to be a meter or so higher or lower than the ATE depth from Pond and Martin (1996).

The FDQ for this site is intermediate for this site, mainly due to the uncertainty in the depth of the water table ATE.

Perrysville (PL). Numerous dikes are present in a 250-m (820 ft) bank exposure, with nearly all dikes in a swarm and one isolated dike away from the swarm. The ground-failure mechanism could not be deduced from data available. Two borings were drilled, one in the swarm and one at the isolated dike.

The minimum $N_{1,60cs}$ for strata that were liquefaction candidates at the swarm was 9.9 bpf (N = 8 bpf), and at the isolated dike was 5.1 bpf (N = 4.5 bpf), at a depth range of 4.3-5.5 m (14-18 ft) below the ground surface ATE. Thus both values of $N_{1,60cs}$ were low. $N_{1,60cs}$ of 5.1 bpf is the minimum possible, but the value of 9.9 bpf is also plausible for the site.

The water table depth ATE from Pond and Martin (1996) is approximately 0.75 m (2.5 ft), with respect to the estimated ground surface ATE. This depth could be as much as 4.6 m (15 ft) too deep.

The FDQ for this site is low because of the uncertainty in the water table depth ATE from Pond and Martin (1996).

Table 1. Guidelines for Selecting a Representative Penetration Resistance Value (Olson et al. 2004)

Ground Failure Mechanism	Sectional View Observations of Marginal Liquefaction	Plan View Observations (any severity of liquefaction) and Sectional View Observations of Severe Liquefaction
Hydraulic fracturing	Designate individual penetration tests as locations of marginal liquefaction or no liquefaction based on proximity to observed liquefaction features. Use lowest value of penetration resistance at each test location.	Use highest minimum value of penetration resistance that is common among multiple penetration tests performed in proximity to individual liquefaction features created by hydraulic fracturing.
Lateral spreading	Designate penetration tests within the probable limits of lateral spread as marginal liquefaction. Designate tests outside these limits as no liquefaction. Use highest minimum value of penetration resistance common among multiple tests for each designation.	Use highest minimum value of penetration resistance that is common among penetration tests scattered along the length of the lateral spread (regardless of their proximity to venting features). This length can be hundreds of meters at many places subjected to strong earthquake shaking.
Surface oscillations	Same as for hydraulic fracturing. Penetration tests should be performed within a few meters of observed liquefaction feature.	Use highest minimum value of penetration resistance that is commonly present (and typically near the base of the fine grained cap) and is located within a few tens of meters of the dikes caused by surface oscillations.
Unknown mechanism	Same as for hydraulic fracturing.	Use lowest value of penetration resistance that is realistically feasible for any of the three candidate mechanisms shown above.

Table 2. Site data for the twelve sites exhibiting paleoliquefaction effects attributed to the Vincennes Earthquake

Site	r_{ec_hypo} (km)	Critical Depth to Liq. ATD	Critical Depth to Liq. ATE	Depth gwt ATE	N measured (bpf)	FC (%)	$N_{1,60cs}$ (bpf)	Failure Mech.	Severity of Liq.	FDQ
VW	18	8.5 m (28 ft)	6.1 m (20 ft)	1.5 m (5 ft)	27	4	30.3	HF	Marg.	High
SM	25	3.7 m (12 ft)	2.4 m (7.75 ft)	0.23 m (0.75 ft)	7	4	8.9	HF	Severe	High
RF	27	5.6 m (18.5 ft)	3.2 m (10.5 ft)	1.2 m (4 ft)	19	4	24.4	LS	Severe	High
PA	37	6.2 m (20.5 ft)	2.4 m (8 ft)	2.3 m (7.5 ft)	12	4	13.6	LS	Mod. to Marg.	High
PB	49	8.5 m (28 ft)	6.1 m (20 ft)	2.3 m (7.5 ft)	20	4	21.5	LS	Severe	High
YO	61	8.5 m (28 ft) 8.2 m (27 ft)	4.9 m (16 ft) 4.7 m (15.5 ft)	3.1 m (10.3 ft)	12 5	4 4	12.1 5.1	LS	Severe to Mod.	Low
MA	80	3.2 m (10.5 ft)	2.3 m (7.5 ft)	1.2 m (4 ft)	9.5	10	13.2	HF or SO	Mod. to Marg.	High
WO	82	4.6 m (15 ft)	2.7 m (9 ft)	1.5 m (5 ft)	7	15	14.1	LS & HF	Mod. to Marg.	High
TH	94	10.5 m (34.5 ft)	5.2 m (17 ft)	0.76 m (2.5 ft)	14.5	4	16.8	HF or SO	Mod. to Marg.	Low
BG	101	7.3 m (24 ft)	5.3 m (17.5 ft)	2.3 m (7.5 ft)	3.5	4	3.5	LS?	Marg.?	Low
NP	135	7.0 m (23 ft)	3.2 m (10.5 ft)	2.0 m (6.5 ft)	6	4	7.1	LS	Mod. to Severe	Inter.
PL	153	7.8 m (25.5 ft) 9.3 m (30.5 ft)	4.3 m (14 ft) 5.5 m (18 ft)	0.75 m (2.5 ft)	8 4.5	4 4	9.9 5.1	??	Mod. to Marg.	Low

Notes:

- Site: Sites analyzed in this study; see Figure 8.
- r_{ec_hypo}: Hypocentral distance to the site computed assuming a focal depth of 10 km and that the horizontal distance from the site to the estimated energy center of the paleoearthquake is equal to the epicentral distance.
- Critical Depth to Liq.: critical depth to liquefaction: ATD - in reference to the ground surface at time of drilling; ATE - in reference to the estimated ground surface at time of earthquake per Pond and Martin (1996).
- Depth gwt ATE: depth to ground water table at time of earthquake (ATE), in reference to the estimated ground surface ATE per Pond and Martin (1996).
- FC: fines content estimated from description given in boring logs of Pond and Martin (1996).
- $N_{1,60cs}$: all adjustments applied to measured SPT N-values are per Youd et al. (2001).
- Failure Mechanism: mode of liquefaction manifestation: LS = lateral spread; HF = hydraulic fracture; SO = surface oscillation; ?? = indeterminate
- Severity of Liq.: severity of liquefaction categorized as: severe, moderate, marginal based on first hand field observations and published reports.
- FDQ: Field Data Quality - categorized as: high, intermediate, and low based on first hand field observations and published reports.

Table 3. Back-calculated a_{max} - M combinations for the twelve sites exhibiting paleoliquefaction effects attributed to the Vincennes Earthquake.

Site	Somerville et al. (2001)						Atkinson and Boore (1995)						Toro et al. (1997)						Campbell (2001, 2003)					
	Energy		Cyclic Stress (SIA)		Cyclic Stress (A&S)		Energy		Cyclic Stress (SIA)		Cyclic Stress (A&S)		Energy		Cyclic Stress (SIA)		Cyclic Stress (A&S)		Energy		Cyclic Stress (SIA)		Cyclic Stress (A&S)	
	a_{max} (g)	M_w	a_{max} (g)	M_w	a_{max} (g)	M_w	a_{max} (g)	M_w	a_{max} (g)	M_w	a_{max} (g)	M_w	a_{max} (g)	M_w	a_{max} (g)	M_w	a_{max} (g)	M_w	a_{max} (g)	M_w	a_{max} (g)	M_w	a_{max} (g)	M_w
VW	0.56	7.6	0.48	7.4	0.49	7.4	0.56	7.3	0.50	7.1	0.53	7.2	0.56	7.4	0.49	7.2	0.51	7.3	0.56	6.7	0.55	6.6	0.63	6.9
SM	0.16	6.2	0.11	5.8	0.16	6.2	0.16	5.1	0.13	4.9	0.22	5.6	0.16	5.8	0.12	5.4	0.18	5.9	0.16	5.2	0.13	4.9	0.21	5.6
RF	0.43	7.6	0.32	7.1	0.34	7.2	0.43	7.3	0.35	6.6	0.39	6.9	0.43	7.5	0.32	7.0	0.35	7.2	0.43	7.1	0.35	6.6	0.40	6.9
PA	0.30	7.3	0.24	7.0	0.26	7.2	0.31	6.8	0.27	6.5	0.31	6.8	0.30	7.3	0.24	7.0	0.26	7.2	0.30	7.0	0.26	6.7	0.29	6.9
PB	0.29	7.5	0.26	7.4	0.27	7.4	0.29	7.3	0.28	7.1	0.29	7.3	0.29	7.7	0.26	7.5	0.26	7.5	0.29	7.5	0.27	7.3	0.27	7.4
YO	0.20	7.3	0.18	7.2	0.19	7.3	0.21	7.0	0.19	6.7	0.22	7.0	0.19	7.4	0.18	7.3	0.18	7.4	0.20	7.3	0.18	7.2	0.19	7.3
	0.13	6.9	0.11	6.7	0.13	6.9	0.16	6.3	0.13	6.0	0.17	6.4	0.13	6.9	0.11	6.7	0.3	6.9	0.14	6.8	0.12	6.5	0.14	6.8
MA	0.20	7.7	0.17	7.5	0.17	7.5	0.20	7.6	0.19	7.2	0.18	7.3	0.19	7.8	0.17	7.6	0.16	7.6	0.20	7.7	0.17	7.5	0.17	7.5
WO	0.20	7.7	0.18	7.6	0.18	7.6	0.20	7.7	0.19	7.4	0.19	7.4	0.19	7.9	0.18	7.8	0.17	7.7	0.20	7.7	0.18	7.6	0.18	7.6
TH	0.17	7.7	0.16	7.6	0.15	7.6	0.17	7.6	0.16	7.4	0.16	7.5	0.16	7.9	0.16	7.8	0.14	7.8	0.18	7.6	0.16	7.5	0.16	7.5
BG	0.09	7.2	0.08	7.1	0.08	7.2	0.11	6.7	0.09	6.3	0.11	6.7	0.09	7.3	0.08	7.1	0.08	7.2	0.10	6.9	0.08	6.7	0.10	6.9
NP	0.12	7.9	0.11	7.8	0.10	7.8	0.12	8.1	0.11	7.7	0.10	7.7	0.12	8.1	0.11	8.0	0.10	7.9	0.13	7.5	0.12	7.3	0.12	7.4
PL[#]	0.10	8.4	0.10	8.4	0.08	8.2	-	-	-	-	-	-	-	-	-	-	0.08	8.4	0.11	8.1	0.10	8.0	0.09	7.9
	0.07	8.0	0.06	7.9	0.06	7.9	0.06	8.3	0.06	8.0	0.06	7.8	0.07	8.2	0.06	8.1	0.05	8.0	0.08	7.6	0.07	7.4	0.07	7.5

Notes:

- Site: Sites analyzed in this investigation; see Figure 8.
- Energy a_{max} and M_w: minimum a_{max} and M_w combination required to induce liquefaction per the energy-based procedure proposed by Green (2001).
- Cyclic Stress (A&S) a_{max} and M_w: minimum a_{max} and M_w combination required to induce liquefaction per the cyclic stress procedure using magnitude scaling factors proposed by Andrus and Stokoe (1997).
- Cyclic Stress (SIA) a_{max} and M_w: minimum a_{max} and M_w combination required to induce liquefaction per the cyclic stress procedure using magnitude scaling factors proposed by Seed et al. (1983).
- For site PL, no site amplification used in back-calculations due to shallow depth to bedrock.
- [#]Calculations for a_{max} and M were terminated and results not presented if computed M > 8.5.

Table 4. Ground motion attenuation relation used in the back-calculations.

Model	Site-to-Source Distance	Magnitude Range	Source Mechanism	Site Condition (Vs: NEHRP Site Class)	a_{max}
Somerville et al. (2001)	r_{jb}: 0 to 500 km	6.0 to 7.5	Non-rift, reverse fault	2830 m/sec: A	geometric mean
Campbell (2001, 2003)	r_{rup}: < 1000 km	5.0 to 8.2	Random fault mechanism	620 m/sec: B/C	geometric mean
Toro et al. (1997)	r_{jb}: 1 to 500 km (emphasis on 1 to 100 km)	5.0 to 8.0	--	1829 m/sec: A	arithmetic mean
Atkinson and Boore (1995)	r_{hypo}: 10 to 500 km	4.0 to 7.25	thrust fault	3800 m/sec: A	median of random component

Notes:

- Site-to-Source Distance: r_{jb} (Joyner-Boore distance) – the closest distance to the rupture surface; r_{rup} – the closest distance to the rupture surface; r_{hypo} – hypocentral distance. See Figure 15. The distance ranges shown are the site-to-source distances for which the models were developed.
- Magnitude Range: Range of earthquake moment magnitudes for which the models were developed.
- Source Mechanisms: The source mechanisms for which the attenuation relations apply.
  - Somerville et al. (2001) allow a_{max} to be computed for rifted and non-rifted domains. Based on Bear et al. (1997) and McBride (2002: personal communication with S.F. Obermeier) a non-rifted domain was assumed for the Wabash Valley fault zone.
  - The data used in developing the Atkinson and Boore (1995) relation was not categorized according to faulting mechanism, but it believed that it predominately came from thrust faults.
- Site Condition: Near surface shear wave velocity of the site; NEHRP site classification (Appendix I).
  - Atkinson and Boore (1995): Atkinson and Boore (1995) list V_s at the depth of the source as 3800 m/sec and go on to state that the near surface amplification due to impedance contrast is negligible. Hence, the near surface shear wave velocity is assumed approximately to be 3800 m/sec.
- a_{max}: Relationship between the a_{max} value computed using the attenuation relations and the peak accelerations of the two horizontal component of motion.
  - Somerville et al. (2001): geometric mean (Somerville, 2004: personal communication with R.A. Green)
  - Toro et al. (1997): Because one of the constants used in developing the ground motions from which this attenuation relation was derived assumes equal partition of energy between the two horizontal components, the a_{max} computed using this relation is most closely related to the arithmetic mean of the peak accelerations of the two horizontal components of motion. (Toro, 2004: personal communication with R.A. Green)

Table I-1. Amplification Ratios (F_a) as a Function of the Site Class and Mapped Short Period Maximum Considered Earthquake Spectral Acceleration (S_s).

Site Class	Mapped Maximum Considered Earthquake Spectral Response Acceleration at Short Periods				
	$S_s \leq 0.25$	$S_s = 0.50$	$S_s = 0.75$	$S_s = 1.00$	$S_s \geq 1.25$
A	0.8	0.8	0.8	0.8	0.8
B	1.0	1.0	1.0	1.0	1.0
C	1.2	1.2	1.1	1.0	1.0
D	1.6	1.4	1.2	1.1	1.0
E	2.5	1.7	1.2	0.9	*a*
F	*a*	*a*	*a*	*a*	*a*

NOTE: Use straight line interpolation for intermediate values of S_s.

[a] Site-specific geotechnical investigation and dynamic site response analyses shall be performed.

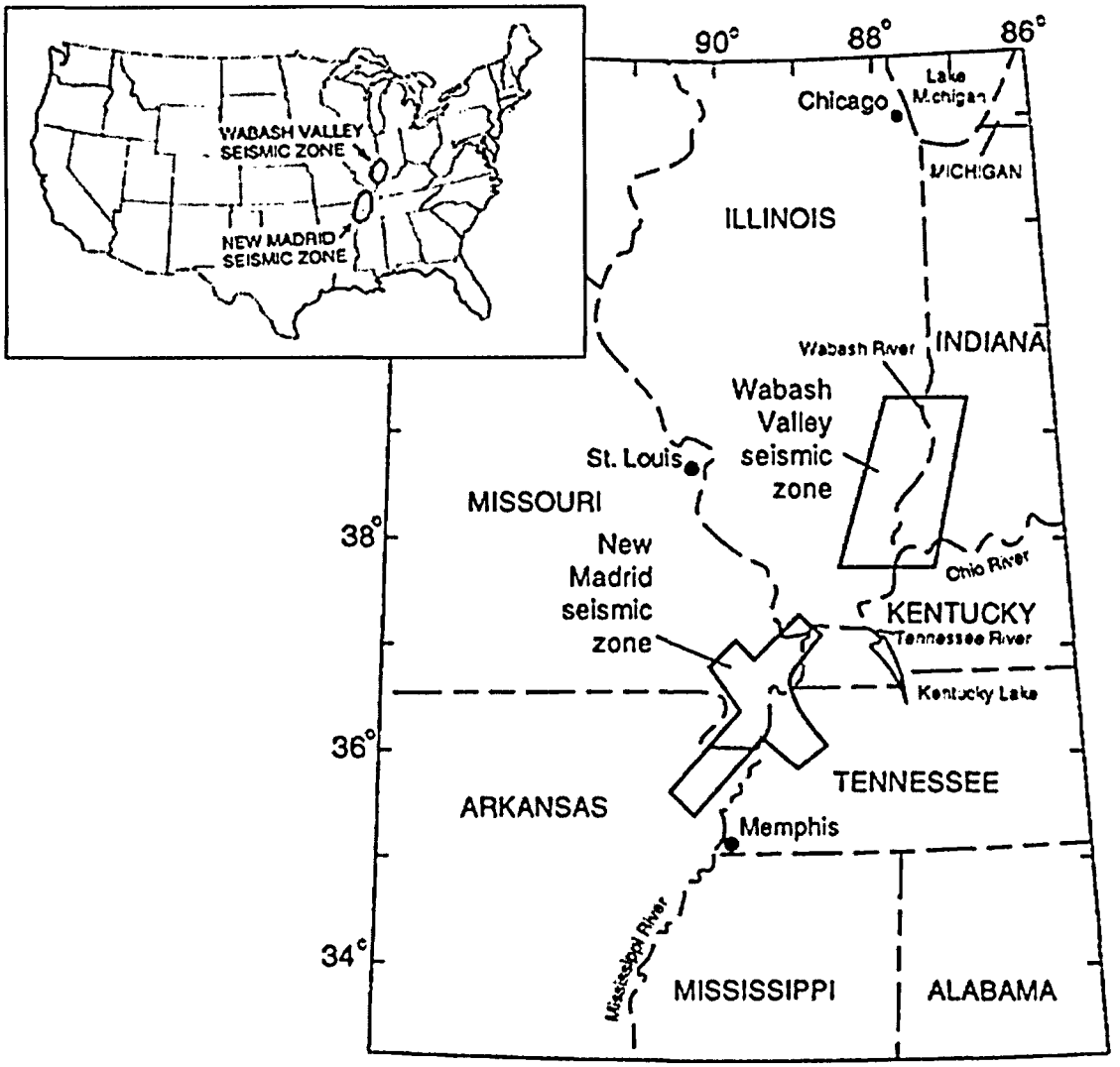

Figure 1. Approximate locations of New Madrid and Wabash Valley Seismic Zones. (Adapted from Obermeier 1998, 1999)

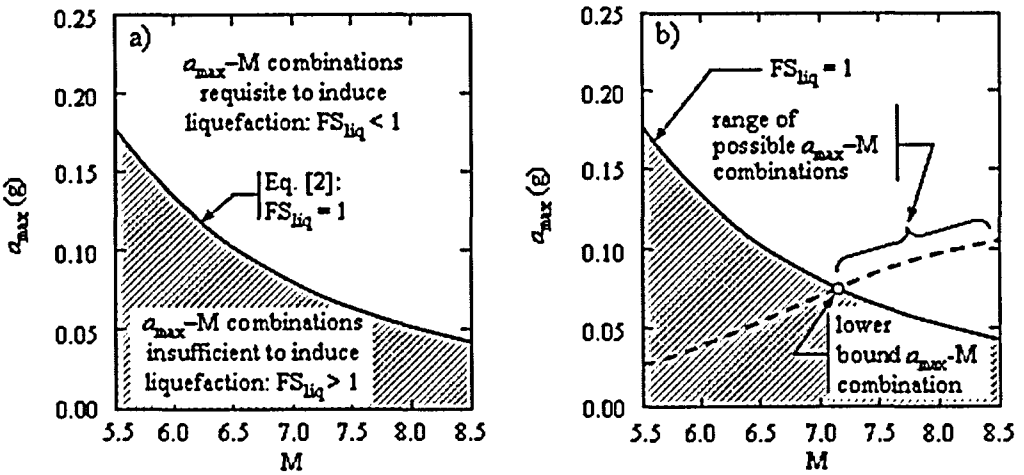

Figure 2. a) a_{max}-M combinations requisite to induce liquefaction for a hypothetical site. b) Determination of lower bound a_{max}-M combination for the same hypothetical site.

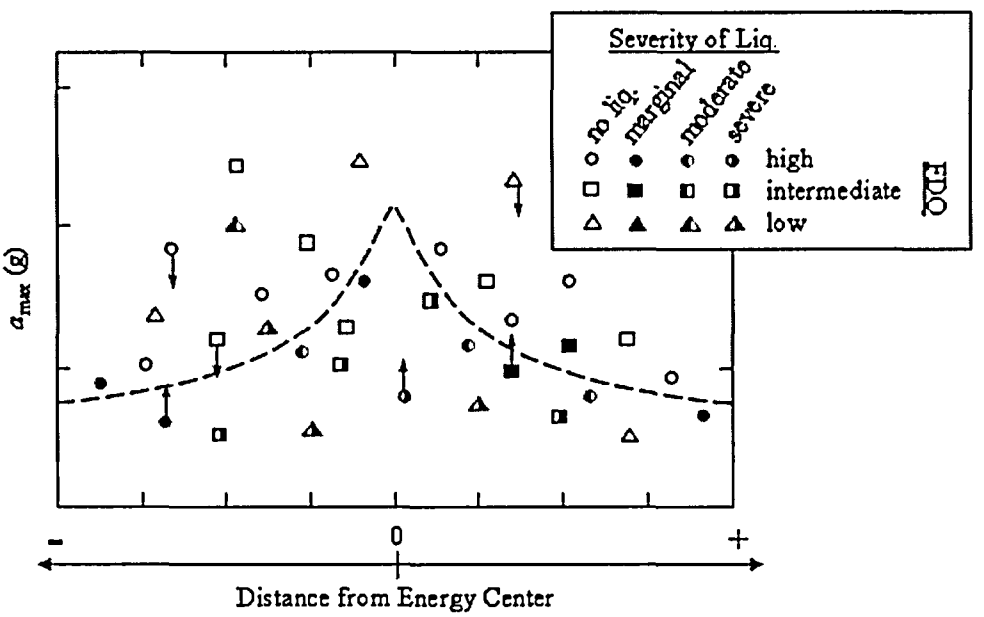

Figure 3. Illustration of proposed regional assessment of paleoliquefaction sites. The filled symbols represent sites that liquefied, and open symbols represent sites of no liquefaction. The field data quality (FDQ) ranks the quality of the field data and geologic interpretation. The upward and downward arrows attached to certain data represent potential aging effects and indicate that back-calculated values for a_{max} are likely on the low and high sides, respectively, as determined from Figure 10 in Olson et al. (2004). The dashed line schematically represents a regionally-appropriate surface peak ground acceleration attenuation relation (including any potential soil amplification effects) that provides reasonable upper bound for liquefaction data and separation for liquefaction and no liquefaction data.

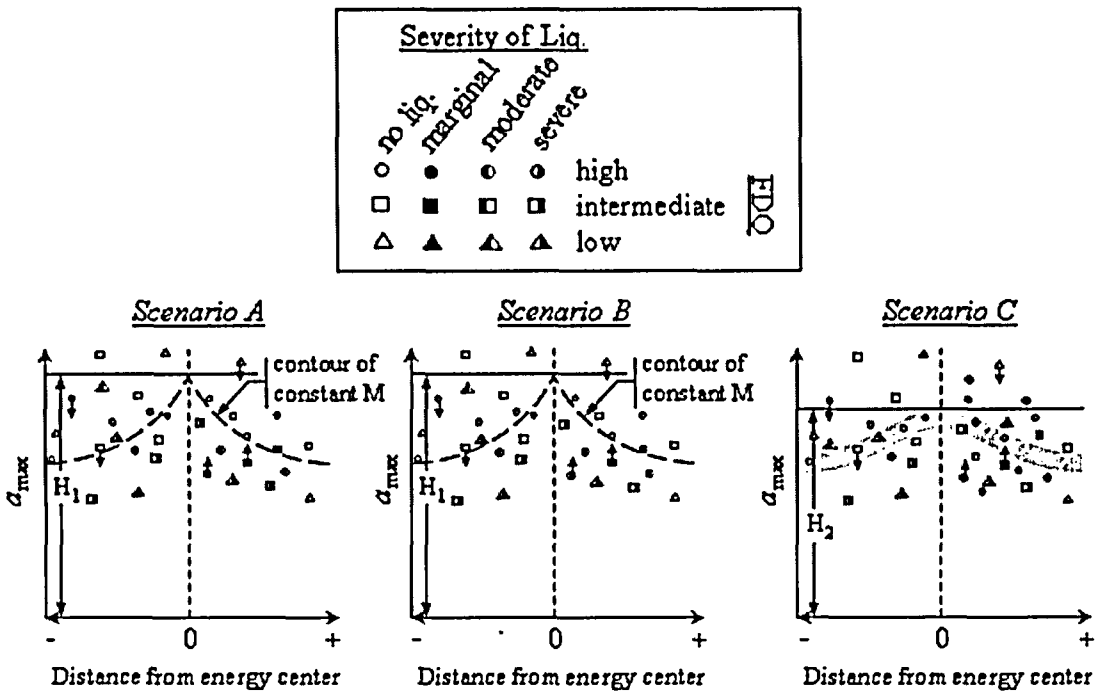

Figure 4. Illustration of potential scenarios that must be considered when integrating the results from back-calculations at multiple, widespread paleoliquefaction sites, where the back-calculations are made using the representative penetration resistance value of Olson et al. (2004). Scenario A is for situation of single large earthquake, located at the energy center. Scenario B is for the same large earthquake located at the provisional location of the energy center, but accompanied by scattered smaller earthquakes in the general vicinity. Scenario C is for several scattered earthquakes located in the general vicinity, but all having smaller values of M that for Scenario A. For the three scenarios, the ages of the earthquakes are indistinguishable from one another using geologic dating techniques.

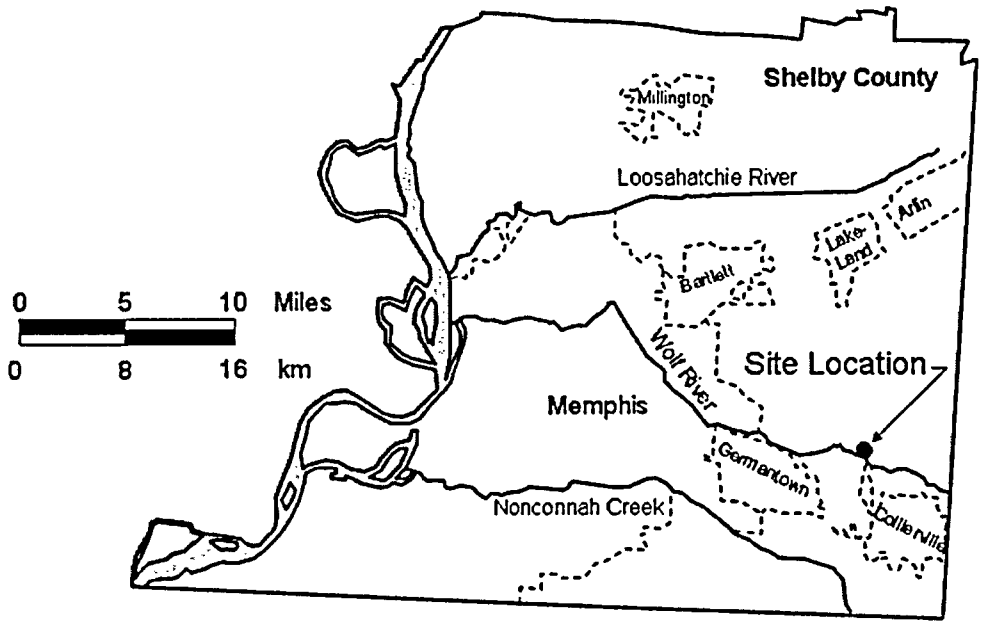

Figure 5. Site study location along the Wolf River (near Memphis, Tennessee) used to illustrate the authors' recommended approach for assessing the significance of effects related to aging, density changes, and other factors affecting liquefaction susceptibility at paleoliquefaction sites. (Adapted from Broughton et al. 2001)

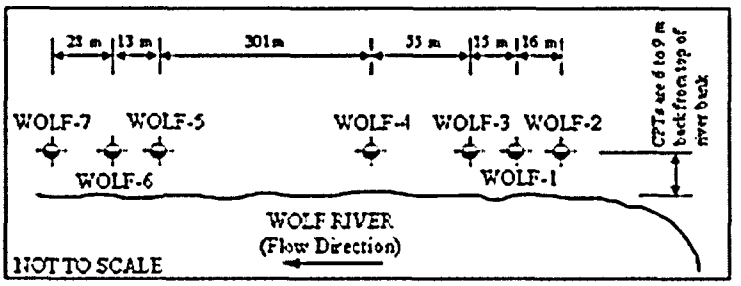

Figure 6. Site map, showing CPT soundings at locations of liquefaction and no liquefaction along Wolf River.

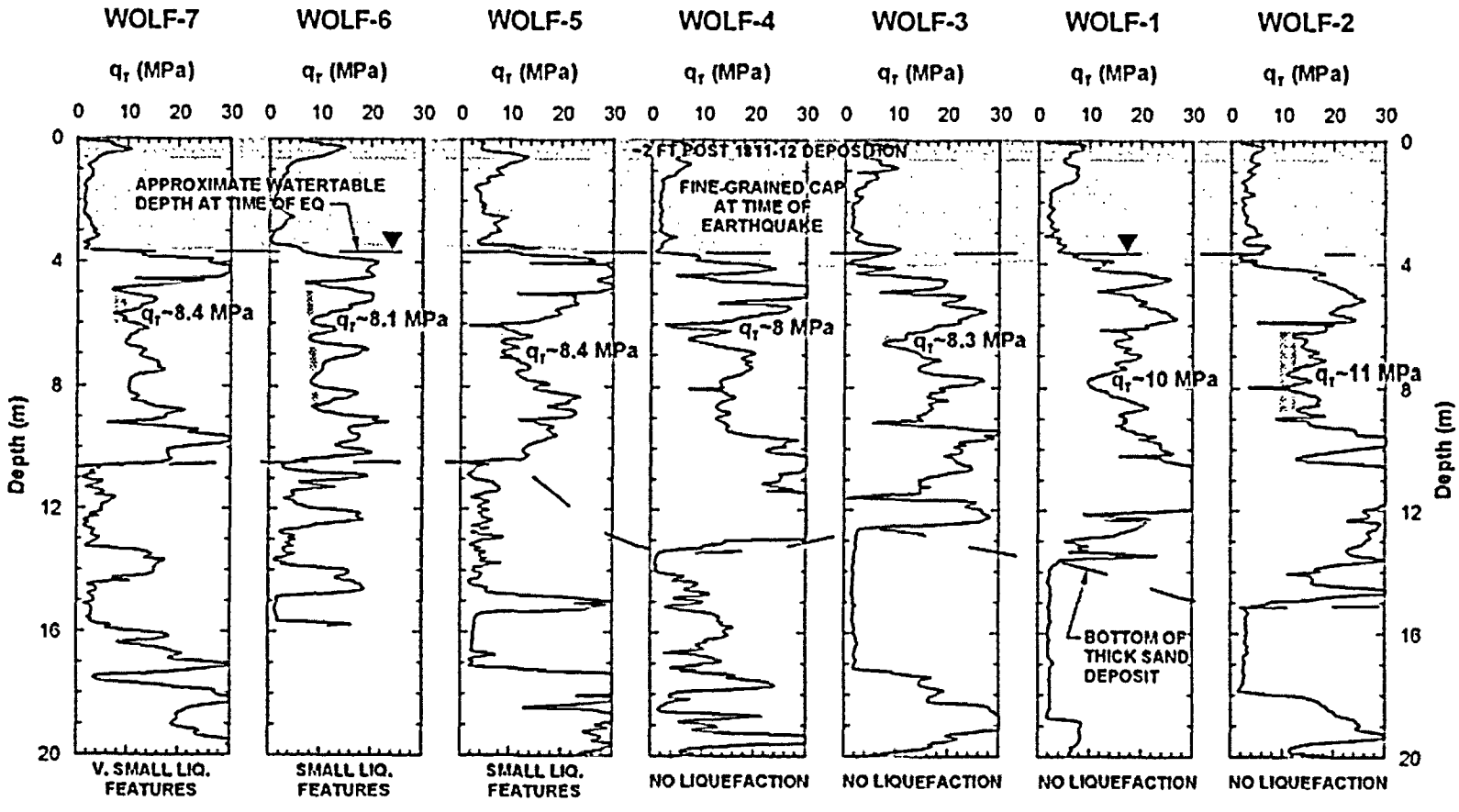

Figure 7. Sectional view of sediments, CPT soundings, and representative CPT values (shown hatched) of tip resistance (q_T) for most liquefiable portion of the profiles. The representative value of q_T corresponds with the depth of liquefaction effects at sites Wolf-5, -6, and –7.

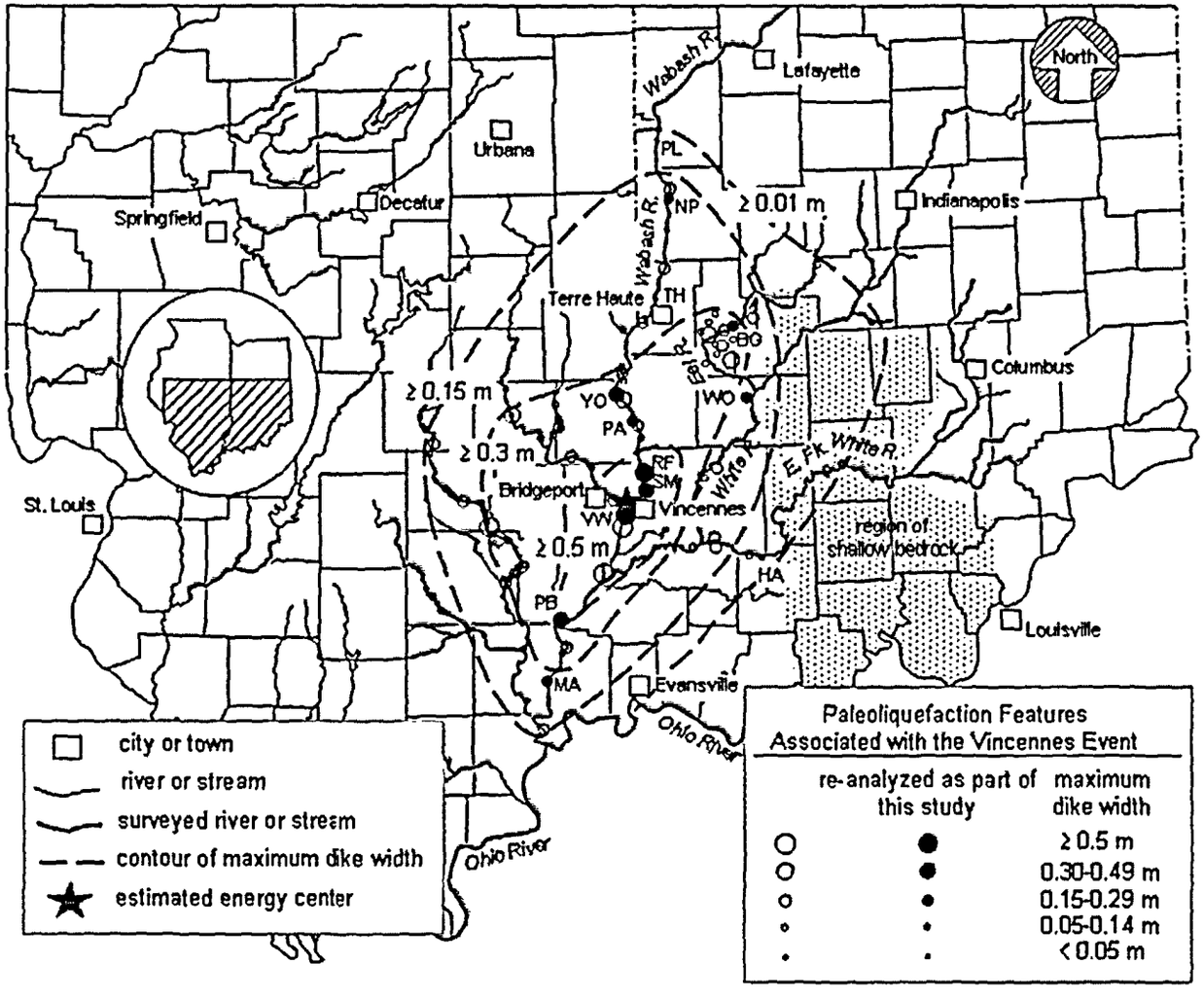

Figure 8. Map of paleoliquefaction sites in the Wabash Valley. (Adapted from Munson and Munson, 1996: Hajic and Wiant, 1997; Obermeier, 1998)

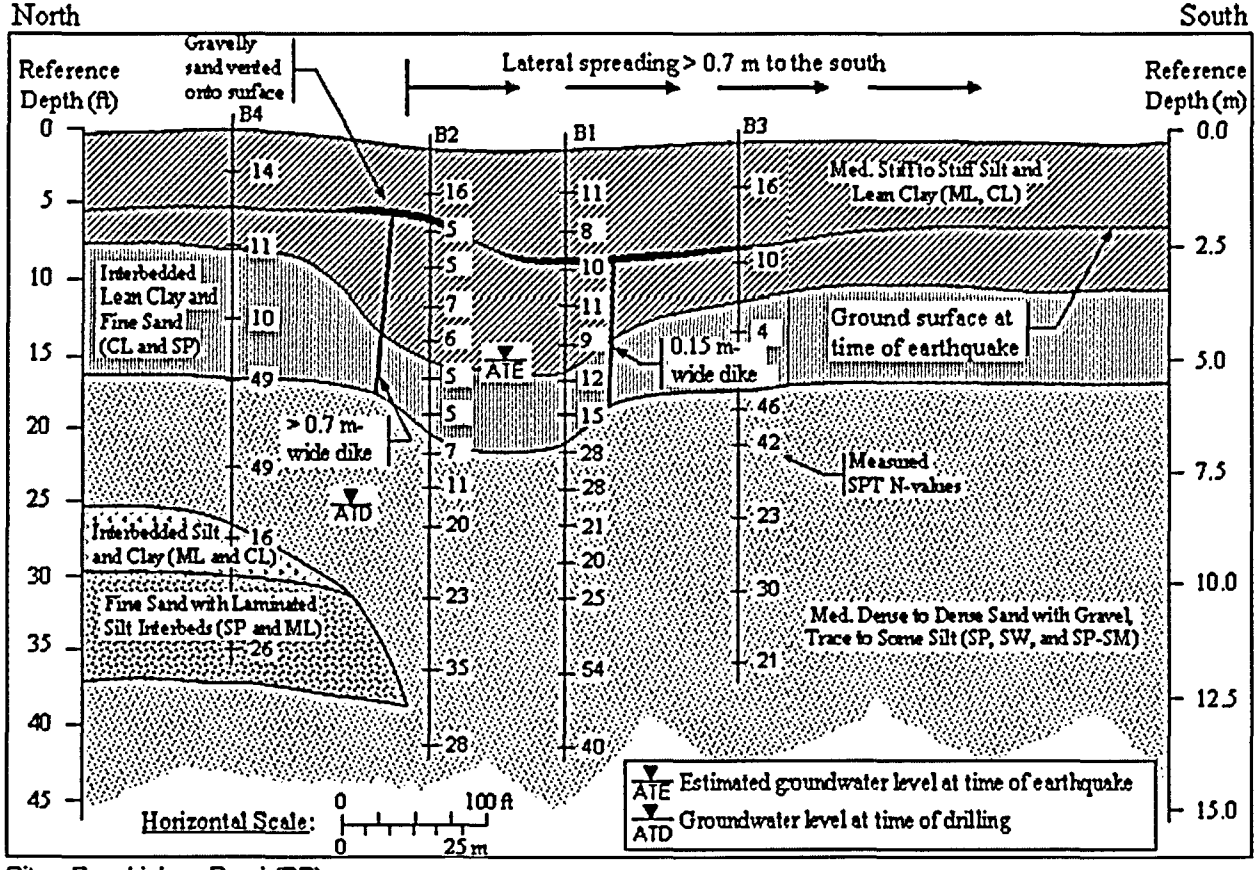

Site: Peankishaw Bend (PB)

Figure 9. Representative vertical section of Site PB. (Adapted from Pond and Martin, 1996)

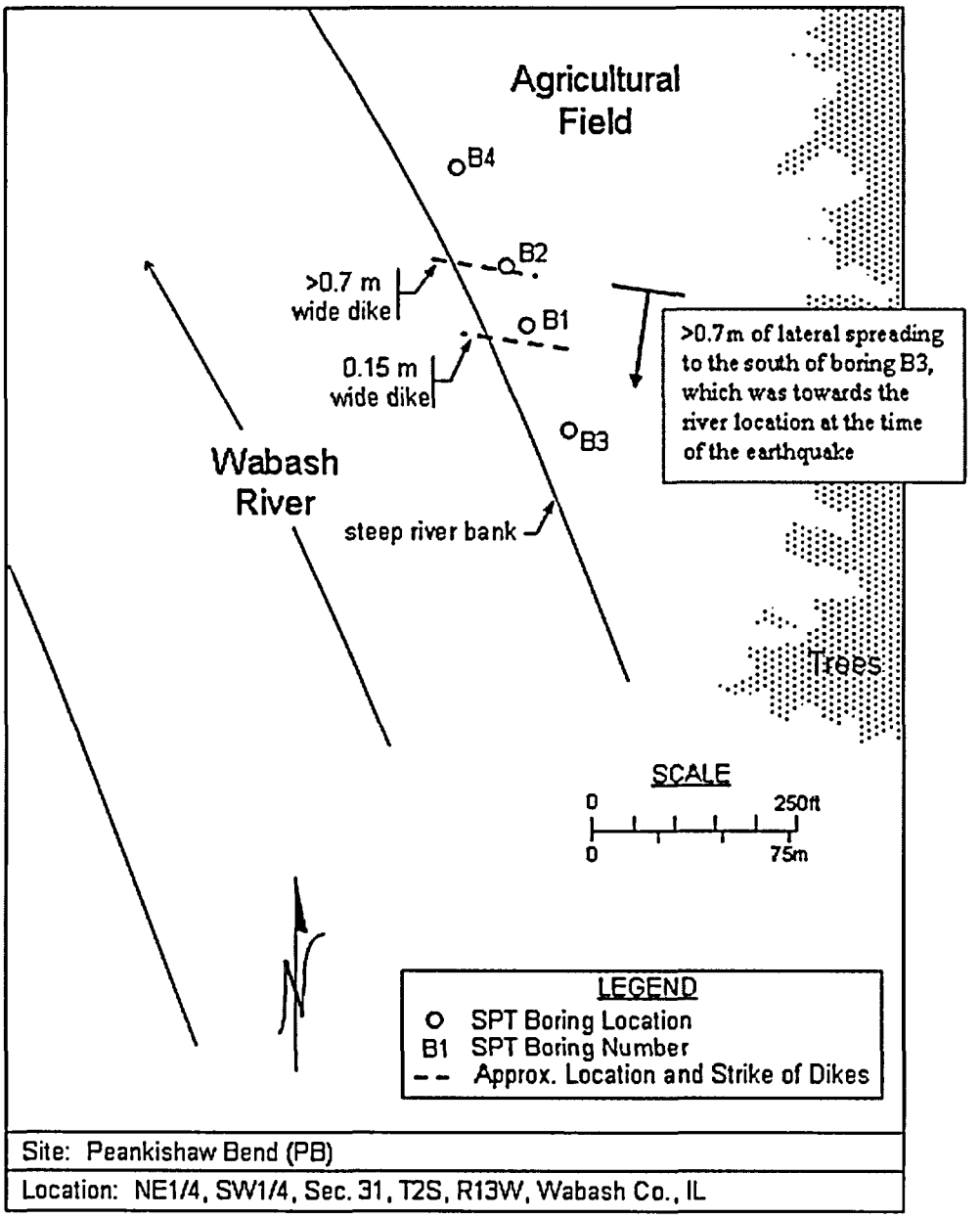

Figure 10. Plan view of Site PB. (Adapted from Pond and Martin, 1996)

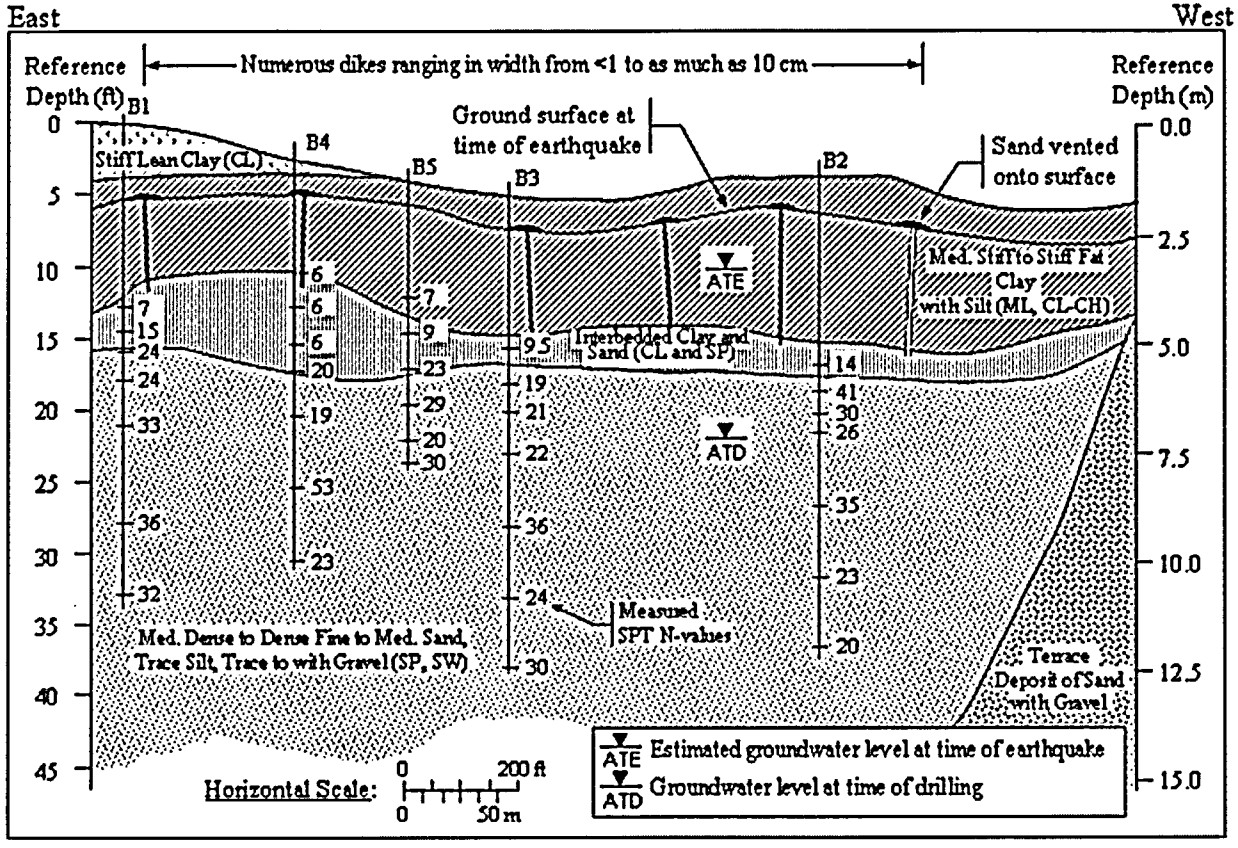

Site: Maunie (MA)

Figure 11. Representative vertical section of Site MA. (Adapted from Pond and Martin, 1996)

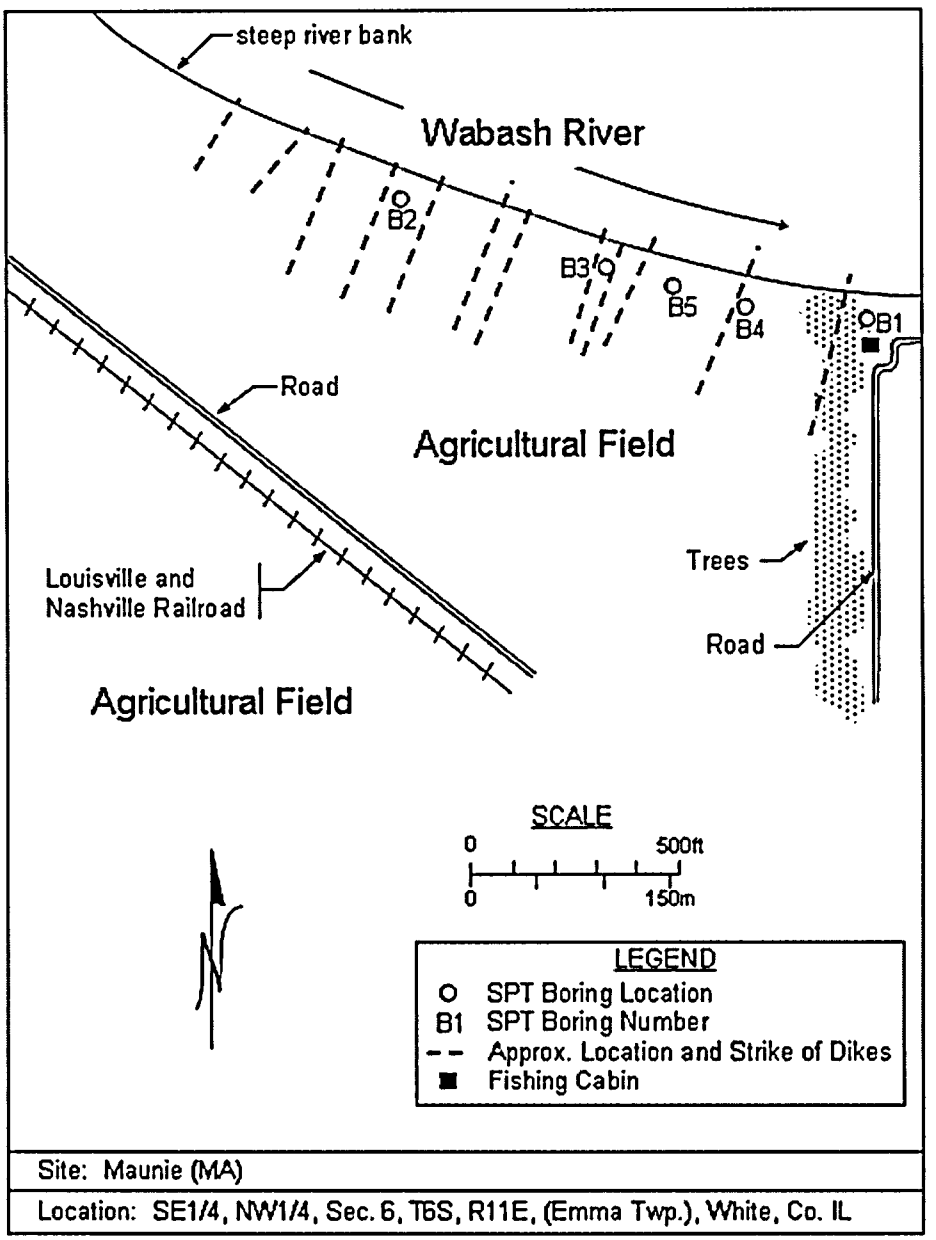

Figure 12. Plan view of Site MA. (Adapted from Pond and Martin, 1996)

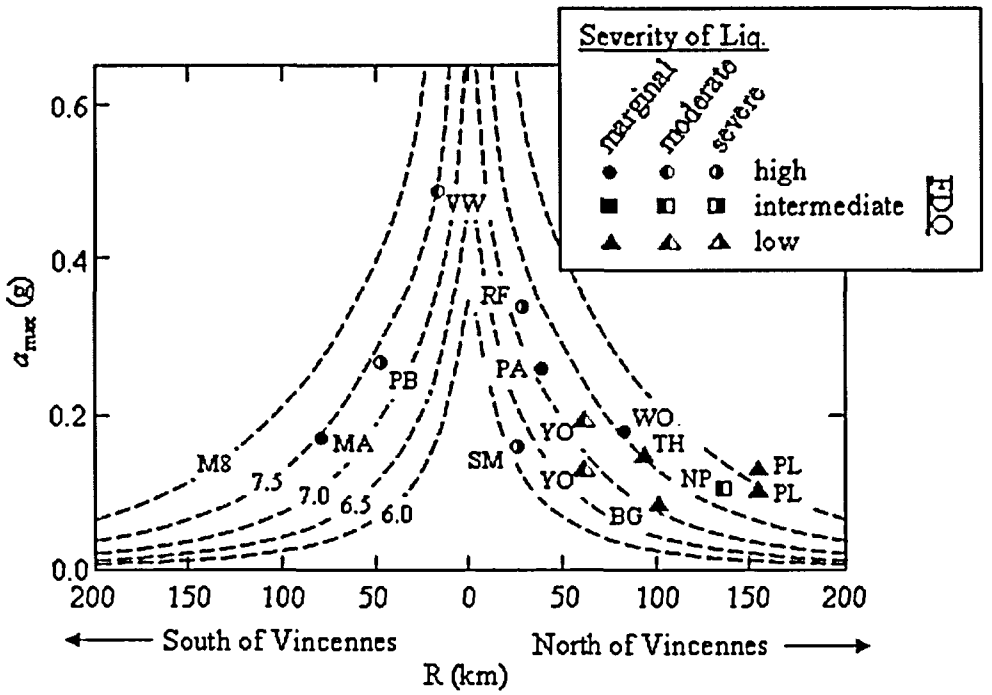

Figure 13a. Regional assessment for the paleoseismic strength of shaking of the Vincennes Earthquake using the attenuation relations proposed by Somerville et al. (2001). The site data and back-calculated values of a_{max}-M are given in Tables 2 and 3. [Note: Two alternative critical depths and failure mechanisms were considered for both YO and PL.]

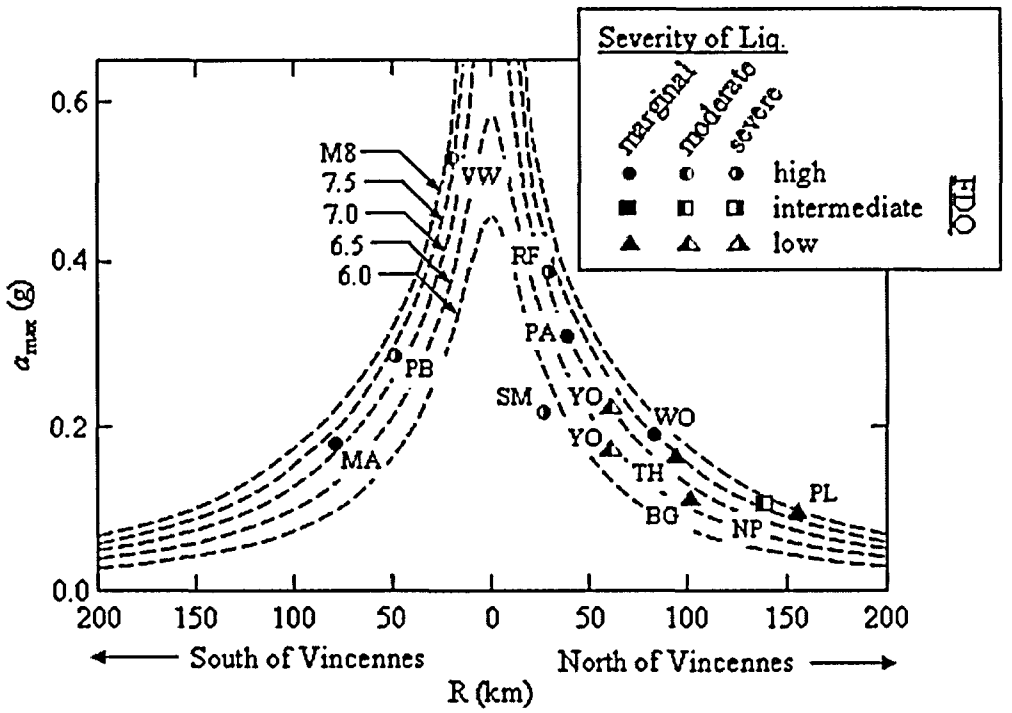

Figure 13b. Regional assessment for the paleoseismic strength of shaking of the Vincennes Earthquake using the attenuation relations proposed by Atkinson and Boore (1995). The site data and back-calculated values of a_{max}-M are given in Tables 2 and 3. [Note: Two alternative critical depths and failure mechanisms were considered for both YO and PL – only one alternative for site PL is plotted in this figure because the other resulted in a back-calculated M>8.5, which was considered unreasonable.]

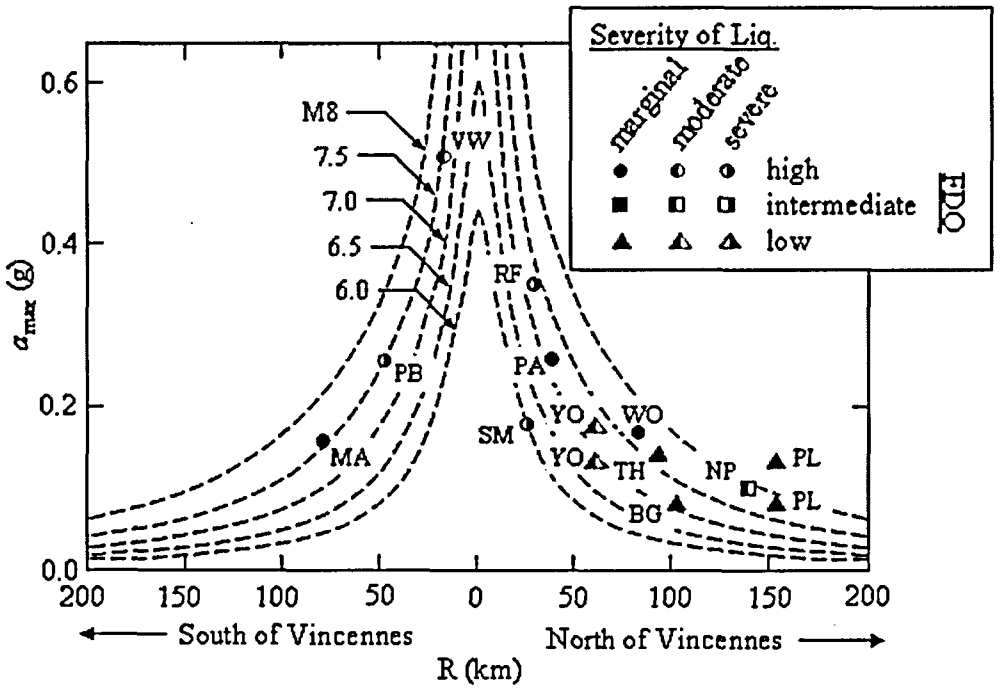

Figure 13c. Regional assessment for the paleoseismic strength of shaking of the Vincennes Earthquake using the attenuation relations proposed by Toro et al. (1997). The site data and back-calculated values of a_{max}-M are given in Tables 2 and 3. [Note: Two alternative critical depths and failure mechanisms were considered for both YO and PL.]

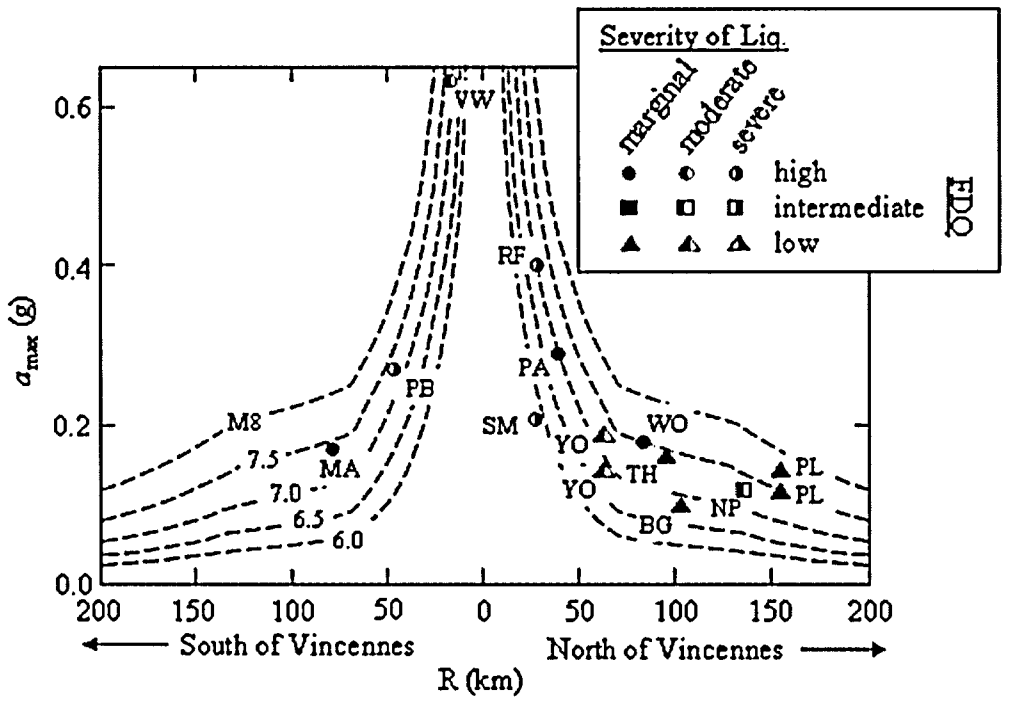

Figure 13d. Regional assessment for the paleoseismic strength of shaking of the Vincennes Earthquake using the attenuation relations proposed by Campbell (2001, 2003). The site data and back-calculated values of a_{max}-M are given in Tables 2 and 3. [Note: Two alternative critical depths and failure mechanisms were considered for both YO and PL.]

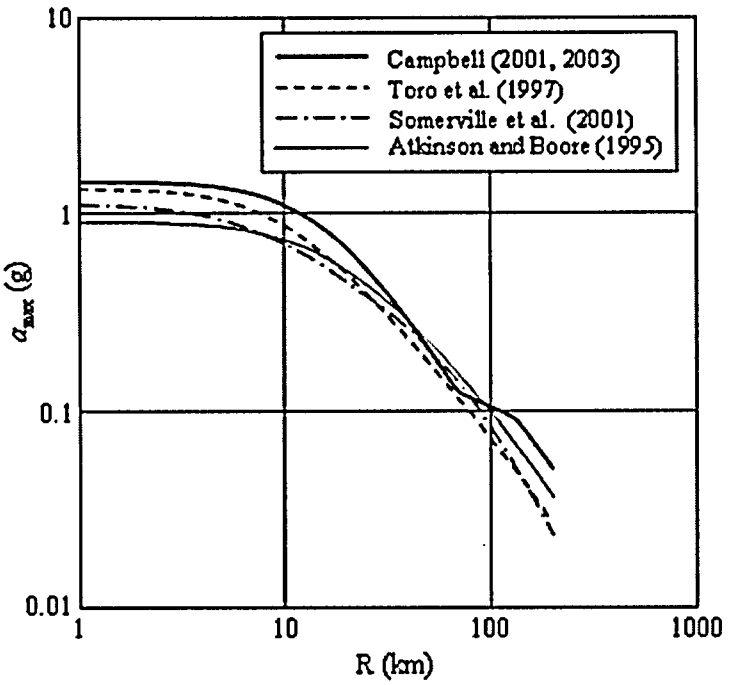

Figure 14a. a_{max} attenuation relations used in the back-calculations: rock sites, M 7.5

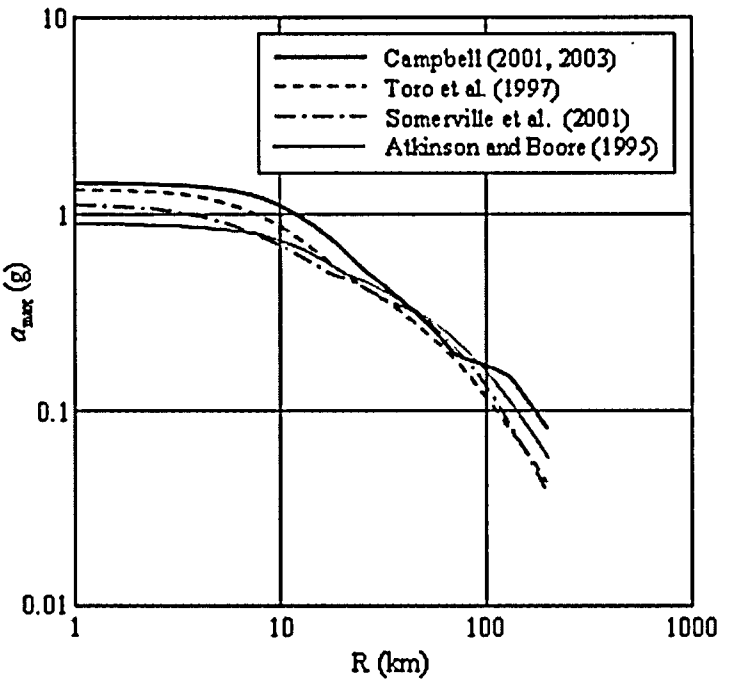

Figure 14b. a_{max} attenuation relations used in the back-calculations: NEHRP Site Class D, M 7.5

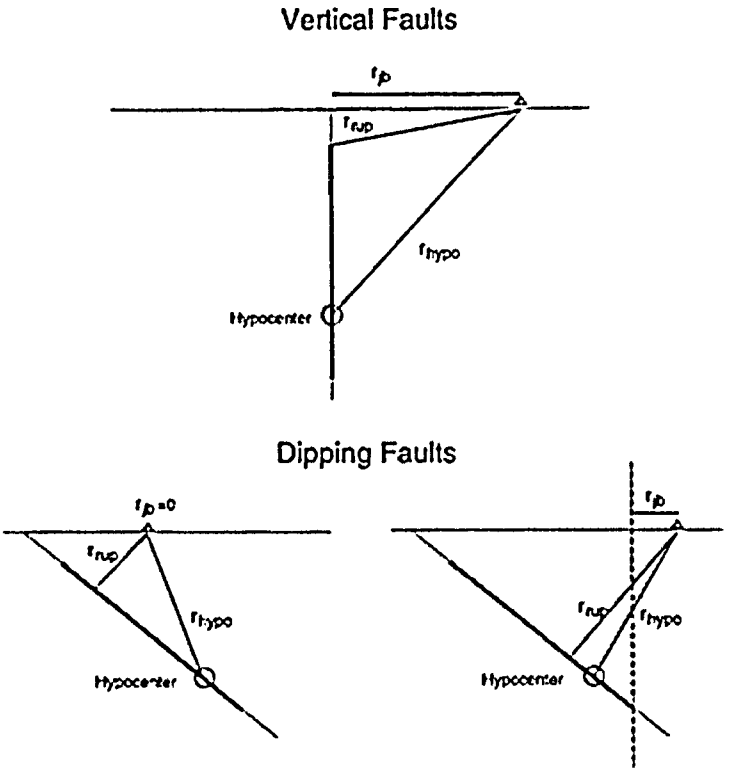

Figure 15. Commonly used measures of site-to-source distance. (Adapted from Abrahamson and Shedlock, 1997).

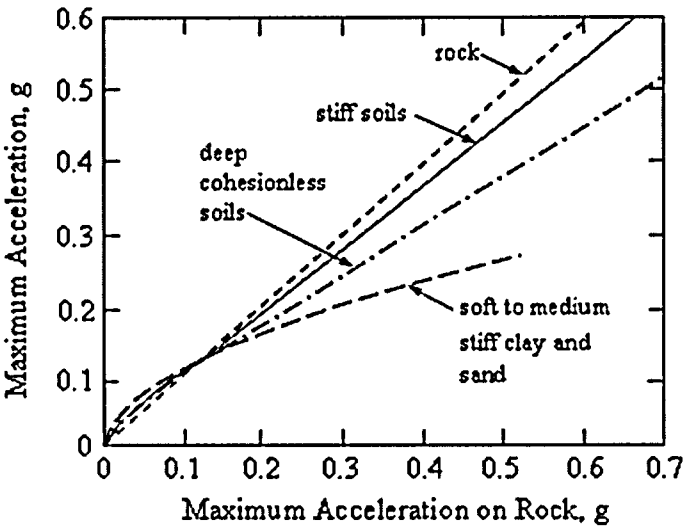

Figure I-1a. Early curves quantifying the amplification ratios as function of site conditions and amplitude of rock acceleration. (Adapted from Seed and Idriss 1982).

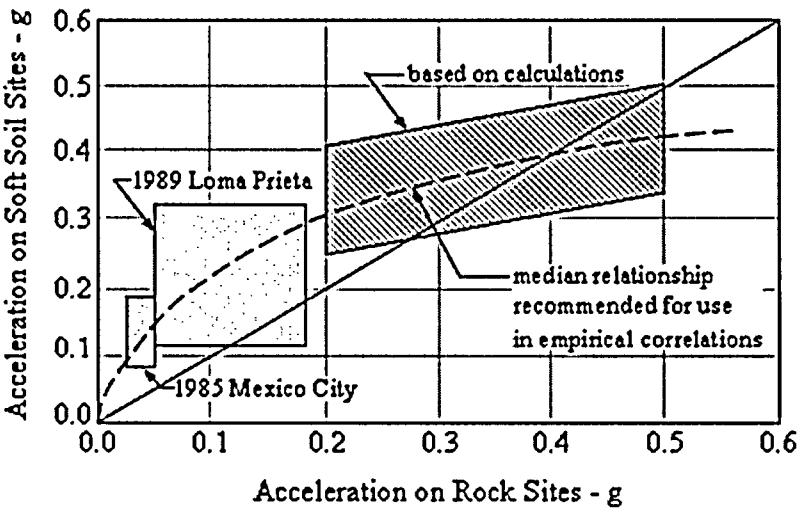

Figure I-1b. Curve quantifying the amplification ratios for soft soil sites. (Adapted from Idriss 1990, 1991).

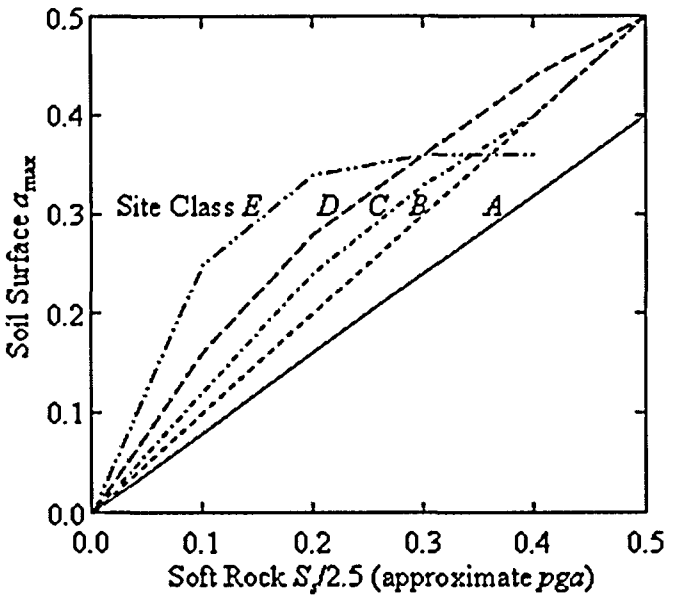

Figure I-2. Curves quantifying the amplification ratios used in the NEHRP provisions, where "soft rock" corresponds to sites falling on the B/C boundary.

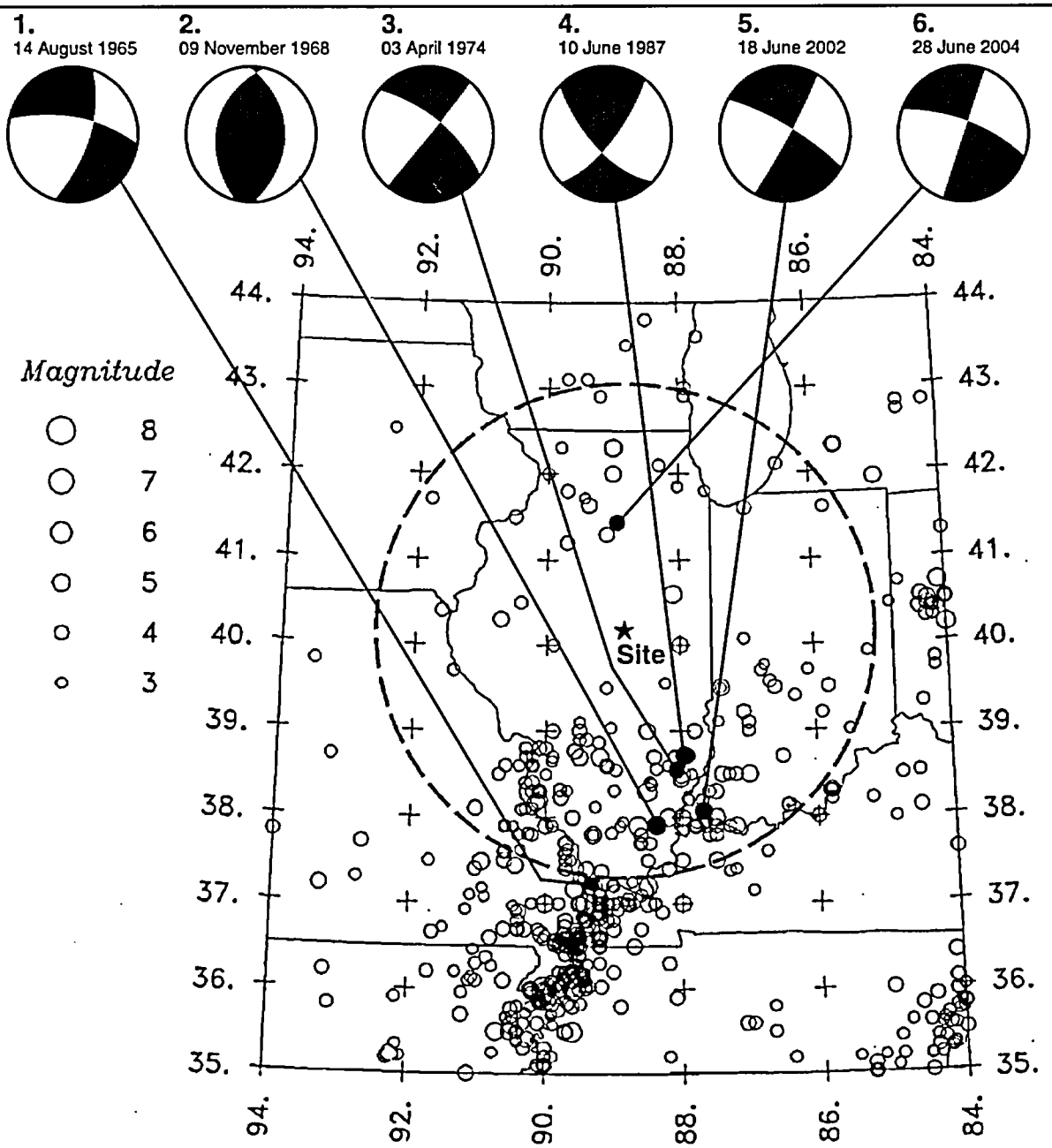

Seismicity for period 1777 to August 1, 2002. Map Symbol sizes are proportional to magnitude. Compressional quadrants in the focal mechanisms are shaded.

Event	Magnitude	Depth
1. 14 August 1965	M 3.6	2 km
2. 09 November 1968	M 5.3	22 km
3. 03 April 1974	M 4.3	15 km
4. 10 June 1987	M 5.0	10 km
5. 18 June 2002	M 4.57	19 km
6. 28 June 2004	M 4.15	7 km

Sources: Herrman (1979); Taylor et al. (1989); http://www.eas.slu.edu/Earthquake_Center/NEW/mechanism.html

Seismic Hazards Report for the EGC ESP Site
Location and Surface-Wave Mechanisms
for Larger Events in Southern Illinois

Figure
2.1-13

S:\1790017935\7935.000\03_0109_esp_fig_2.1-13(55).ai (2004-09-28, 11:35)

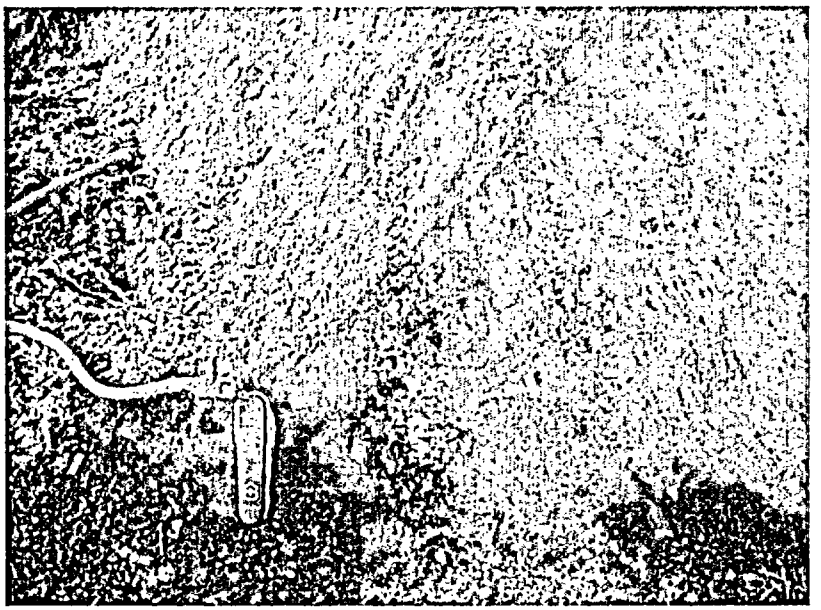

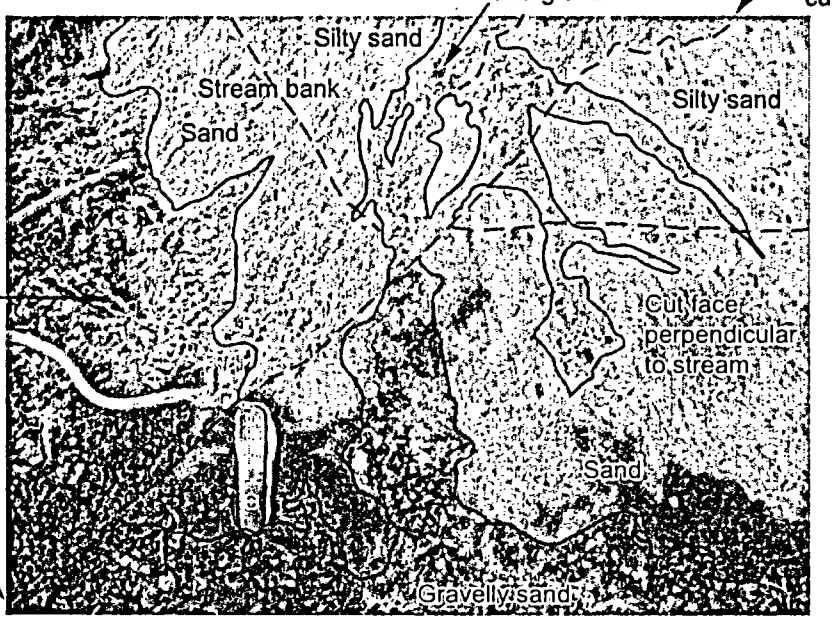

Note that:
1. Dike widens downward.
2. Gravelly sand fill fines upward.
3. Dike walls are sharp and irregular.
4. Dike is roughly tabular.
5. Dike occurs in clear association with source material.
6. Weathering within dike suggests it is relatively old.

Seismic Hazards Report for the EGC ESP Site
Photographs of Dike 1 at Locality SC 25

Figure
B-1-13A

S:\17900\7935\7935.000\03_0303_sect01\individual_photos_09041_fig_b1-13A(09.10).ai

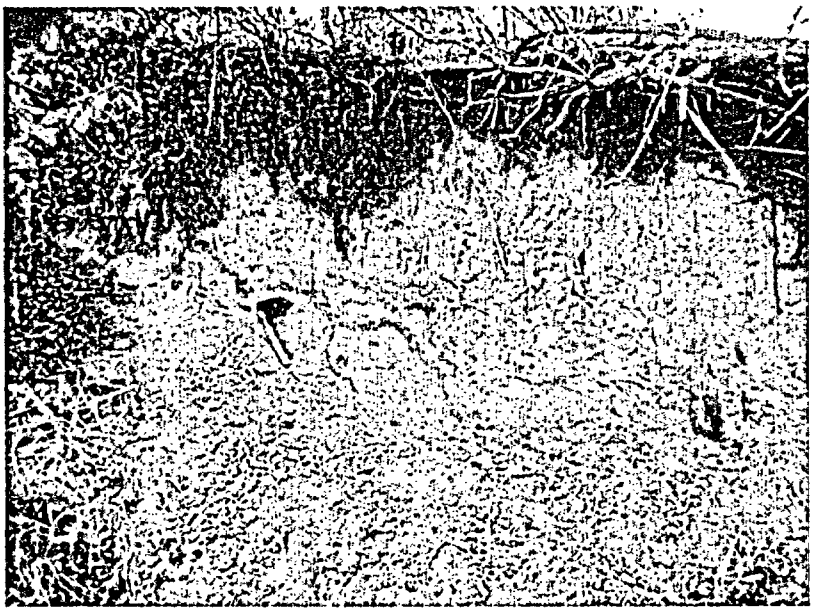

Bank rises approximately 12 feet above water level

Note that:

1. Dike widens downward.
2. Gravelly sand fill fines upward.
3. Dike walls are sharp and irregular.
4. Dike is roughly tabular.
5. Dike occurs in clear association with source material.
6. Weathering within dike suggests it is relatively old.

Seismic Hazards Report for the EGC ESP Site
Photographs of Dike 1 at Locality SC 25

Figure
B-1-13B

S:\17900\179357935.000\03_0303_sect\individual_photos_0904_fig_b1-13B(10).ai

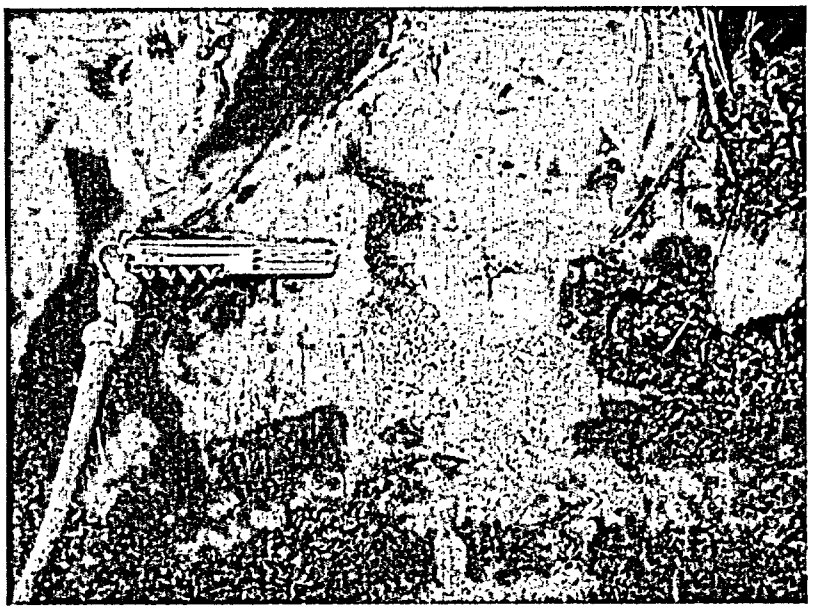

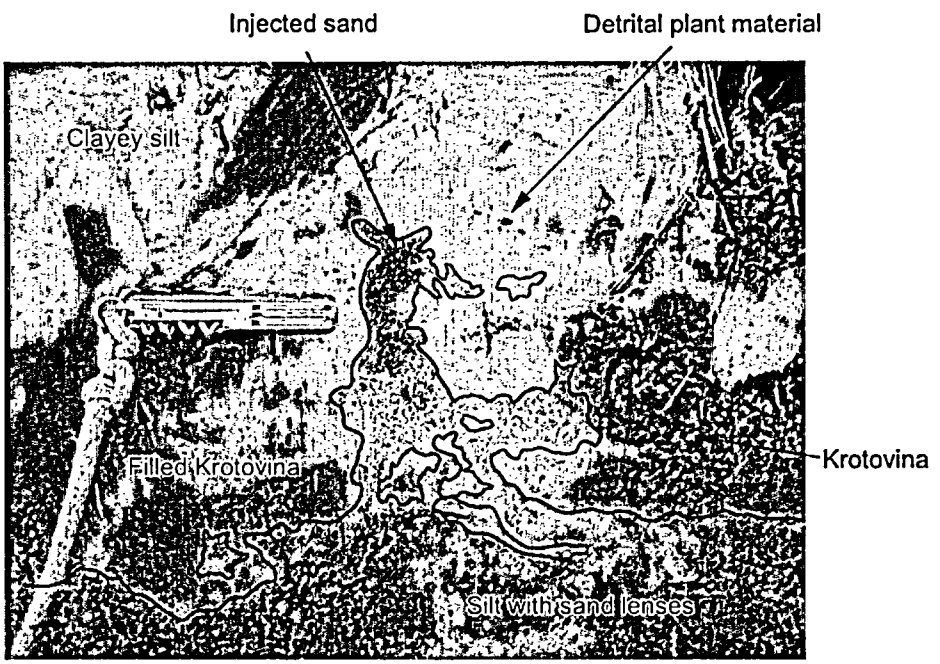

Note that:

1. Dike widens downward.
2. Sand in filling fines upwards.
3. Contacts are sharp and irregular.
4. Dike occurs in clear association with source material.
5. Dike includes clasts of silty clay, apparently ripped from its walls.
6. Maximum dike width is 1.5 in.

Seismic Hazards Report for the EGC ESP Site
Photograph of Dike 2 at Locality SC 19

Figure
B-1-14

s:\17900\79351\7935.000\03_0303_sect\11_fig_b1-14(07)_0904.ai

Note: Knife is 8 in. long

Seismic Hazards Report for the EGC ESP Site

Photographs of Parts of Dike 1 at Locality M 6

Figure

B-1-15A

s:\17900\179357\935.000\03_0303_sect\1\individual_photos_0904_fig_B1-15A(13).ai

Seismic Hazards Report for the EGC ESP Site

Photographs of Parts of Dike 1 at Locality M 6

Figure **B-1-15B**

s:\17900\79351\7935.000\03_0303_sect b1\individual_photos_0904_fig_B1-15B(12).ai

Non-GDS

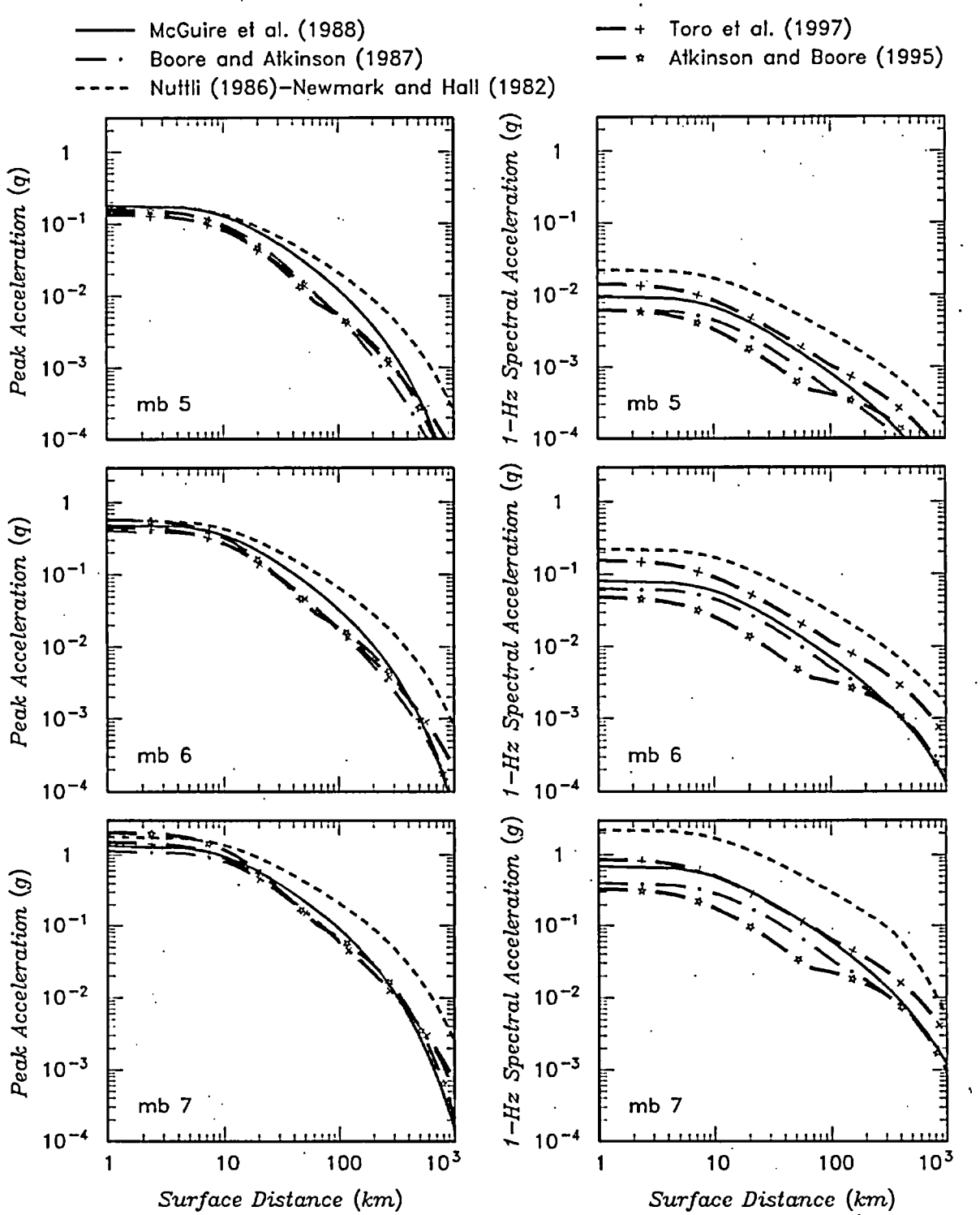

Seismic Hazards Report for the EGC ESP Site

Comparison of Median Ground Motion Relationships Used in EPRI-SOG Study with Recently Developed Relationships

Figure **2.2-2**

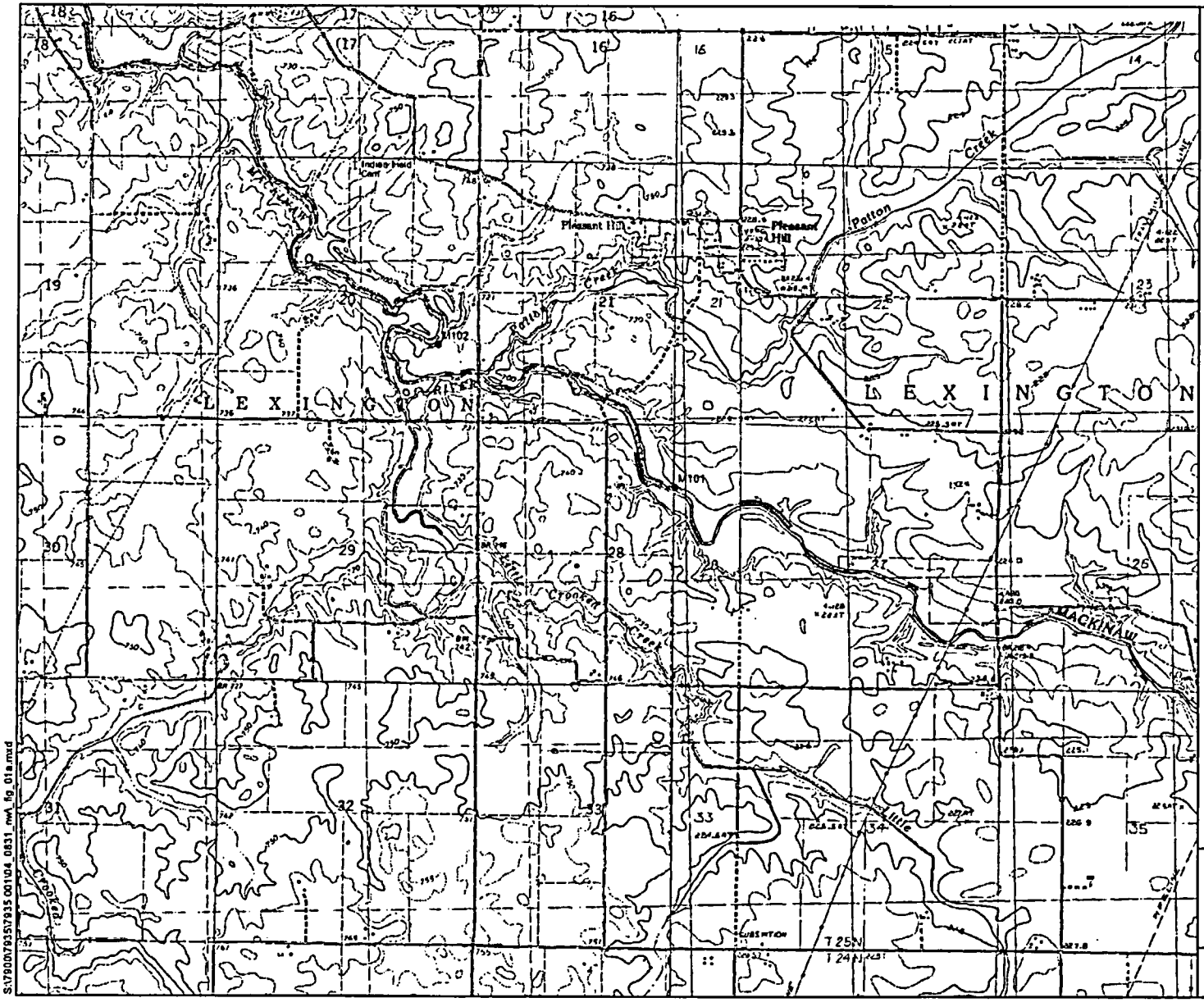

Explanation

- Late Pleistocene Till or Glacial Drift
- Later Pleistocene/Pre-Hypsithermic Holocene Alluvium
- Post-Hypsithermic Holocene Alluvium
- Stations described in Field Notes

Solid lines indicate relatively continuous exposures that were annotated on field maps. Dotted lines indicate 'Target Reaches': River reaches that intersect mapped soil types (from Soil Surveys) likely to be developed on older alluvium (Latest Pleistocene or Pre-Hypsithermic Holocene). These reaches were observed during field reconnaissance, and many included exposures of older alluvium, but they were not recorded because they contained no liquefaction features. Reaches that are not colored generally represent modern floodplains or low terraces underlain by late Holocene alluvium that was not well exposed.

N

0 2,000 Feet

Base map modified from 7.5' U.S.G.S. Cooksville and Merna, Illinois topographic quadrangles.

Seismic Hazards Report for the EGC ESP Site-RAI 2.5.2-6

Locations of Stream Bank Exposures Observed during Paleoliquefaction Field Reconnaissance, Mackinaw River

Figure

2.5.2-6-1A

S:\179001793\7935.001\04_0831_rwA_fig_01a.mxd

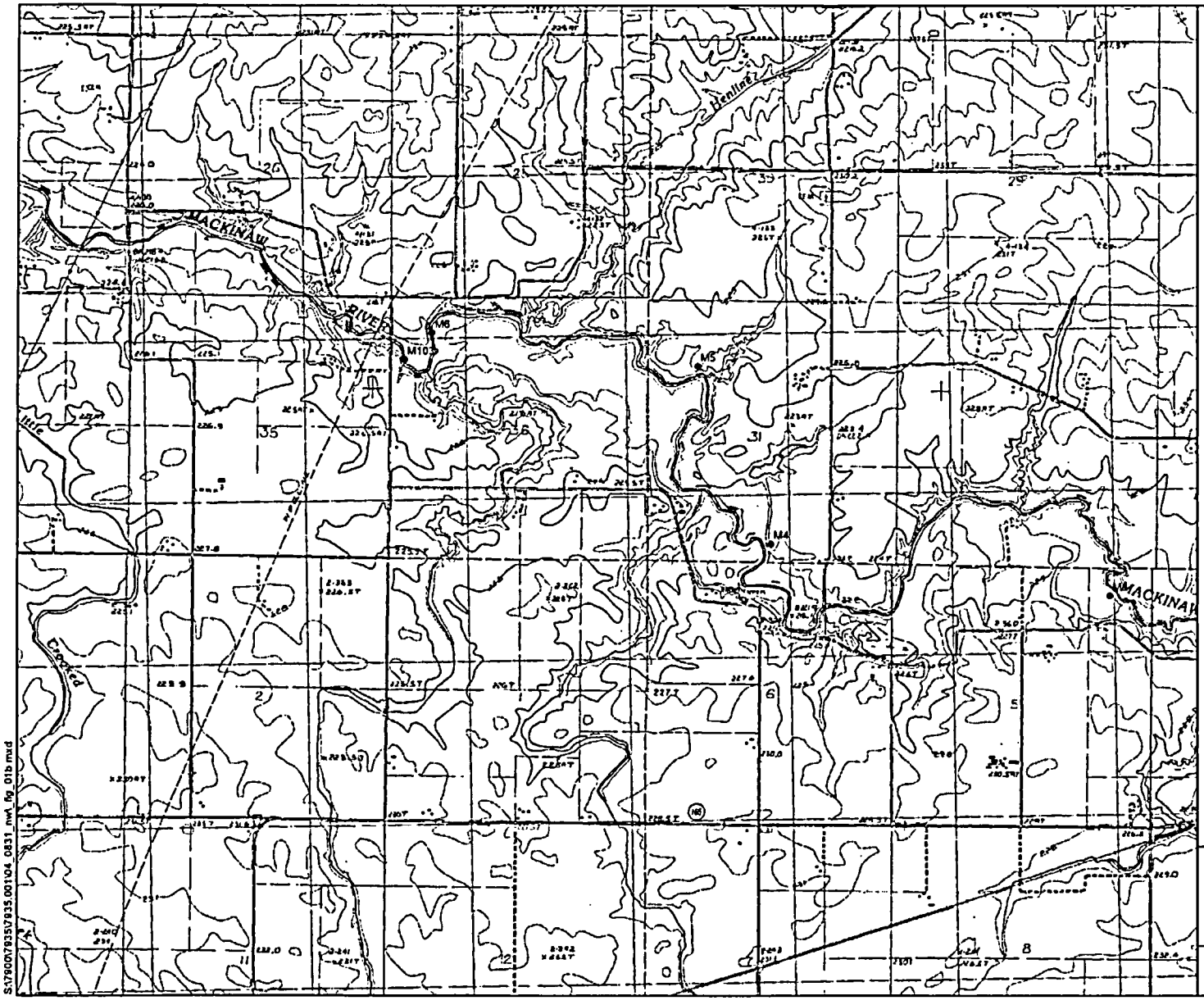

Explanation

- Late Pleistocene Till or Glacial Drift
- Later Pleistocene/Pre-Hypsithermic Holocene Alluvium
- Post-Hypsithermic Holocene Alluvium
- Stations described in Field Notes

Solid lines indicate relatively continuous exposures that were annotated on field maps. Dotted lines indicate 'Target Reaches'; River reaches that intersect mapped soil types (from Soil Surveys) likely to be developed on older alluvium (Latest Pleistocene or Pre-Hypsithermic Holocene). These reaches were observed during field reconnaissance, and many included exposures of older alluvium, but they were not recorded because they contained no liquefaction features. Reaches that are not colored generally represent modern floodplains or low terraces underlain by late Holocene alluvium that was not well exposed.

N

0 2,000 Feet

Base map modified from 7.5' U.S.G.S. Cooksville, Illinois topographic quadrangle.

Seismic Hazards Report for the EGC ESP Site-RAI 2.5.2-6

Locations of Stream Bank Exposures Observed during Paleoliquefaction Field Reconnaissance, Mackinaw River

Figure

2.5.2-6-1B

S:\7900\7935\7935.001\04_0831_nwk_fig_01b.mxd

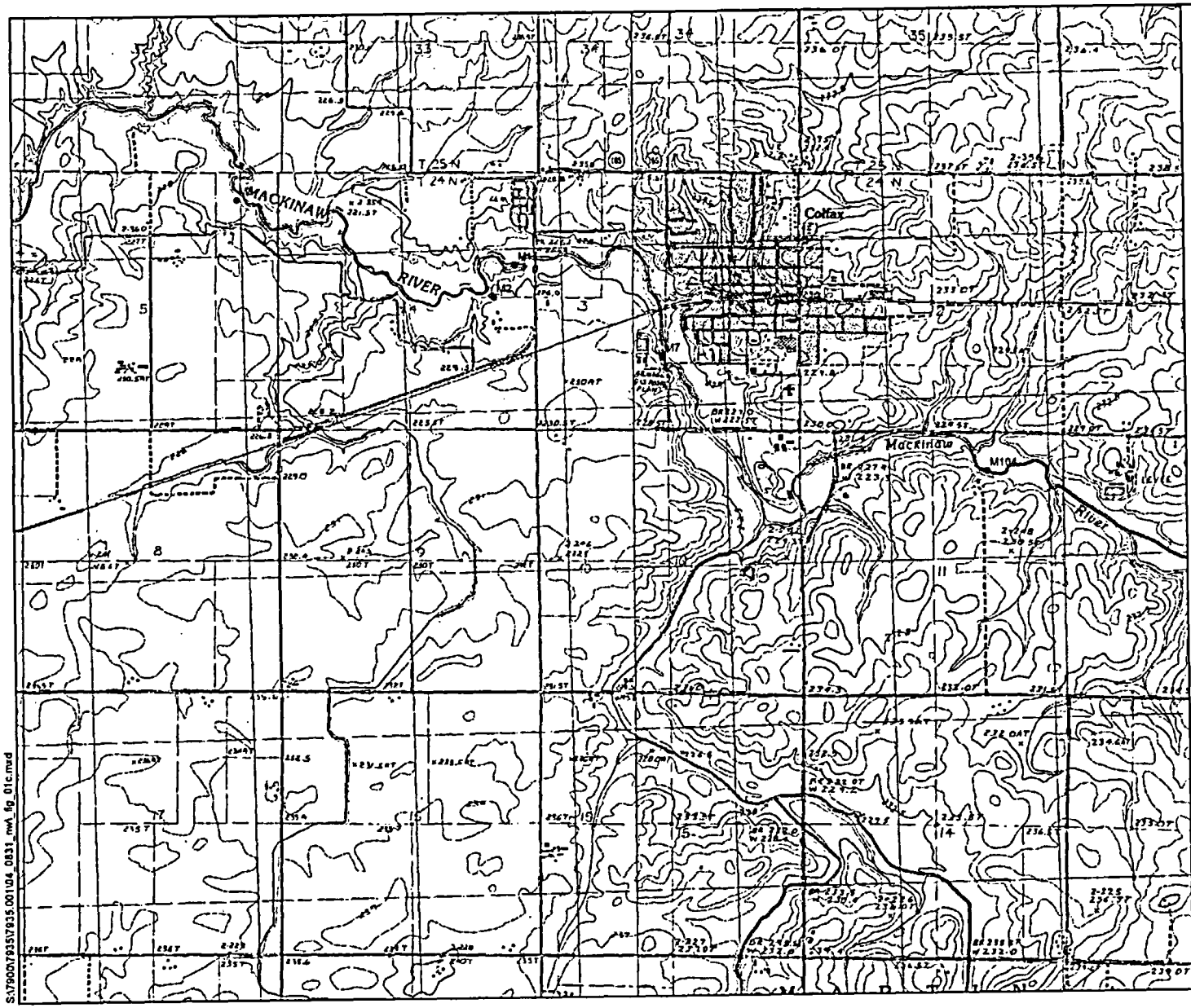

Explanation

- Late Pleistocene Till or Glacial Drift
- Later Pleistocene/Pre-Hypsithermic Holocene Alluvium
- Post-Hypsithermic Holocene Alluvium
- Stations described in Field Notes

Solid lines indicate relatively continuous exposures that were annotated on field maps. Dotted lines indicate 'Target Reaches'; River reaches that intersect mapped soil types (from Soil Surveys) likely to be developed on older alluvium (Latest Pleistocene or Pre-Hypsithermic Holocene). These reaches were observed during field reconnaissance, and many included exposures of older alluvium, but they were not recorded because they contained no liquefaction features. Reaches that are not colored generally represent modern floodplains or low terraces underlain by late Holocene alluvium that was not well exposed.

N

0 2,000 Feet

Base map modified from 7.5' U.S.G.S. Cooksville and Colfax, Illinois topographic quadrangles.

Seismic Hazards Report for the EGC ESP Site-RAI 2.5.2-6

Locations of Stream Bank Exposures Observed during Paleoliquefaction Field Reconnaissance, Mackinaw River

Figure

2.5.2-6-1C

S:\7900\179351\7935.001\04_0831_mvt_fig_01c.mxd

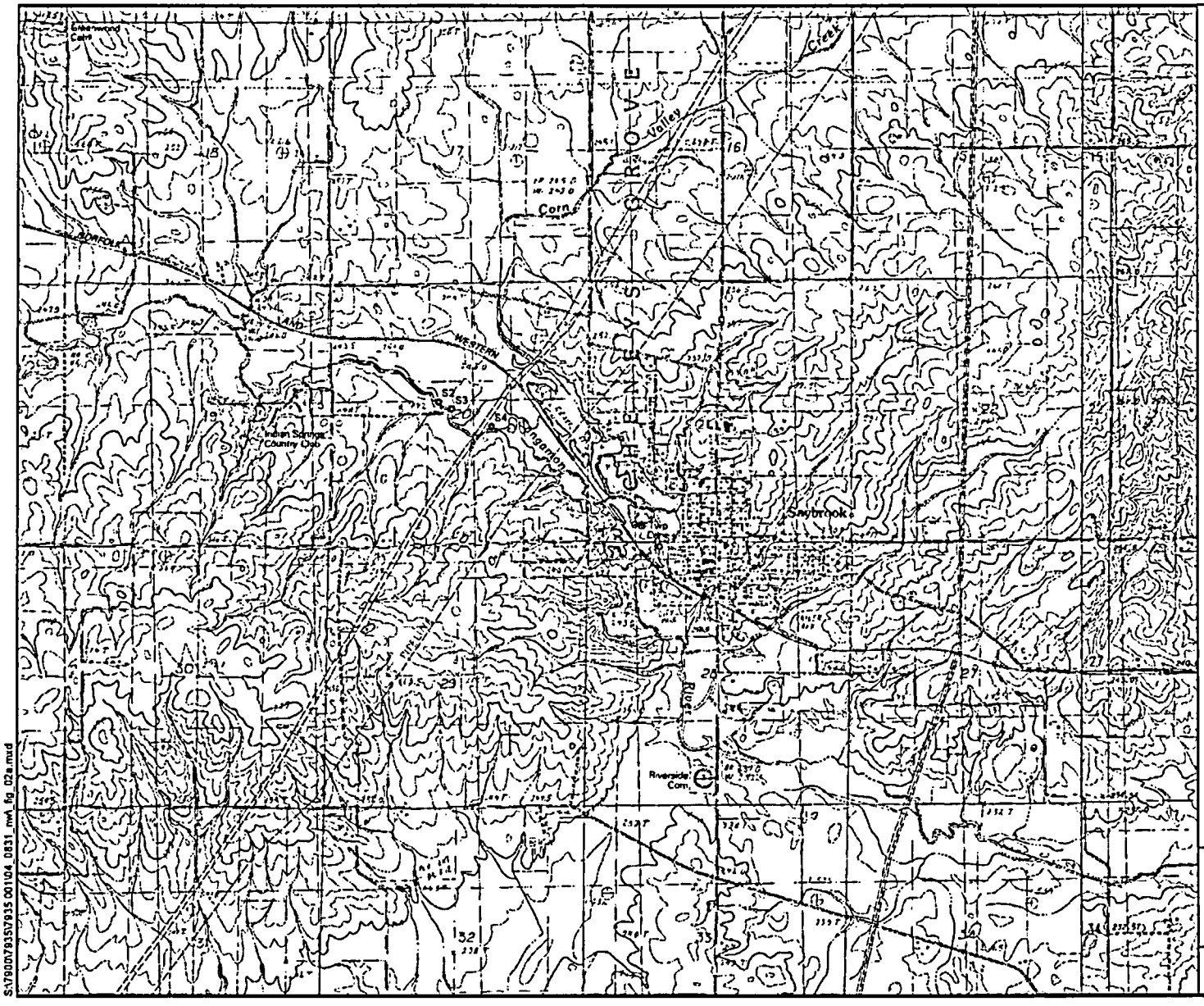

Explanation

- Late Pleistocene Till or Glacial Drift
- Later Pleistocene/Pre-Hypsithermic Holocene Alluvium
- Post-Hypsithermic Holocene Alluvium
- Stations described in Field Notes

Solid lines indicate relatively continuous exposures that were annotated on field maps. Dotted lines indicate 'Target Reaches': River reaches that intersect mapped soil types (from Soil Surveys) likely to be developed on older alluvium (Latest Pleistocene or Pre-Hypsithermic Holocene). These reaches were observed during field reconnaissance, and many included exposures of older alluvium, but they were not recorded because they contained no liquefaction features. Reaches that are not colored generally represent modern floodplains or low terraces underlain by late Holocene alluvium that was not well exposed.

N

0 2,000 Feet

Base map modified from 7.5' U.S.G.S. Saybrook and Gibson City West, Illinois topographic quadrangles.

Seismic Hazards Report for the EGC ESP Site-RAI 2.5.2-6

Locations of Stream Bank Exposures Observed during Paleoliquefaction Field Reconnaissance, Sangamon River

Figure

2.5.2-6-2A

S:\7900\7935\7935001\04_0831_rwl_fig_02a.mxd

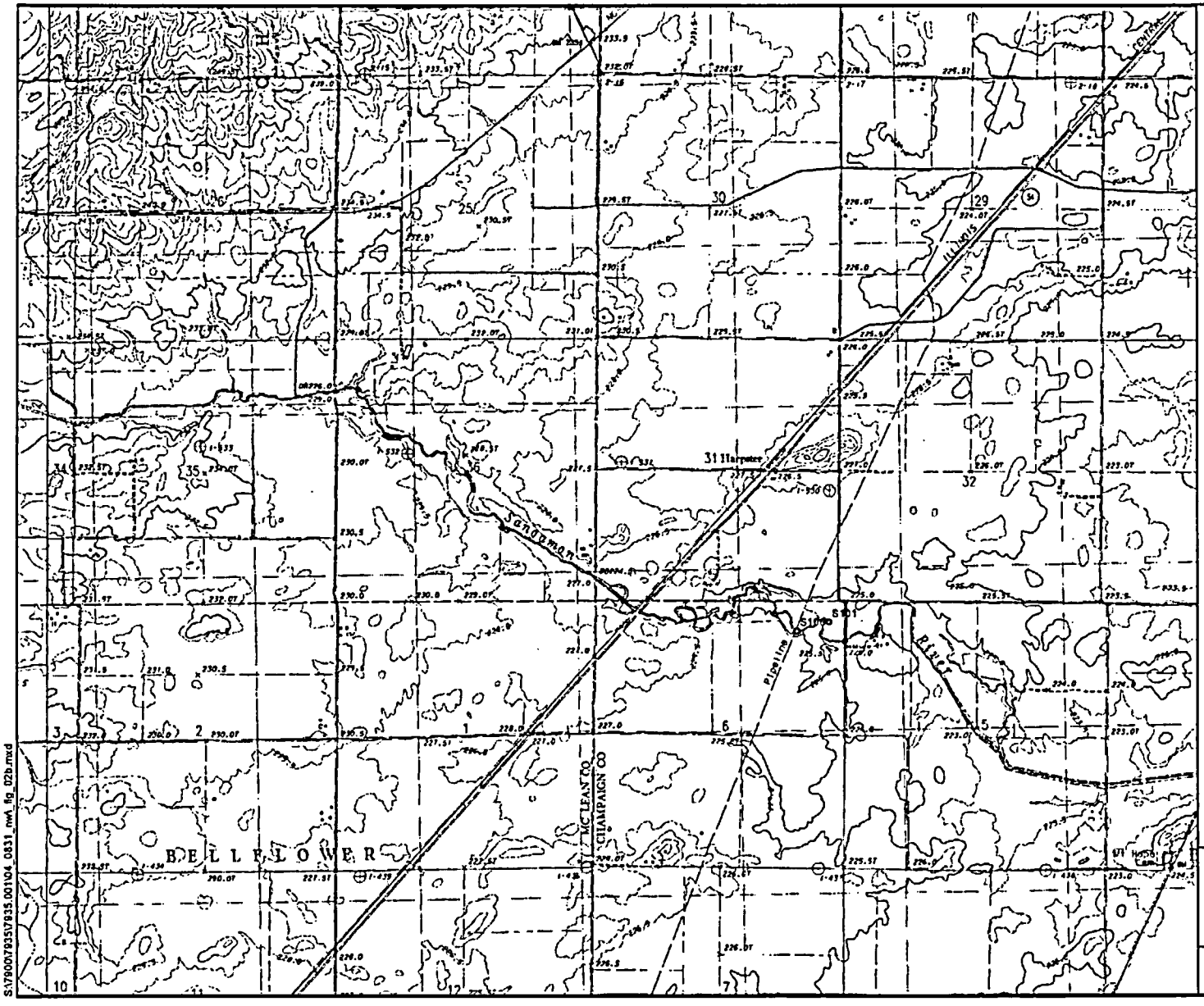

Explanation

- Late Pleistocene Till or Glacial Drift
- Later Pleistocene/Pre-Hypsithermic Holocene Alluvium
- Post-Hypsithermic Holocene Alluvium
- Stations described in Field Notes

Solid lines indicate relatively continuous exposures that were annotated on field maps. Dotted lines indicate 'Target Reaches': River reaches that intersect mapped soil types (from Soil Surveys) likely to be developed on older alluvium (Latest Pleistocene or Pre-Hypsithermic Holocene). These reaches were observed during field reconnaissance, and many included exposures of older alluvium, but they were not recorded because they contained no liquefaction features. Reaches that are not colored generally represent modern floodplains or low terraces underlain by late Holocene alluvium that was not well exposed.

0 2,000 Feet

Base map modified from 7.5' U.S.G.S. Gibson City West, Illinois topographic quadrangle.

Seismic Hazards Report for the EGC ESP Site-RAI 2.5.2-6

Locations of Stream Bank Exposures Observed during Paleoliquefaction Field Reconnaissance, Sangamon River

Figure

2.5.2-6-2B

S:\7900079357935.001\04_0831_mxd_fig_02b.mxd

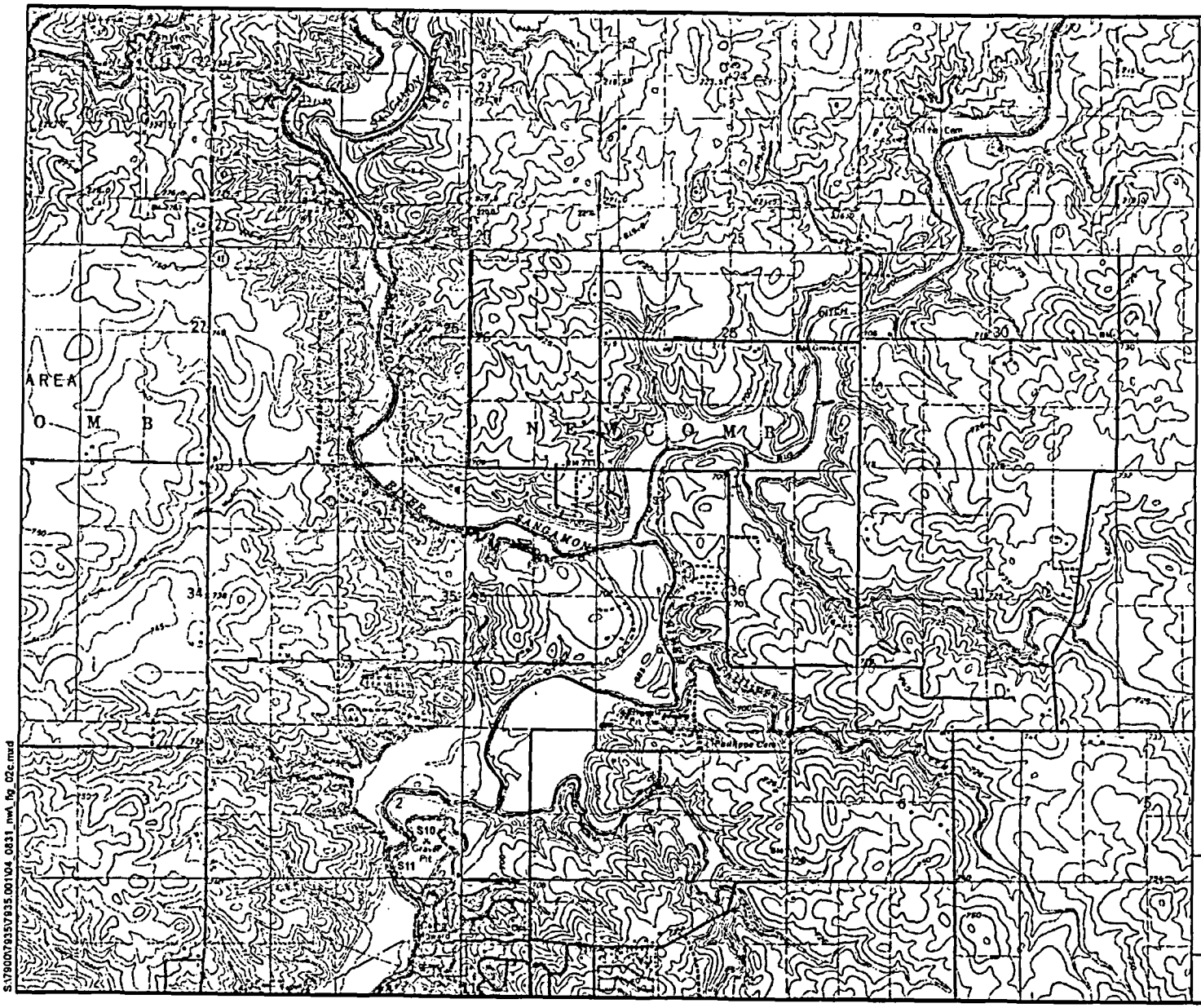

Explanation

- Late Pleistocene Till or Glacial Drift
- Later Pleistocene/Pre-Hypsithermic Holocene Alluvium
- Post-Hypsithermic Holocene Alluvium
- Stations described in Field Notes

Solid lines indicate relatively continuous exposures that were annotated on field maps. Dotted lines indicate 'Target Reaches': River reaches that intersect mapped soil types (from Soil Surveys) likely to be developed on older alluvium (Latest Pleistocene or Pre-Hypsithermic Holocene). These reaches were observed during field reconnaissance, and many included exposures of older alluvium, but they were not recorded because they contained no liquefaction features. Reaches that are not colored generally represent modern floodplains or low terraces underlain by late Holocene alluvium that was not well exposed.

N

0 2,000 Feet

Base map modified from 7.5' U.S.G.S. Fisher, Foosland, Mahomet, and Rising, Illinois topographic quadrangles.

Seismic Hazards Report for the EGC ESP Site-RAI 2.5.2-6

Locations of Stream Bank Exposures Observed during Paleoliquefaction Field Reconnaissance, Sangamon River

Figure

2.5.2-6-2C

S:\7900\7935\7935.001\04_0831_nwl_fig_02c.mxd

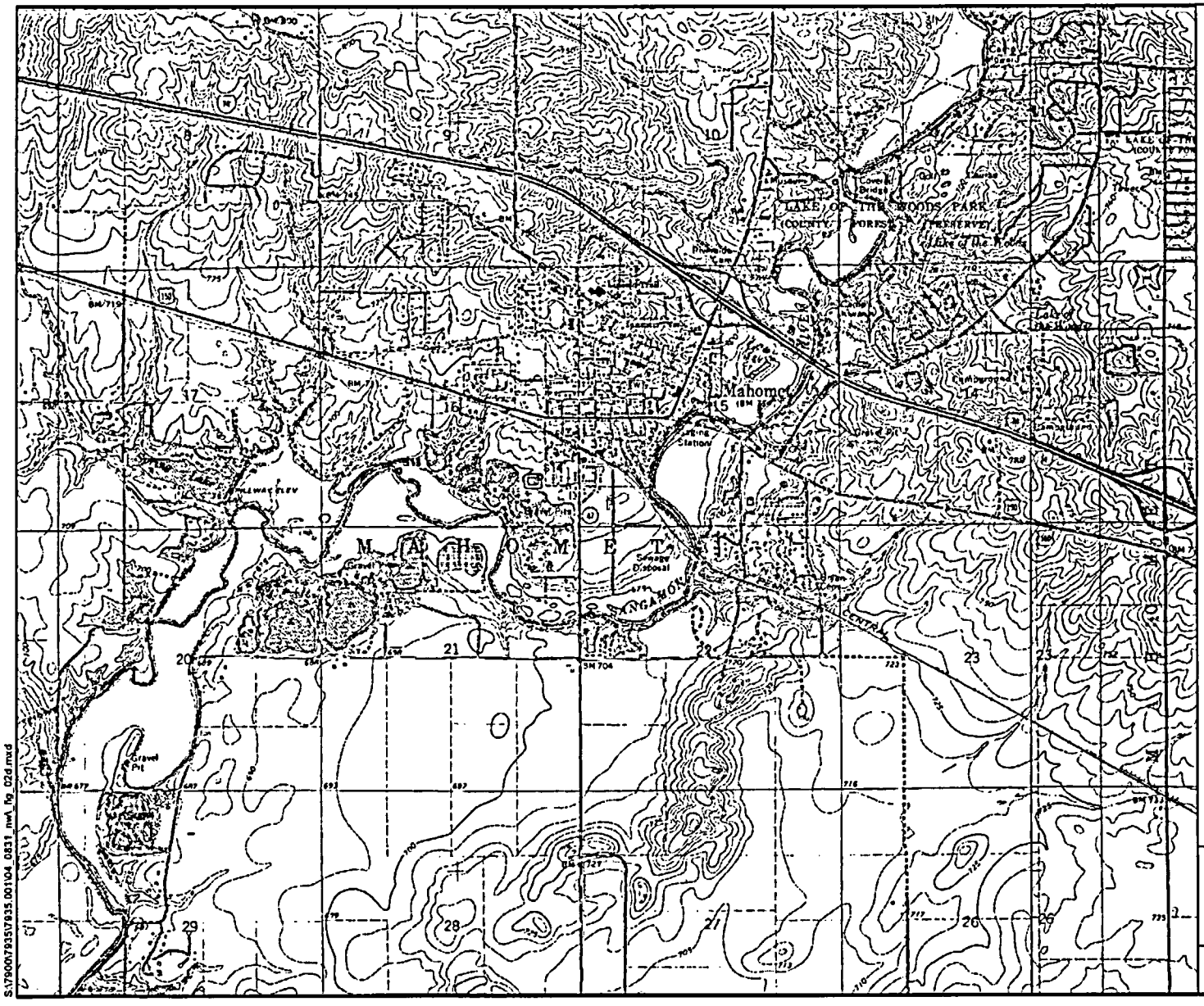

S:\7900\7935\7935.001\04_0831_mxd_fig_02d.mxd

Seismic Hazards Report for the EGC ESP Site-RAI 2.5.2-6

Locations of Stream Bank Exposures Observed during Paleoliquefaction Field Reconnaissance, Sangamon River

Figure

2.5.2-6-2D

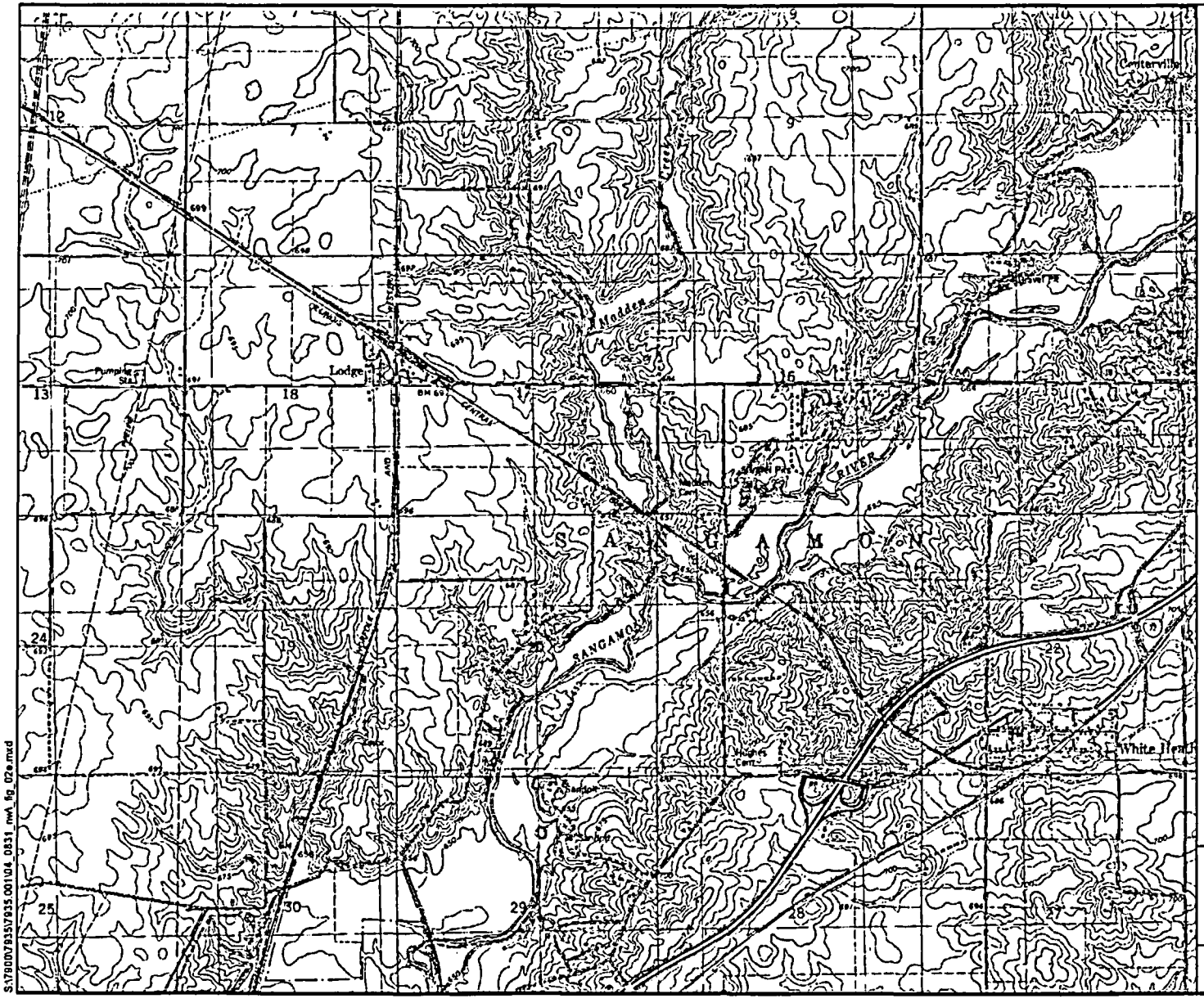

S:\7000\7835\7835.001\04_0831_mxA_fig_02e.mxd

Explanation

- Late Pleistocene Till or Glacial Drift
- Later Pleistocene/Pre-Hypsithermic Holocene Alluvium
- Post-Hypsithermic Holocene Alluvium
- Stations described in Field Notes

Solid lines indicate relatively continuous exposures that were annotated on field maps. Dotted lines indicate 'Target Reaches': River reaches that intersect mapped soil types (from Soil Surveys) likely to be developed on older alluvium (Latest Pleistocene or Pre-Hypsithermic Holocene). These reaches were observed during field reconnaissance, and many included exposures of older alluvium, but they were not recorded because they contained no liquefaction features. Reaches that are not colored generally represent modern floodplains or low terraces underlain by late Holocene alluvium that was not well exposed.

N

0 2,000 Feet

Base map modified from 7.5' U.S.G.S. Monticello, Illinois topographic quadrangle.

Seismic Hazards Report for the EGC ESP Site-RAI 2.5.2-6

Locations of Stream Bank Exposures Observed during Paleoliquefaction Field Reconnaissance, Sangamon River

Figure

2.5.2-6-2E

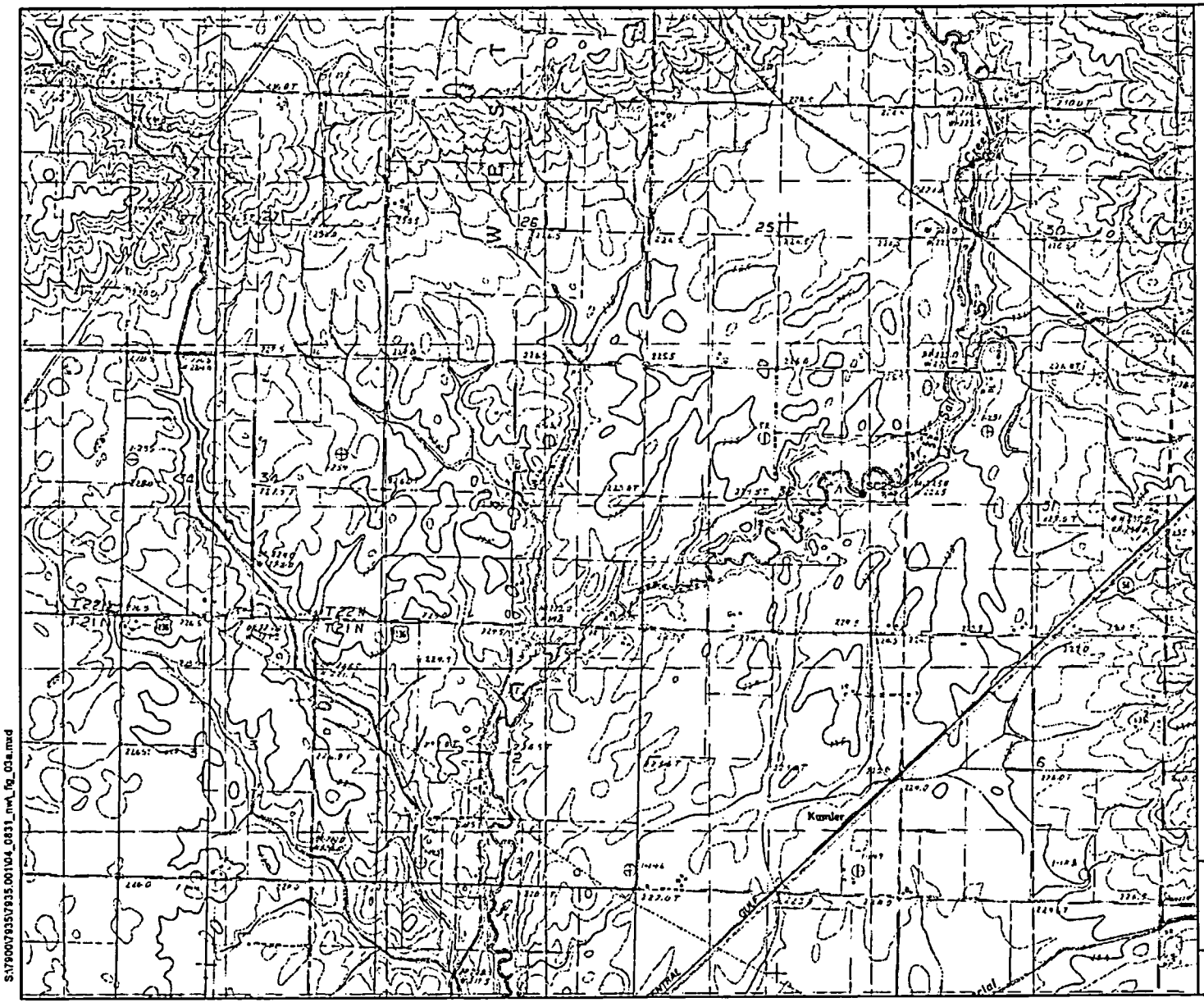

Explanation

- Late Pleistocene Till or Glacial Drift
- Later Pleistocene/Pre-Hypsithermic Holocene Alluvium
- Post-Hypsithermic Holocene Alluvium
- Stations described in Field Notes

Solid lines indicate relatively continuous exposures that were annotated on field maps. Dotted lines indicate 'Target Reaches'; River reaches that intersect mapped soil types (from Soil Surveys) likely to be developed on older alluvium (Latest Pleistocene or Pre-Hypsithermic Holocene). These reaches were observed during field reconnaissance, and many included exposures of older alluvium, but they were not recorded because they contained no liquefaction features. Reaches that are not colored generally represent modern floodplains or low terraces underlain by late Holocene alluvium that was not well exposed.

N

0 2,000 Feet

Base map modified from 7.5' U.S.G.S. Bellflower and Farmer City North, Illinois topographic quadrangles.

Seismic Hazards Report for the EGC ESP Site-RAI 2.5.2-6

Locations of Stream Bank Exposures Observed during Paleoliquefaction Field Reconnaissance, Salt Creek

Figure

2.5.2-6-3A

S:\179001793517935.001\04_0831_nwk_fig_03a.mxd

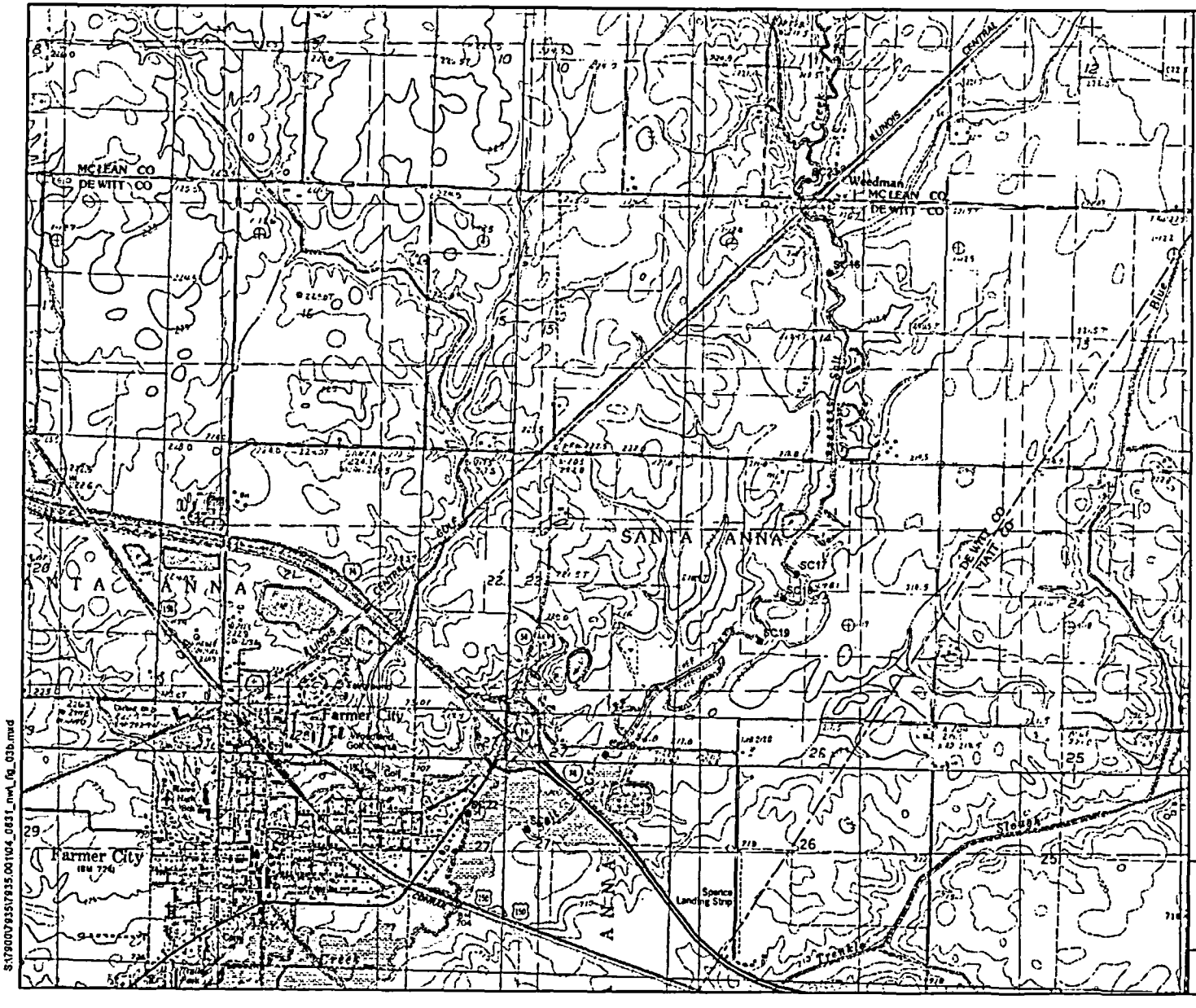

S:\1790007935\7935.001\04_0831_rwt_fig_03b.mxd

Seismic Hazards Report for the EGC ESP Site-RAI 2.5.2-6

Locations of Stream Bank Exposures Observed during Paleoliquefaction Field Reconnaissance, Salt Creek

Figure

2.5.2-6-3B

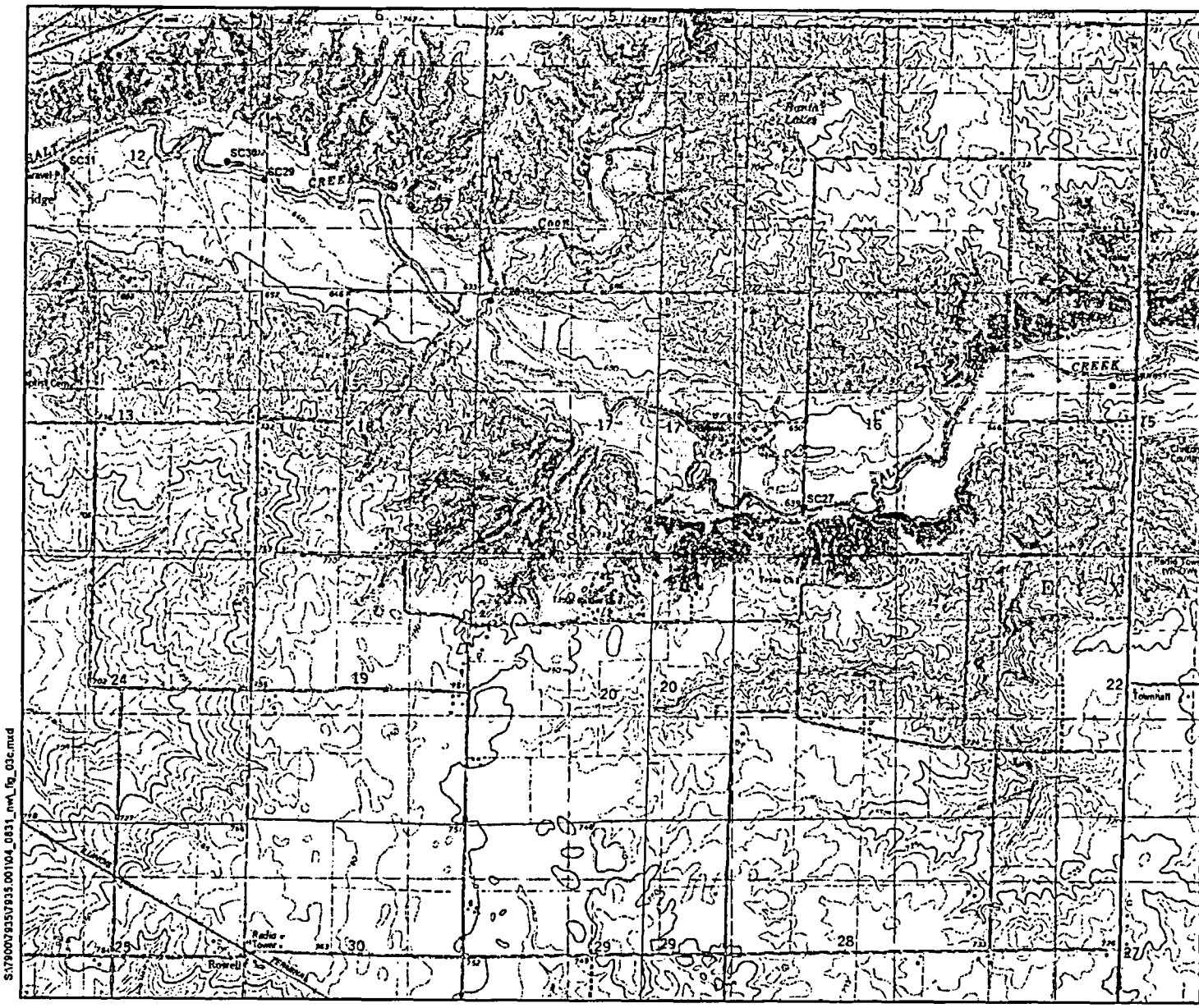

Explanation

- Late Pleistocene Till or *Glacial Drift*
- Later Pleistocene/Pre-Hypsithermic Holocene Alluvium
- Post-Hypsithermic Holocene Alluvium
- Stations described in Field Notes

Solid lines indicate relatively continuous exposures that were annotated on field maps. Dotted lines indicate 'Target Reaches': River reaches that intersect mapped soil types (from Soil Surveys) likely to be developed on older alluvium (Latest Pleistocene or Pre-Hypsithermic Holocene). These reaches were observed during field reconnaissance, and many included exposures of older alluvium, but they were not recorded because they contained no liquefaction features. Reaches that are not colored generally represent modern floodplains or low terraces underlain by late Holocene alluvium that was not well exposed.

Base map modified from 7.5' U.S.G.S. Maroa and Kenney, Illinois topographic quadrangles.

Seismic Hazards Report for the EGC ESP Site-RAI 2.5.2-6

Locations of Stream Bank Exposures Observed during Paleoliquefaction Field Reconnaissance, Salt Creek

Figure

2.5.2-6-3C

S:\7900\7935\7935.001\04_0831_mxd_fig_03c.mxd

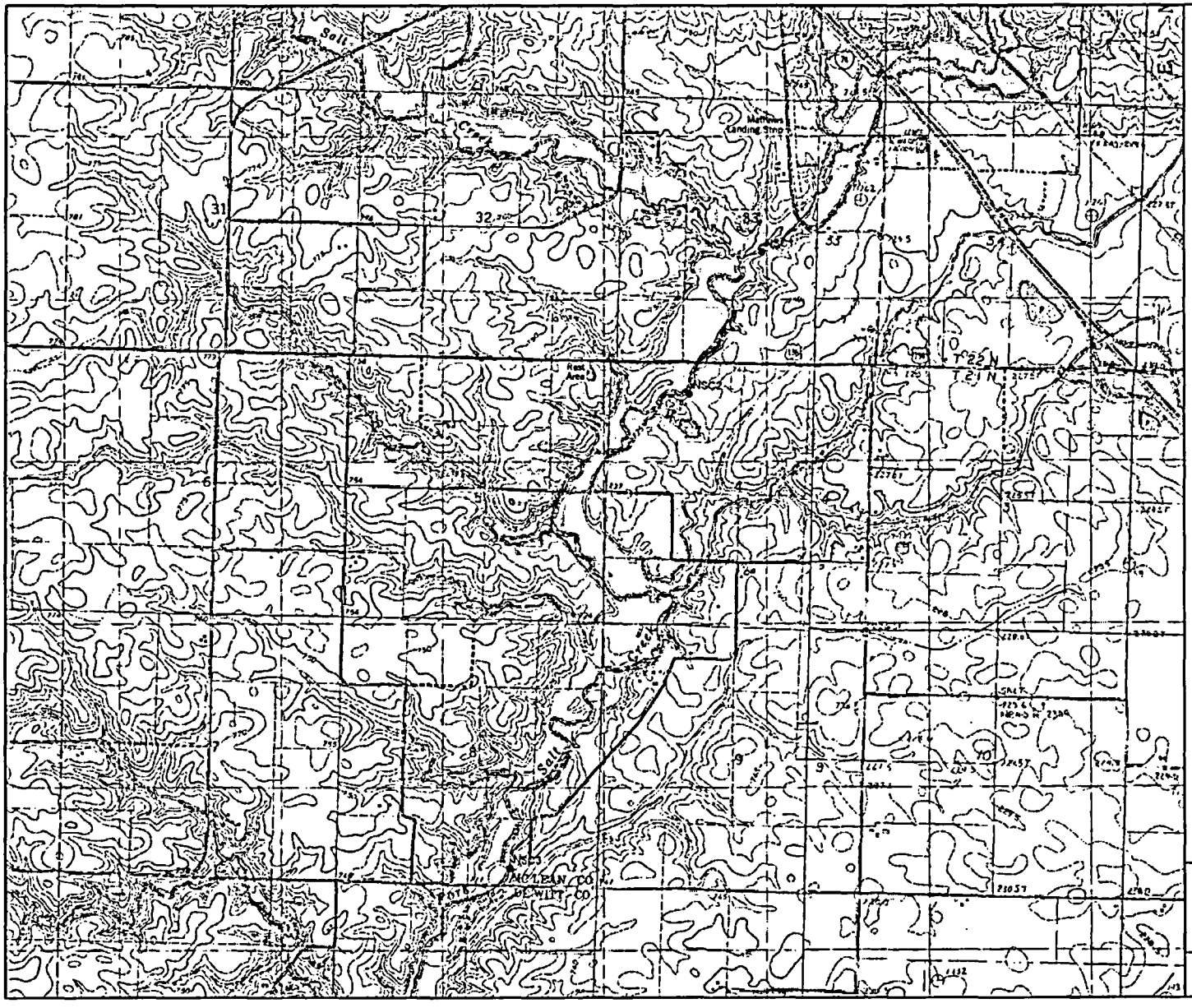

Explanation

- Late Pleistocene Till or Glacial Drift
- Later Pleistocene/Pre-Hypsithermic Holocene Alluvium
- Post-Hypsithermic Holocene Alluvium
- Stations described in Field Notes

Solid lines indicate relatively continuous exposures that were annotated on field maps. Dotted lines indicate 'Target Reaches': River reaches that intersect mapped soil types (from Soil Surveys) likely to be developed on older alluvium (Latest Pleistocene or Pre-Hypsithermic Holocene). These reaches were observed during field reconnaissance, and many included exposures of older alluvium, but they were not recorded because they contained no liquefaction features. Reaches that are not colored generally represent *modern floodplains or low terraces underlain by late* Holocene alluvium that was not well exposed.

N

0 2,000 Feet

Base map modified from 7.5' U.S.G.S. Farmer City North and Leroy, Illinois topographic quadrangles.

Seismic Hazards Report for the EGC ESP Site-RAI 2.5.2-6

Locations of Stream Bank Exposures Observed during Paleoliquefaction Field Reconnaissance, North Fork Salt Creek

Figure

2.5.2-6-4A

S:\7900\79357935.001\04_0831_nwt_0g_04a.mxd